

The near-continuum mechanism for extended Boltzmann theory: the non-equilibrium relaxation

Sha Liu^{123†}, Ningchao Ding^{1‡}, Ming Fang⁴, Hao Jin¹, Rui Zhang¹, Congshan Zhuo¹²³ and Chengwen Zhong¹²³

¹School of Aeronautics, Northwestern Polytechnical University, Xi'an, Shaanxi 710072, China

²National Key Laboratory of Aircraft Configuration Design, Northwestern Polytechnical University, Xi'an, Shaanxi 710072, China

³Institute of Extreme Mechanics, Northwestern Polytechnical University, Xi'an, Shaanxi 710072, China

⁴China Aerodynamics Research and Development Center, Mianyang, Sichuan 621000, China

(Received xx; revised xx; accepted xx)

The collision phenomenon of polyatomic gases is described by the collision operator of extended Boltzmann equation or the energy-exchange model in particle direct simulations, for example, the Borgnakke-Larsen model. The later one is well developed and widely used in rarefied flow predictions. However, as a collision kernel, it does not guarantee the intrinsic detailed balance and is not integrable in moment calculations, thereby resulting in a lack of comprehensive knowledge of the near-continuum relaxation mechanism, along with the associated macroscopic transport coefficients and concrete relaxation model equation. In this work, the Pullin equation, which possesses an integrable collision kernel and satisfies the detailed balance constraint, is adopted as an extended Boltzmann equation for the theoretical analysis of near-continuum relaxation mechanisms. For clarity, only the translational and rotational degrees are considered in this work. Explicit analytical expressions for the temporal relaxation of macroscopic variables, including the stress force, (translational/rotational) temperature and (translational/rotational) heat flux, are obtained at the first time. This is achieved by approximating the distribution function in mixed Hermite space for translation and Laguerre space for rotation and computing the collision operator moments, enabling a direct description of macroscopic non-equilibrium evolution. Based on the same elementary moment (integral) of collision operator, the macroscopic transport coefficients is found in Chapman-Enskog framework. The long-standing speculation, that thermal conduction coefficient should be depended on the degrees of thermal non-equilibrium, is rigorously confirmed and evaluated. When thermal equilibrium is enforced, the present thermal conduction coefficients can be degenerated to the famous results of Mason and Monchick. Given the correct relaxation rate, a Rykov-type novel relaxation model for Pullin equation is proposed. It can recover the interaction of translational and rotational heat fluxes in relaxation process, which is ignored in the widely used Rykov equation. Finally, the precision of this new Rykov-type equation is examined using a series of benchmark test cases.

Key words: kinetic theory, rarefied gas flow

† Email address for correspondence: shaliu@nwpu.edu.cn

‡ Email address for correspondence: dingnc@mail.nwpu.edu.cn

MSC Codes (*Optional*) Please enter your MSC Codes here

1. Introduction

Gas kinetic theory, originally established by Maxwell and Boltzmann (Cercignani & Lampis 1971; Bird 1970; Chapman & Cowling 1990), was developed to describe dilute gas flows under rarefied and micro-nano-scale conditions, and has since been extended to model a wide range of particle systems, including photons (Sun *et al.* 2015, 2017; Dreicer 1964; Li *et al.* 2020b), plasmas (Liu & Xu 2017; Pu & Xu 2025), phonons (Zhang & Guo 2021; Guo & Xu 2016; Liu *et al.* 2024; Zhang *et al.* 2017), and neutrons (Tan *et al.* 2019; Zhou & Guo 2020; Tan *et al.* 2020). The distribution function $f(\mathbf{x}, \mathbf{c}, t)$, which is the fundamental field variable of the gas kinetic theory, represents the number density of molecules with velocity \mathbf{c} at spatial coordinates \mathbf{x} and time t . It can be viewed as dividing the macroscopic field variables, for example the momentum, into microscopic molecules with different molecular momentum. By doing so, the fundamental property of rarefied and micro-nano flows, which can be expressed as the velocity distribution of molecules significantly deviates from the normal distribution (the Maxwellian distribution in gas kinetic theory), can be accurately captured. In other words, the gas kinetic theory can provide a comprehensive description of the non-normal (non-equilibrium) molecular system, along with a physically rigorous framework, which should be adopted in studying the non-equilibrium phenomena in rarefied and micro-nano flows. This theoretical foundation has yielded profound insights into a series of complex flow phenomena (Cercignani 2000), including the Knudsen layer (Guo & Zheng 2008; Gusarov & Smurov 2002; Zhang *et al.* 2006) and the Knudsen paradox (Akhlaghi *et al.* 2023). To extend the scope of gas kinetic theory to broader scale ranges, primarily in the context of numerical prediction methods, modern scale-adaptive strategy, such as a series of unified modeling approaches (Xu & Huang 2010; Guo *et al.* 2013; Chen *et al.* 2019; Yang *et al.* 2019; Gallis & Torczynski 2011; Fei *et al.* 2020; Zhang *et al.* 2019), asymptotic preserving Monte Carlo (Ren *et al.* 2014), the general synthetic iterative scheme (Wu *et al.* 2014), and time-relaxed Monte Carlo (Fei 2023) has been successful in accommodating the near-continuum flows and even the entire flow scale (regime) spanning from rarefied to continuum flows. On the other hand, in the context of theoretical analysis, rigorous connections between gas kinetic theory and continuum aerodynamics have been derived through the Chapman-Enskog (C-E) expansion (Chapman & Cowling 1990), along with the moment methods (Grad 1958; Torrilhon 2016; Struchtrup & Torrilhon 2003; Cai & Li 2010; Jiang *et al.* 2019), yielding a system of constitutive relations and corresponding transport coefficients (such as thermal conductivity and viscosity) (Kremer 2010).

However, significant challenges arise when accounting for the internal degrees of freedom within molecule structures (e.g., rotational, vibrational and electronic motions). Due to the lack of exact and analytically integrable differential collision cross-section, which is the pivot of a governing equation, formulating an accurate extended Boltzmann equation (EBE) becomes considerably difficult (Nagnibeda & Kustova 2009; Gamba & Pavić-Čolić 2023; Pavić-Čolić & Simić 2022). Consequently, the theoretical derivation of the corresponding transport coefficients, which should be based on a given master equation, also becomes difficult. The master equation corresponds to rarefied and micro-nano-flows, while the transport coefficients are for both continuum flows (in constitutive relations for diffusion, stress and heat flux) and rarefied flows (in constructing model equation for EBE). So far,

almost all experimental data for transport coefficients, such as those published by National Institute of Standards and Technology (NIST 2025), are predominantly confined to the thermal equilibrium condition where temperatures for all degrees of freedom are equal. This situation renders the acquisition of reliable transport coefficients particularly challenging under the common thermal non-equilibrium condition. These limitations in both the master equation and the corresponding transport coefficients hampers both the understanding of fundamental physics and the numerical simulations of flow fields, especially in scenarios of aerospace engineering and micro-nano-manufacturing, where thermal non-equilibrium are pervasive due to the much less molecular collisions. Therefore, experimental works in the electric arc shock tube (EAST) (Cruden 2014; Park 1989) are conducted, which primarily focus on the acquisition of the relaxation time for internal energy and the chemical reaction rate (Nagnibeda & Kustova 2009), but without involving the transport coefficients. On the other hand, in scenarios of numerical prediction, the development of scale-adaptive methods for simulating the entire flow regime often relies on the model equation (Holway 1966; Rykov 1975) which is a mathematical simplification of EBE, and its modeling constrains include these very transport coefficients.

To address these challenges, a possible route involves the following steps: (1) finding or constructing an analytically integrable EBE; (2) rigorously deriving the non-equilibrium relaxation rate based on EBE, and obtaining the transport coefficient using the same methodology; (3) constructing and validating the relaxation model equation for the EBE. The subsequent paragraphs in this section review the background relevant to these three objectives. To ensure clarity throughout the derivation process and facilitate understanding of the underlying mechanisms, this study focuses exclusively on the rotational degrees of freedom. Other internal degrees of freedom can be treated analogously.

The key to constructing EBE lies in the accurate definition of the collision kernel, which determines the post-collision states of a particle pair based on their pre-collision states. This mapping relationship is precisely realized by the mechanism of the differential collision cross-section in the EBE framework. The construction of EBE, which entails defining a specific differential collision cross-section, primarily follows two routes: the state-to-state (StS) and the phenomenological approaches.

For StS-based EBE, the critical differential collision cross-sections are fitted or constructed based on molecular dynamics (MD) experimental results (Müller-Plathe 1997; Hu *et al.* 2025) as well as potential energy surfaces (PES) obtained from quantum mechanical (Szabo & Ostlund 2012) or simplified computational methods (Ebner *et al.* 1976; te Vrugt *et al.* 2020). However, the construction of the StS database is constrained by the limited accuracy and high computational cost. Addressing the challenge of improving the accuracy of state-to-state simulations, a series of quantum-classical hybrid methods have been developed. For instance, the mixed quantum-classical method (Billing 2003) employs quantum mechanical treatment for vibrational degrees of freedom and vibration-rotation coupling terms, while applying classical mechanics to translational and rotational degrees of freedom. Furthermore, classical mechanics can also be applied to the vibrational degrees of freedom to improve computational efficiency, as exemplified by the quasi-classical trajectory (QCT) method (Karplus *et al.* 1965). Although the QCT method is computationally efficient, its accuracy must be evaluated against results with higher theoretical accuracy. On the other hand, the accuracy of PES can also be enhanced by adjusting parameters for short-range interactions and linear collision configurations (Hong *et al.* 2020). Currently, the PES established for the corresponding EBE exhibit fluctuations in precision due to the fact that no single method has been proven to possess optimal accuracy.

Furthermore, both MD simulations and PES calculations require highly detailed pre-collision molecular information (including the relative positions of internal atoms, vibrational

velocities along bond directions, rotational velocities about three axes, etc.), leading to immense computational and experimental demands due to the high dimensionality and large number of discrete states involved. Even though StS collision kernels incorporated into the EBE retain only discrete energy level information through fitting procedures, the number of required discrete energy levels remains substantial. Due to the high costs and computational complexity involved, the development of a comprehensive state-to-state database faces significant challenges. In the early stages, to address the issue of prohibitive computational costs in potential energy surface calculations, methods such as spline interpolation and nonlinear fitting techniques based on many-body expansions and functional forms were successfully applied to triatomic systems (Schatz 1989). However, for reactive systems involving more than four atoms, these interpolated PES suffer from substantial computational costs, significantly limiting the speed of dynamical potential energy calculations. In recent years, the rapid development of neural network fitting techniques and artificial intelligence has brought new solutions to the problem of high computational cost in PES calculations. The relevant applications aim to reduce the computational load and improve the efficiency of database establishment while ensuring the accuracy of PES (Hong *et al.* 2023; Li *et al.* 2020a).

It follows that once StS differential collision cross-sections are obtained, they can be incorporated using the framework of the Wang Chang-Uhlenbeck (WCU) equations (WANG-CHANG & Uhlenbeck 1951). This framework effectively treats different internal energy states as distinct species. In fact, the WCU formalism represents an early exploration of constructing the EBE under the StS model, although accurate StS differential collision cross-sections were unavailable at that time, thus requiring approximation schemes to derive macroscopic transport properties, specifically viscosity, diffusion, and thermal conductivity coefficients (WANG-CHANG & Uhlenbeck 1951). The growing availability of established StS databases enhances the feasibility of this framework, as its application relies on detailed databases covering various temperature ranges and different degrees of thermal non-equilibrium generated by the aforementioned work (Hong *et al.* 2020; Jiang *et al.* 2024). On the other hand, the WCU framework assumes by default that the internal energy states of molecules do not affect their translational motion. This treatment is also widely used in the model construction in Direct Simulation Monte Carlo (DSMC) methods (Borgnakke & Larsen 1975). However, some studies based on modeling practices have proposed that the influence of internal states on molecular collisional cross-sections should be taken into account (Gamba & Pavić-Čolić 2023). Nevertheless, there is currently a relative lack of experimental or computational support to substantiate such work.

Phenomenological EBE, in contrast, simplifies the detailed pre-collision state information by considering only translational velocity and internal energy (e.g., rotational energy, vibrational energy). Ordinary with the decoupled influence of translational and internal energy on the collision model, the translation of a collision pair is modeled by the traditional model such as the variable hard-sphere (VHS) model, while energy exchange mechanisms are modeled separately. This methodological modeling is implemented either at the theoretical level in the mathematical construction of EBE (Pullin 1978) or at the particle simulation level via specific procedures (Borgnakke & Larsen 1975) to construct the stochastic collision process. Throughout the modeling process, strict compliance with the detailed balance principle must be maintained (Cercignani 2000). Regarding energy exchange mechanisms, phenomenological models generally employ two approaches: either probabilistically selecting between fully elastic and fully inelastic collisions (Bird 1978, 1976), or directly distributing energy according to predefined probability parameters (Pullin 1978).

It is noteworthy that research on collision processes involving internal energy exchange

for rarefied flow predictions has historically been predominantly conducted using the DSMC method. For modeling collisions of polyatomic gas molecules, the early energy sink model (Bird 1976) was used, with subsequent widespread adoption of the Borgnakke-Larsen (BL) model in later studies (Borgnakke & Larsen 1975). The energy sink model checks the equilibrium relationship between translational and internal energy for every colliding pair and relaxes all imbalance. However, the energy sink model distorts the high-velocity tail of the translational velocity equilibrium distribution. This issue was resolved by Borgnakke in the BL model (Bird 1978). The BL model simulates energy exchange probabilistically, assuming that only a fraction of colliding pairs undergo completely inelastic collisions, while the remainder collide elastically. For the completely inelastic collisions, the BL model samples both the post-collision translational energy (and thus the relative translational velocity) and the internal energy from their respective local equilibrium distributions (statistically determined from all molecules within a computational cell), while rigorously conserving total energy. Crucially, each sampling step must satisfy the constraint of the residual energy remaining from the previous step. However, it has not been conclusively proven that the BL model satisfies detailed balance principle. The BL model significantly broadened the applicability of DSMC, cementing its role as the primary model and method for simulating rarefied flows (Boyd 1993; Valentini *et al.* 2023). However, it is essential to emphasize that the BL model was constructed specifically for direct simulation of the collision process. Consequently, its collision cross-section lacks an explicit integrable functional form. This limitation makes it difficult to derive analytical expressions for transport coefficients (e.g., viscosity, thermal conductivity) from the BL model, hindering further theoretical and completeness investigations.

Another seminal work in phenomenological EBE is Pullin's pioneering model (Pullin 1978). The phenomenological energy exchange component of its collision model employs a beta distribution to redistribute energy between colliding pairs, explicitly ensuring adherence to the important principle of detailed balance. Simultaneously, a governing equation with an analytically tractable form was constructed. Specifically, Pullin leveraged the mathematical property of the beta distribution enabling the decomposition of a normal distribution into multiple normal distributions (Pullin 1978), thereby preserving analytical integrability. Furthermore, the additional free parameter in the beta function allows for ensuring correct energy partitioning and matching macroscopic transport coefficients. Critically, incorporating the principle of detailed balance for the collision process guarantees collisional reversibility and the theoretical completeness of the equation within the framework of gas kinetic theory. Building upon similar energy redistribution concepts, Pavic *et al.* (Gamba & Pavić-Čolić 2023) also proposed a collision model accounting for the increased collision likelihood of particles possessing high translational and high internal energy, constructing an EBE tailored for polyatomic gases.

It is noteworthy that in the field of numerical computation, directly solving the Boltzmann equation poses significant challenges due to its mathematical complexity (specifically, the nonlinear multiple integrals in the collision term) and its physical stiffness. Although several representative efforts have addressed these difficulties (Aristov 2001; Morris *et al.* 2011; Clarke *et al.* 2012), both StS EBE and phenomenological EBE remain susceptible to the curse of dimensionality. To address this limitation, a series of model equations approximating the full Boltzmann transport equation and extended Boltzmann transport equation(EBTE) have been developed. These primarily fall into two categories: BGK-type model equations (also termed relaxation-type models) (Bhatnagar *et al.* 1954; Morse 1964; Shakhov 1968; Rykov & Skobelkin 1978) and Fokker-Planck-type model equations (Lebowitz *et al.* 1960; Pawula 1967; Yano *et al.* 2009; Gorji *et al.* 2011). Focusing on relaxation models for EBTE incorporating rotational energy, key contributions include the Rykov model (Rykov 1975) and

ES-BGK model (Holway 1966). The Rykov model adjusts Hermite polynomial coefficients to recover the correct thermal conductivity (Rykov 1975). However, it assumes independent relaxation of translational and rotational heat fluxes, a feature inconsistent with the actual physical relaxation process (Wu *et al.* 2015). While the ES-BGK model is grounded in the principle of maximum entropy, it suffers from similar unphysical limitations as the Rykov model. Furthermore, its reliance on an anisotropic Gaussian distribution restricts its ability to achieve exact relaxation for higher-order moments. Regarding Fokker-Planck models, the cubic-FP model has also been extended to include rotational energy (Gorji *et al.* 2011).

Historically, constructing relaxation-type models (e.g., the Rykov model), particularly concerning their asymptotic preserving (AP) properties, centered on the guiding principle of recovering correct transport coefficients via C-E expansion. However, achieving the correct relaxation rates is a broader and more fundamental requirement. When accurate relaxation rates are attained, the correct macroscopic transport coefficients are naturally recovered. This critical point will be elaborated upon in detail in Section 2 of this work. Moreover, within both the C-E expansion and relaxation rate frameworks, the moment integration of the collision term constitutes a fundamental element. This integration exhibits significant universality across theoretical studies, particularly in deriving transport coefficients. Eucken analytically demonstrated that under thermal non-equilibrium conditions (where translational and rotational temperatures differ), the thermal conductivity coefficients contributing to the total heat flux differ for gradients in translational temperature versus rotational temperature, quantified by the Eucken factor (Eucken 1913). In pursuit of its accurate value, Mason and Monchick (Mason & Monchick 1962) started from the WCU equations and employed the rigid sphere model to perform a series of mathematical simplifications, including the assumptions of perfectly elastic collisions. They subsequently applied a conceptual equivalence treatment to the transport coefficients deferred in the original WCU formulation. This allowed them to derive expressions for the thermal relaxation coefficient and the Eucken factor for molecules with rotational energy via a simplified C-E expansion. Conversely, Wu *et al.* numerically explored and attempted to calibrate the near-equilibrium relaxation processes of translational and rotational heat fluxes using DSMC-BL simulations on benchmark problems, providing a contrasting perspective to theoretical results of Mason (Li *et al.* 2021). This numerical calibration formed the basis for constructing a relaxation-type model equation. However, it is crucial to recognize that numerical calibration outcomes can exhibit significant variations depending on the specific physical problem and the resulting form of the distribution function.

Hence, the present work aims to derive analytical relaxation rates for molecular gases through theoretical formulation and, based on the obtained rates, to analyze thermal non-equilibrium relaxation processes and construct a kinetic model. The remainder of this paper is organized as follows. In § 2, an approximate distribution function constructed via Hermite and Laguerre polynomial expansions is employed to approximate the near-equilibrium state. This enables the theoretical derivation of relaxation rates based on Pullin's energy exchange model, along with an optimization of the energy partitioning parameter. Using the derived relaxation rates, the thermal non-equilibrium relaxation process is analyzed, and the relationship between relaxation rates and macroscopic transport coefficients is elucidated. In § 3, a Rykov-type kinetic model is developed using the previously derived relaxation rates, and the connection between relaxation rates and transport coefficients in the kinetic model is discussed. In § 4, the proposed kinetic model is validated through DSMC simulations in both zero-dimensional relaxation and typical rarefied gas flows (e.g., normal shock wave, planar Couette flow, lid-driven cavity flow, and hypersonic flow past cylinder) with comparisons made against the Rykov model. Finally, conclusions are presented in § 5.

2. Relaxation rate

The relaxation process about a non-equilibrium gas system towards its equilibrium state is determined by the momentum and energy exchange between collision pairs, which is characterized by the relaxation rates of non-equilibrium variables from macroscopic point of view. Analytical expressions for these relaxation rates can be obtained by calculating the moments of collision operator in EBE. In this work, the phenomenological Pullin equation (Pullin 1978) is adopted, which starts from a generalized polyatomic Boltzmann equation and utilizes the beta function to partition energy between collision pairs. Compared to the widely used and also phenomenological BL model for DSMC simulations, the Pullin's collision model satisfies the crucial detailed balance principle. Furthermore, when the Pullin's model is employed as the collision kernel for a master equation, the moments (relaxation rates) can be analytically obtained. Therefore, the Pullin equation can be used for both numerical prediction and theoretical analysis, and the later one is important for the strictness of the extension works in gas kinetic theory.

The following of this section is structured as follows: the original Pullin equation is outlined in Subsection 2.1, along with a proof of its detailed balance property. Subsection 2.2 is a derivation of relaxation rates, where combined Hermite and Laguerre expansions are used for approximating the non-equilibrium distribution, and extra standard integral terms are introduced. Subsection 2.3 presents an analysis of the derived macroscopic relaxation rates and establishes the links between the relaxation rates and the transport coefficients through the C-E expansion.

2.1. Pullin equation and detailed balance

To characterize a molecular system via the distribution function within the framework of gas kinetic theory, the conventional phase (spanned by time t , spatial coordinates \mathbf{x} , and molecular velocity \mathbf{c}) must be extended to account for internal motions of molecules. This extension introduces an additional independent variable, which may be selected as the internal energy ϵ , the discrete quantum states, or a generalized energy coordinate (in terms of momentum) $\mathbf{q} = \{\mathbf{q}_1, \mathbf{q}_2 \dots \mathbf{q}_v\}$, where v denotes the number of rotational degrees of freedom considered in this work. When the generalized energy coordinate \mathbf{q} is adopted, the resulting distribution function takes the form $F(t, \mathbf{x}, \mathbf{c}, \mathbf{q})$. In the absence of external forces and heat sources, the corresponding generalized Boltzmann equation (Chapman & Cowling 1990) is given by:

$$\frac{\partial F_1}{\partial t} + \mathbf{c}_1 \cdot \frac{\partial F_1}{\partial \mathbf{x}} = \iint \dots \int (F_1' F_2' - F_1 F_2) g \hat{\sigma} d\mathbf{e}' d\mathbf{c}_2 d\mathbf{q}_2, \quad (2.1)$$

where the left hand side of this equation represents the free-transport term, while the right hand side corresponds to the binary collision term. The subscripts “1” and “2” distinguish the two molecules in a collision pair, and the prime symbol denotes post-collision quantities. Within the collision integral, g is the relative speed of the colliding pair, $d\mathbf{e}' = \sin \chi d\chi d\theta$ is the solid angle element for the post-collision relative velocity \mathbf{g}' (where χ is the deflection angle and θ is the azimuth angle), and $\hat{\sigma} = \hat{\sigma}(g, \mathbf{q}_1, \mathbf{q}_2, \chi, \theta)$ is the differential cross-section, which serves as the kernel of the collision operator.

Based rigorously on the generalized Boltzmann equation, the phenomenological Pullin equation (Pullin 1978) is formulated as follows:

$$\frac{\partial f_1}{\partial t} + \mathbf{c}_1 \cdot \frac{\partial f_1}{\partial \mathbf{x}} = \iint \dots \int [f_1' f_2' \mathcal{J} - f_1 f_2] g \sigma R(\epsilon | \epsilon') d\mathbf{e}' d\epsilon' d\mathbf{c}_2 d\epsilon_2. \quad (2.2)$$

In the Pullin equation, the detailed description of the generalized coordinates \mathbf{q} is reduced to the internal energy ϵ , yielding a reduced distribution function $f(t, \mathbf{x}, \mathbf{c}, \epsilon)$. Correspondingly,

the differential cross-section $\hat{\sigma}(g, \mathbf{q}_1, \mathbf{q}_2, \chi, \theta)$ in the generalized Boltzmann equation is reduced to the product form $\sigma(g, \chi, \theta)R(\epsilon|\epsilon')$, where $R(\epsilon|\epsilon')$ denotes the transition probability from the pre-collision energy state $\epsilon = (\epsilon_1, \epsilon_2, \epsilon_t)$ to the post-collision state ϵ' . Here, ϵ_i represents the internal energy of a molecule and ϵ_t the translational energy of the collision pair. The term $\sigma(g, \chi, \theta)$ is identical to the traditional elastic collision model, such as the inverse-power potential or its equivalent VHS model in DSMC. That implies that velocity deflection (scattering) and internal energy transfer are independent, which is consistent with mainstream DSMC practice and also serves to simplify the analytical procedure. As a result of this decoupling, internal motion (particularly its directional aspect) is disregarded in the scattering process, rendering the azimuth angle θ in $\sigma(g, \chi, \theta)$ a dummy variable. The factor $\mathcal{J} = (\epsilon_1 \epsilon_2 / \epsilon'_1 \epsilon'_2)^{\zeta-1}$ originates from the degeneracy of generalized energy coordinates, as embodied by the relation $f(t, \mathbf{x}, \mathbf{c}, \epsilon) \propto \epsilon^{\zeta-1} F(t, \mathbf{x}, \mathbf{c}, \mathbf{q})$ (Pullin 1978). For notational brevity in subsequent expressions, $\zeta = \nu/2$ is defined. Since the differential cross-section $\sigma(g, \chi, \theta)$ is the well-established elastic scattering cross-section, the central task in constructing the Pullin model reduces to identifying a suitable energy transition probability $R(\epsilon|\epsilon')$ that satisfies the fundamental requirements of a differential cross-section: (1) energy conservation $\epsilon = \epsilon'$; (2) nonnegativity $R(\epsilon|\epsilon') > 0$; (3) normalization $\int R(\epsilon|\epsilon') d\epsilon' = 1$. These basic properties are proved in (Pullin 1978). In the present work, we provide a detailed examination of an important and more advanced property of the Pullin equation, the detailed balance property, as a supplement to the original derivation.

It is noteworthy that the physical process governed by $R(\epsilon|\epsilon')$ corresponds to a redistribution of internal energy between the two molecules during a collision. In the Pullin model, this redistribution is controlled by a set of random variables $\mathbf{s} = (s_1, s_2, s_3, s_4, s_5)$, where each $s_i \in (0, 1)$ follows a beta distribution of the form:

$$\beta \langle s_i | b_1, b_2 \rangle = \frac{1}{B(b_1, b_2)} s_i^{b_1-1} (1 - s_i)^{b_2-1}, \quad (2.3)$$

where $B(b_1, b_2)$ denotes the standard beta function, and the shape parameters b_1 and b_2 vary for each s_i . The energy transition during a forward collision proceeds in two steps. First, the active energy ϵ_a of the colliding pair is drawn from the pre-collision energies ϵ_1, ϵ_2 and ϵ_t according to the following expression:

$$\epsilon_a = s_1 \epsilon_1 + s_2 \epsilon_2 + s_3 \epsilon_t, \quad (2.4)$$

where s_1, s_2 and s_3 follow the beta distributions $\beta \langle s_1 | \phi\zeta, (1 - \phi)\zeta \rangle$, $\beta \langle s_2 | \phi\zeta, (1 - \phi)\zeta \rangle$ and $\beta \langle s_3 | \psi\eta, (1 - \psi)\eta \rangle$, respectively. Here, ϕ and ψ are the two key parameters in the Pullin model, which will be determined in Section 2.2 based on the rotational collision number Z_{rot} and the energy equal-partition principle. The parameter $\eta = 2 - 2/\alpha$ is an external parameter from the elastic collision model, with α denoting the index of the inverse-power potential. Then, the active energy is partitioned among the post-collision internal energy (ϵ'_1 and ϵ'_2) and the post-collision translational energy ϵ'_t as follows:

$$\begin{aligned} \epsilon'_1 &= (1 - s_1) \epsilon_1 + s_5 s_4 \epsilon_a, \\ \epsilon'_2 &= (1 - s_2) \epsilon_2 + s_5 (1 - s_4) \epsilon_a, \\ \epsilon'_t &= (1 - s_3) \epsilon_t + (1 - s_5) \epsilon_a, \end{aligned} \quad (2.5)$$

where s_4 and s_5 follow the beta distributions $\beta \langle s_4 | \phi\zeta, \phi\zeta \rangle$ and $\beta \langle s_5 | 2\phi\zeta, \psi\eta \rangle$, respectively.

On the other hand, for the inverse collision process, to ensure an exactly reversed transition

from ϵ' to ϵ , \mathbf{s}' must satisfy the following relations.

$$\begin{aligned}s'_1 &= \epsilon_1^{(r)} / (\epsilon_1^{(r)} + \epsilon_1^{(i)}), \\s'_2 &= \epsilon_2^{(r)} / (\epsilon_2^{(r)} + \epsilon_2^{(i)}), \\s'_3 &= \epsilon_t^{(r)} / (\epsilon_t^{(r)} + \epsilon_t^{(i)}), \\s'_4 &= \epsilon_1^{(a)} / (\epsilon_1^{(a)} + \epsilon_2^{(a)}), \\s'_5 &= (\epsilon_1^{(a)} + \epsilon_2^{(a)}) / \epsilon_a,\end{aligned}\quad (2.6)$$

where the superscripts (a), (i), (r) denote the active, inert and redistribution energy components, respectively. For clarity, the corresponding energies are defined as follows:

$$\begin{aligned}\epsilon_1^{(a)} &= s_1 \epsilon_1, & \epsilon_2^{(a)} &= s_2 \epsilon_2, & \epsilon_t^{(a)} &= s_3 \epsilon_t, \\ \epsilon_1^{(i)} &= (1 - s_1) \epsilon_1, & \epsilon_2^{(i)} &= (1 - s_2) \epsilon_2, & \epsilon_t^{(i)} &= (1 - s_3) \epsilon_t, \\ \epsilon_1^{(r)} &= s_4 s_5 \epsilon_a, & \epsilon_2^{(r)} &= (1 - s_4) s_5 \epsilon_a, & \epsilon_t^{(r)} &= (1 - s_5) \epsilon_a.\end{aligned}\quad (2.7)$$

Here, s'_1 , s'_2 and s'_3 serve to decompose a post-collision energy into the inert and redistribution parts in forward collision, while s'_4 and s'_5 function to partition the total active energy into $\epsilon_1^{(a)}$, $\epsilon_2^{(a)}$ and $\epsilon_t^{(a)}$. This configuration of \mathbf{s}' ensures an exactly reversible process and will subsequently guarantee the detailed balance property derived below. Then, the inverse collision parameters \mathbf{s}' can be reformulated in terms of the forward collision parameters as:

$$\begin{aligned}s'_1 &= s_4 s_5 \epsilon_a / \epsilon'_1, \\s'_2 &= (1 - s_4) s_5 \epsilon_a / \epsilon'_2, \\s'_3 &= (1 - s_5) \epsilon_a / \epsilon'_t, \\s'_4 &= s_1 \epsilon_1 / (s_1 \epsilon_1 + s_2 \epsilon_2), \\s'_5 &= (s_1 \epsilon_1 + s_2 \epsilon_2) / \epsilon_a.\end{aligned}\quad (2.8)$$

Note that the active energy remains invariant under this transformation, i.e., $\epsilon'_a = \epsilon_a$. Together with the deflection angle $\chi' = \chi$ and the relative speed $g' = \sqrt{4\epsilon'_t/m}$ (where m is the molecular mass), the impact parameters for inverse collision are fully determined. Therefore, the transition probability $R(\epsilon | \epsilon')$ in the Pullin equation can be constructed as:

$$R(\epsilon | \epsilon') d\epsilon' = \int h(\mathbf{s}) ds, \quad (2.9)$$

where $h(\mathbf{s})$ denotes the joint probability density of the forward variables, given by the product of beta distributions:

$$\begin{aligned}h(\mathbf{s}) = & \beta \langle s_1 | \phi \zeta, (1 - \phi) \zeta \rangle \beta \langle s_2 | \phi \zeta, (1 - \phi) \zeta \rangle \beta \langle s_3 | \psi \eta, (1 - \psi) \eta \rangle \\& \cdot \beta \langle s_4 | \phi \zeta, \phi \zeta \rangle \beta \langle s_5 | 2\phi \zeta, \psi \eta \rangle.\end{aligned}\quad (2.10)$$

Finally, the specific form of Pullin equation can be expressed as:

$$\frac{\partial f_1}{\partial t} + \mathbf{c}_1 \cdot \frac{\partial f_1}{\partial \mathbf{x}} = \int \dots \int [f_1' f_2' \mathcal{J} - f_1 f_2] g \sigma d\mathbf{e}' h(\mathbf{s}) ds d\mathbf{c}_2 d\epsilon_2, \quad (2.11)$$

which is now ready for verification of the detailed balance property.

It is noteworthy that the physical interpretation of the detailed balance property is that the probability of an inverse collision is identical to its corresponding forward collision. For

Equation (2.11), the following equality must be established:

$$\sigma g \epsilon_1^{\zeta-1} \epsilon_2^{\zeta-1} h(\mathbf{s}) d\mathbf{e}' ds d\mathbf{c}_1 d\mathbf{c}_2 d\epsilon_1 d\epsilon_2 = \sigma' g' \epsilon_1'^{\zeta-1} \epsilon_2'^{\zeta-1} h(\mathbf{s}') d\mathbf{e}' ds' d\mathbf{c}'_1 d\mathbf{c}'_2 d\epsilon'_1 d\epsilon'_2. \quad (2.12)$$

In the current form, however, the functional dependence between the integration variables and the integrand is not explicitly revealed. To facilitate the proof, it is therefore necessary to reformulate the proposition. Noting that the molecular velocities \mathbf{c}_1 and \mathbf{c}_2 can be expressed in the terms of relative velocity \mathbf{g} and the center-of-mass velocity \mathbf{G} (there is $d\mathbf{c}_1 d\mathbf{c}_2 = dg d\mathbf{G}$), and the same holds for the inverse collision. This transformation is essential because the integrand explicitly depends on $g = |\mathbf{g}|$. Furthermore, momentum conservation in a binary collision implies $\mathbf{G} = \mathbf{G}'$. Since $d\mathbf{G}$ and $d\mathbf{G}'$ are irrelevant to the integrand, they can be omitted in subsequent steps. On the other hand, the differential dg can be written as $g^2 \sin(\theta_g) dg d\theta_g d\phi_g$. Neither θ_g nor ϕ_g appears in the integrand, and $\sin(\theta_g)$ is eliminated by integrating θ_g over $(0, \pi)$. Moreover, since $\chi' = \chi$, and $d\mathbf{e}' = \sin \chi d\chi d\theta$, the solid angle $d\mathbf{e}'$ also cancels out. Consequently, the detailed balance condition to be verified reduces to the simplified form:

$$\sigma g^3 \epsilon_1^{\zeta-1} \epsilon_2^{\zeta-1} h(\mathbf{s}) ds dg d\epsilon_1 d\epsilon_2 = \sigma' g'^3 \epsilon_1'^{\zeta-1} \epsilon_2'^{\zeta-1} h(\mathbf{s}') ds' dg' d\epsilon'_1 d\epsilon'_2. \quad (2.13)$$

Using the relations $\sigma' g'^{4/\alpha} = \sigma g^{4/\alpha}$ and $(g/2m)dg = d\epsilon_t$, the expression can be further simplified to:

$$\epsilon_t^{\eta-1} \epsilon_1^{\zeta-1} \epsilon_2^{\zeta-1} h(\mathbf{s}) ds d\epsilon_t d\epsilon_1 d\epsilon_2 = \epsilon_t'^{\eta-1} \epsilon_1'^{\zeta-1} \epsilon_2'^{\zeta-1} h(\mathbf{s}') ds' d\epsilon'_t d\epsilon'_1 d\epsilon'_2. \quad (2.14)$$

Multiplying both sides of this equation by $\exp(-\epsilon_t - \epsilon_1 - \epsilon_2)$ and introducing the gamma distribution defined as:

$$\gamma \langle x | a \rangle = [1/\Gamma(a)] x^{a-1} e^{-x}, \quad (2.15)$$

where $\Gamma(a)$ is the gamma function. Then Equation (2.12) finally becomes:

$$\gamma \langle \epsilon_1' | \zeta \rangle \gamma \langle \epsilon_2' | \zeta \rangle \gamma \langle \epsilon_t' | \eta \rangle h(\mathbf{s}') d\epsilon' ds' = \gamma \langle \epsilon_1 | \zeta \rangle \gamma \langle \epsilon_2 | \zeta \rangle \gamma \langle \epsilon_t | \eta \rangle h(\mathbf{s}) d\epsilon ds. \quad (2.16)$$

At this point, the propositional expression is sufficiently clear and concise. Then, the proof proceeds from the following expression, denoted by R :

$$R = \gamma \langle \epsilon_1 | \zeta \rangle \gamma \langle \epsilon_2 | \zeta \rangle \gamma \langle \epsilon_t | \eta \rangle \frac{h(\mathbf{s}) ds_1 ds_2 ds_3 ds_4 ds_5 d\epsilon_1 d\epsilon_2}{h(\mathbf{s}') ds'_1 ds'_2 ds'_3 ds'_4 ds'_5 d\epsilon'_t d\epsilon'_1 d\epsilon'_2}. \quad (2.17)$$

The relation between beta and gamma distributions enables the decomposition of one gamma distribution into a product of two gamma distributions as follows:

$$\begin{aligned} \gamma \langle x | a_1 + a_2 \rangle \beta(z | a_1, a_2) dx dz &= \gamma \langle x_1 | a_1 \rangle \gamma \langle x_2 | a_2 \rangle dx_1 dx_2, \\ x_1 = a_1 x, \quad x_2 = a_2 x. \end{aligned} \quad (2.18)$$

Therefore, the gamma distributions in Equation (2.17) are decomposed successively by the beta distributions in $h(\mathbf{s})$, which corresponds to the physical energy redistribution process and ensures mathematical consistency.

First, the terms associated with the forward collision process are calculated, in which s_1 ,

s_2 and s_3 extract the active energy components from ϵ_1 , ϵ_2 and ϵ_t . At this step, R becomes:

$$R = \left\{ \gamma \left\langle \epsilon_1^{(a)} \middle| \phi \zeta \right\rangle \gamma \left\langle \epsilon_2^{(a)} \middle| \phi \zeta \right\rangle \gamma \left\langle \epsilon_t^{(a)} \middle| \psi \eta \right\rangle \frac{d\epsilon_t^{(a)} d\epsilon_1^{(a)} d\epsilon_2^{(a)}}{ds'_4 ds'_5} \right\} \\ \cdot \gamma \left\langle \epsilon_1^{(i)} \middle| (1 - \phi) \zeta \right\rangle \gamma \left\langle \epsilon_2^{(i)} \middle| (1 - \phi) \zeta \right\rangle \gamma \left\langle \epsilon_t^{(i)} \middle| (1 - \psi) \eta \right\rangle \\ \cdot \frac{\beta \langle s_4 | \phi \zeta, \phi \zeta \rangle \beta \langle s_5 | 2\phi \zeta, \psi \eta \rangle ds_4 ds_5 d\epsilon_t^{(i)} d\epsilon_1^{(i)} d\epsilon_2^{(i)}}{h(s') ds'_1 ds'_2 ds'_3 d\epsilon'_1 d\epsilon'_2 d\epsilon'_2}. \quad (2.19)$$

Next, the terms enclosed in the curly brackets are considered. Given the presence of ds'_4 and ds'_5 in the expressions, the inverse collision process must be introduced. Based on Equation (2.6), the reverse process governed by s'_4 and s'_5 can be expressed as follows:

$$\gamma \langle \epsilon_a | 2\phi \zeta + \psi \eta \rangle \beta \langle s'_4 | \phi \zeta, \phi \zeta \rangle \beta \langle s'_5 | 2\phi \zeta, \psi \eta \rangle d\epsilon_a ds'_4 ds'_5 \\ = \gamma \left\langle \epsilon_1^{(a)} \middle| \phi \zeta \right\rangle \gamma \left\langle \epsilon_2^{(a)} \middle| \phi \zeta \right\rangle \gamma \left\langle \epsilon_t^{(a)} \middle| \psi \eta \right\rangle d\epsilon_1^{(a)} d\epsilon_2^{(a)} d\epsilon_t^{(a)}. \quad (2.20)$$

Here, following Equation (2.20), the active energy components $\epsilon_1^{(a)}$, $\epsilon_2^{(a)}$ and $\epsilon_t^{(a)}$ are recombined into the total active energy ϵ_a . Therefore, by inserting Equation (2.20) into Equation (2.19), R further becomes:

$$R = \{ \gamma \langle \epsilon_a | 2\phi \zeta + (1 - \psi) \eta \rangle \beta \langle s_4 | \phi \zeta, \phi \zeta \rangle \beta \langle s_5 | 2\phi \zeta, \psi \eta \rangle ds_4 ds_5 \} \\ \cdot \gamma \left\langle \epsilon_1^{(i)} \middle| (1 - \phi) \zeta \right\rangle \gamma \left\langle \epsilon_2^{(i)} \middle| (1 - \phi) \zeta \right\rangle \gamma \left\langle \epsilon_t^{(i)} \middle| (1 - \psi) \eta \right\rangle \\ \cdot \frac{d\epsilon_a d\epsilon_t^{(i)} d\epsilon_1^{(i)} d\epsilon_2^{(i)}}{\beta \langle s_1' | \phi \zeta, (1 - \phi) \zeta \rangle \beta \langle s_2' | \phi \zeta, (1 - \phi) \zeta \rangle \beta \langle s_3' | \psi \eta, (1 - \psi) \eta \rangle ds'_1 ds'_2 ds'_3 d\epsilon'_1 d\epsilon'_2}. \quad (2.21)$$

Following the procedure, the forward process governed by s_4 and s_5 within the curly brackets of Equation (2.21) is evaluated. After rearrangement, R reduces to the following form:

$$R = \frac{\gamma \left\langle \epsilon_1^{(i)} \middle| (1 - \phi) \zeta \right\rangle \gamma \left\langle \epsilon_2^{(i)} \middle| (1 - \phi) \zeta \right\rangle \gamma \left\langle \epsilon_t^{(i)} \middle| (1 - \psi) \eta \right\rangle \gamma \left\langle \epsilon_1^{(r)} \middle| \phi \zeta \right\rangle \gamma \left\langle \epsilon_2^{(r)} \middle| \phi \zeta \right\rangle \gamma \left\langle \epsilon_t^{(r)} \middle| \psi \eta \right\rangle}{\beta \langle s'_1 | \phi \zeta, (1 - \phi) \zeta \rangle \beta \langle s'_2 | \phi \zeta, (1 - \phi) \zeta \rangle \beta \langle s'_3 | \psi \eta, (1 - \psi) \eta \rangle} \\ \cdot \frac{d\epsilon_t^{(r)} d\epsilon_1^{(r)} d\epsilon_2^{(r)} d\epsilon_t^{(i)} d\epsilon_1^{(i)} d\epsilon_2^{(i)}}{ds'_1 ds'_2 ds'_3 d\epsilon'_1 d\epsilon'_2}. \quad (2.22)$$

Equation (2.22) describes the reverse process governed by s'_1 , s'_2 and s'_t , expressed as:

$$\gamma \left\langle \epsilon_1^{(i)} \middle| (1 - \phi) \zeta \right\rangle \gamma \left\langle \epsilon_1^{(r)} \middle| \phi \zeta \right\rangle d\epsilon_1^{(i)} d\epsilon_1^{(r)} = \gamma \langle \epsilon'_1 | \zeta \rangle \beta \langle s'_1 | \phi \zeta, (1 - \phi) \zeta \rangle d\epsilon'_1 ds'_1, \\ \gamma \left\langle \epsilon_2^{(i)} \middle| (1 - \phi) \zeta \right\rangle \gamma \left\langle \epsilon_2^{(r)} \middle| \phi \zeta \right\rangle d\epsilon_2^{(i)} d\epsilon_2^{(r)} = \gamma \langle \epsilon'_2 | \zeta \rangle \beta \langle s'_2 | \phi \zeta, (1 - \phi) \zeta \rangle d\epsilon'_2 ds'_2, \quad (2.23) \\ \gamma \left\langle \epsilon_t^{(i)} \middle| (1 - \psi) \eta \right\rangle \gamma \left\langle \epsilon_t^{(r)} \middle| \psi \eta \right\rangle d\epsilon_t^{(i)} d\epsilon_t^{(r)} = \gamma \langle \epsilon'_t | \eta \rangle \beta \langle s'_3 | \psi \eta, (1 - \psi) \eta \rangle d\epsilon'_t ds'_3,$$

where the inert and redistribution energies recombine to form the post-collision energy. Substituting Equation (2.23) into Equation (2.22), the final form of R simplifies to:

$$R = \gamma \langle \epsilon'_1 | \zeta \rangle \gamma \langle \epsilon'_2 | \zeta \rangle \gamma \langle \epsilon'_t | \eta \rangle. \quad (2.24)$$

With this, the proposition is proved. To briefly summarize, the detailed balance property of Pullin model replies on two key elements: (1) the use of the beta function to probabilistically

redistribute energies and its mathematical property for decomposing gamma distributions, and (2) the consistent definition of the inverse collision parameters s' .

Similar to the BL model, the Pullin model was originally developed for DSMC simulations of polyatomic gases. Although it has not seen widespread adoption, primarily due to its moderately high computational cost, the Pullin model offers distinct advantages in terms of analytical tractability and strict adherence to detailed balance principle, making it particularly suitable for theoretical investigations.

2.2. Analytical relaxation rate

Time relaxation rates of non-equilibrium variables are essential in constructing thermal non-equilibrium governing equations. These variables include pressure tensor \mathbf{p} , translational and rotational temperatures (T_t, T_r), translational and rotational heat fluxes ($\mathbf{q}_t, \mathbf{q}_r$), corresponding to both flow non-equilibrium and thermal non-equilibrium. For example, they serve as source terms in the thermal Navier-Stokes equations for continuum flows and the moment equations for low-speed rarefied flows, and provide essential modeling constraints for BGK-type and Fokker-Planck-type models for Boltzmann equation, which are widely used in constructing numerical schemes for multi-scale flows. Also, these relaxation rates share all the elementary integrals with the C-E expansion that connects the microscopic gas-kinetic theory with the macroscopic aerodynamics, and are also necessary for characterizing entropy evolution in non-equilibrium thermodynamics (Desvillettes & Villani 2005).

To determine these relaxation rates, the phase-space integrals (moments) of a generalized Boltzmann equation should be calculated. However, the collision term cannot be analytically integrated when adopting the widely used BL model as the collision kernel. This is because of the forced energy conservation in sampling post-collision energies, which must be enforced in the BL for correct physical modeling. But, this treatment leads to multi-dimensional bounded integrations over the Maxwell-Boltzmann distribution for sampling post-collision energies, which consequently leads to nested error functions that cannot be analytically integrated. Therefore, the Pullin equation is adopted in the analytical derivations in this work, which is both analytically integrable and satisfies the detailed balance condition.

2.2.1. Approximate distribution function

Prior to calculating the moments of collision term, a definitive analytical approximation for the non-equilibrium distribution function must be constructed first. Accordingly, the following quasi-equilibrium distribution function is introduced, which serves as the basis for the approximate distribution function in subsequent procedures:

$$f^{(0)} = n \left(\frac{m}{2\pi k T_t} \right)^{\frac{3}{2}} e^{-\frac{mc^2}{2kT_t}} \cdot \frac{\epsilon^{\frac{\nu}{2}-1}}{\Gamma\left(\frac{\nu}{2}\right) (kT_r)^{\frac{\nu}{2}}} e^{-\frac{\epsilon}{kT_r}}. \quad (2.25)$$

This quasi-equilibrium distribution is a joint Maxwell-Boltzmann distribution, employing a Maxwell distribution for translational velocity and a Boltzmann distribution for internal energy. It is noteworthy that translational temperature T_t is used in Maxwell distribution and rotational temperature T_r is used in Boltzmann distribution. This configuration is used in (WANG-CHANG & Uhlenbeck 1951) to handle strong thermal non-equilibrium where T_t and T_r exhibit a large departure. In contrast, the approach, choosing the averaged temperature T in equilibrium state Eq. (2.25) and expressing the difference of T_t and T_r by a second-order perturbation, can only handle small departures in different temperatures (weak thermal non-equilibrium).

Owing to the distinct functional forms of the equilibrium distributions for particle velocity and internal energy, the approximate distribution function is expanded in a coupled orthogonal

basis comprising Hermite and Laguerre polynomials. The equilibrium distribution function for translational velocity corresponds to the weight function of the Hermite polynomial, $\omega_H(\xi) = e^{-\xi^2/2}/(2\pi)^{\frac{3}{2}}$, where $\xi = C/\sqrt{m/2kT_t}$ is the dimensionless thermal velocity. Correspondingly, the equilibrium distribution for internal energy corresponds to the weight function of the Laguerre polynomial, $\omega_L(\varepsilon) = \varepsilon^N e^{-\varepsilon}$, where $\varepsilon = \epsilon/(kT_r)$ is the dimensionless internal energy. Based on the weight functions, the Hermite and Laguerre polynomials can be generated as:

$$H_{i_1 i_2 \dots i_N}(\xi) = \frac{(-1)^N}{\omega_H(\xi)} \frac{\partial^N \omega_H(\xi)}{\partial \xi_{i_1} \partial \xi_{i_2} \dots \partial \xi_{i_N}}, \quad (2.26)$$

$$L_N(\varepsilon) = \frac{\varepsilon^N}{\omega_L(\varepsilon) N!} \frac{d^N \omega_L(\varepsilon)}{d \varepsilon^N}. \quad (2.27)$$

The approximate distribution function is expanded in a series of Hermite polynomials Eq. (2.26) and Laguerre polynomials Eq. (2.27) as follows:

$$f = f^{(0)} \left(a + a_i H_i + \frac{1}{2} a_{ij} H_{ij} + \dots + \frac{1}{N!} a_{i_1 i_2 \dots i_N} H_{i_1 i_2 \dots i_N} + \dots \right) \cdot (b_0 + b_1 L_1 + \dots + b_N L_N + \dots), \quad (2.28)$$

where $a_{i_1 i_2 \dots i_N}(\mathbf{x}, t)$ and $b_N(\mathbf{x}, t)$ denote tensor coefficients dependent on spatial coordinate \mathbf{x} and time t . To accurately characterize non-equilibrium states, the constructed approximate distribution function should ensure the accuracy of key macroscopic quantities, including mass density $\rho(\mathbf{x}, t)$, bulk velocity $\mathbf{v}(\mathbf{x}, t)$, pressure deviator $p_{\langle ij \rangle}(\mathbf{x}, t)$, translational temperature $T_t(\mathbf{x}, t)$, rotational temperature $T_r(\mathbf{x}, t)$, translational heat flux $\mathbf{q}_t(\mathbf{x}, t)$ and rotational heat flux $\mathbf{q}_r(\mathbf{x}, t)$. For simplicity, the (\mathbf{x}, t) notation of subsequent macroscopic variables is omitted. These macroscopic quantities can be calculated from the moment of the distribution function:

$$\begin{aligned} \rho &= \int m f d\mathbf{c} d\epsilon, \quad 0 = \int m C_i f d\mathbf{c} d\epsilon, \\ T_t &= \frac{1}{3nk} \int m C^2 f d\mathbf{c} d\epsilon, \quad T_r = \frac{2}{vnk} \int \epsilon f d\mathbf{c} d\epsilon, \\ p_{\langle ij \rangle} &= \int m C_{\langle i} C_{j \rangle} f d\mathbf{c} d\epsilon, \quad q_{t,i} = \int \frac{1}{2} m C^2 C_i f d\mathbf{c} d\epsilon, \\ q_{r,i} &= \int \epsilon C_i f d\mathbf{c} d\epsilon. \end{aligned} \quad (2.29)$$

In Equation (2.28), the order of the Hermite polynomials corresponds to the power of particle velocity, and the order of the Laguerre polynomials to internal energy. To recover these key macroscopic quantities in Eq. (2.29), the approximate distribution function is constructed using Hermite polynomials up to third order and Laguerre polynomials up to first order. The explicit expressions of the Hermite and Laguerre polynomials used are given as follows:

$$\begin{cases} H = 1, \\ H_i = \xi_i, \\ H_{ij} = \xi_i \xi_j - \delta_{ij}, \\ H_{ijj} = \xi_i \xi_j \xi_j - 5\xi_i, \end{cases} \quad \begin{cases} L_0 = 1, \\ L_1 = -\varepsilon + 1. \end{cases} \quad (2.30)$$

Thus, with the accurate recovery of key macroscopic quantities, the expansion of the

approximate distribution function is truncated as follows:

$$f = f^{(0)} \left(\left(a + a_i H_i + \frac{1}{2} a_{ij} H_{ij} + \frac{1}{10} a_{ijj} H_{ijj} \right) \cdot b_0 + (a + a_i H_i) \cdot b_1 L_1 \right). \quad (2.31)$$

The coefficients $a_{i_1 i_2 \dots i_N}$ and b_N can be solved by substituting and integrating the approximate distribution function Eq. (2.31) into the macroscopic moment Eq. (2.29). The specific expression for the approximate distribution function can be written as:

$$f = f^{(0)} \left(1 + \frac{p \langle ij \rangle}{2n k T_t} \xi_i \xi_j + \frac{q_{t,i}}{5mn} \left(\frac{m}{k T_t} \right)^{\frac{3}{2}} \left(\xi_i \xi^2 - 5 \xi_i \right) + \frac{2}{\nu} q_{r,i} \sqrt{\frac{m}{k T_t}} \frac{1}{n k T_r} \left(\varepsilon - \frac{\nu}{2} \right) \xi_i \right). \quad (2.32)$$

At this stage, the explicit expression of the approximate distribution function is derived. This expression is also commonly used within the moment methods where the non-equilibrium macroscopic quantities are typically expressed by constitutive relations derived via the C-E expansion.

2.2.2. Integration and simplification of the relaxation rates

The relaxation rates can be derived by taking moments of the collision term in the Pullin equation. Therefore, the moment balance equations of the Pullin equation must be provided. Multiplying both sides of Pullin equation Eq. (2.11) by an arbitrary function $\varphi = \varphi(\mathbf{x}, \mathbf{c}, \epsilon, t)$ and integrating over phase space $d\mathbf{c}_1 d\epsilon_1$ yields the moment balance equation:

$$\int \varphi \frac{\partial f_1}{\partial t} d\mathbf{c}_1 d\epsilon_1 + \int \varphi \frac{\partial f_1}{\partial \mathbf{x}} \cdot \mathbf{c}_1 d\mathbf{c}_1 d\epsilon_1 = \int \dots \int \varphi [f'_1 f'_2 \mathcal{J} - f_1 f_2] g \sigma d\mathbf{e}' h(\mathbf{s}) d\mathbf{s} d\mathbf{c}_1 d\mathbf{c}_2 d\epsilon_1 d\epsilon_2. \quad (2.33)$$

where $\mathcal{J} = (\epsilon_1 \epsilon_2 / \epsilon'_1 \epsilon'_2)^{\zeta-1}$. In frameworks that calculate moments of the collision term, such as the C-E expansion, it is typically necessary to simplify the collision term using the detailed balance relation. According to Pullin's detailed balance relation Eq. (2.12), the differential operators satisfy the following transformation relation:

$$g \sigma d\mathbf{e}' h(\mathbf{s}) d\mathbf{s} d\mathbf{c}_1 d\mathbf{c}_2 d\epsilon_1 d\epsilon_2 = \left(\frac{\epsilon'_1 \epsilon'_2}{\epsilon_1 \epsilon_2} \right)^{\zeta-1} \cdot g' \sigma' d\mathbf{e} h(\mathbf{s}') d\mathbf{s}' d\mathbf{c}'_1 d\mathbf{c}'_2 d\epsilon'_1 d\epsilon'_2, \quad (2.34)$$

Additionally, Liouville's theorem states the conservation of phase-space volume for an ensemble of systems with same Hamiltonian function. Specifically, if at time t these occupy an infinitesimal volume of the phase space, at any other time they occupy an equal volume (Chapman & Cowling 1990). The Hamiltonian of the Pullin model is well-established (Pullin 1978). Therefore, according to Liouville's theorem, the phase spaces of the pre-collision and post-collision states satisfy $d\mathbf{c}_1 d\epsilon_1 d\mathbf{c}_2 d\epsilon_2 = d\mathbf{c}'_1 d\epsilon'_1 d\mathbf{c}'_2 d\epsilon'_2$. Based on Liouville's theorem and the reversibility of collisions, the transformation $(\mathbf{c}_1, \mathbf{c}_2, \epsilon_1, \epsilon_2) \leftrightarrow (\mathbf{c}'_1, \mathbf{c}'_2, \epsilon'_1, \epsilon'_2)$ is applied to the first term $f'_1 f'_2$ of the collision term within Eq. (2.33). Subsequently, to unify the integration domain, the first term of the collision integral is further simplified via detailed

balance relation Eq. (2.34), specifically:

$$\begin{aligned}
& \int \dots \int \varphi [f'_1 f'_2 \mathcal{J} - f_1 f_2] g \sigma d\mathbf{e}' h(\mathbf{s}) d\mathbf{s} d\mathbf{c}_1 d\mathbf{c}_2 d\epsilon_1 d\epsilon_2 \\
&= \int \dots \int \varphi \left[f'_1 f'_2 \left(\frac{\epsilon_1 \epsilon_2}{\epsilon'_1 \epsilon'_2} \right)^{\zeta-1} - f_1 f_2 \right] g \sigma d\mathbf{e}' h(\mathbf{s}) d\mathbf{s} d\mathbf{c}_1 d\mathbf{c}_2 d\epsilon_1 d\epsilon_2 \\
&= \int \dots \int \varphi' f_1 f_2 \left(\frac{\epsilon'_1 \epsilon'_2}{\epsilon_1 \epsilon_2} \right)^{\zeta-1} g' \sigma' d\mathbf{e}' h(\mathbf{s}') d\mathbf{s}' d\mathbf{c}'_1 d\mathbf{c}'_2 d\epsilon'_1 d\epsilon'_2 - \\
& \quad \int \dots \int \varphi f_1 f_2 g \sigma d\mathbf{e}' h(\mathbf{s}) d\mathbf{s} d\mathbf{c}_1 d\mathbf{c}_2 d\epsilon_1 d\epsilon_2 \\
&= \int \dots \int \varphi' f_1 f_2 g \sigma d\mathbf{e}' h(\mathbf{s}) d\mathbf{s} d\mathbf{c}_1 d\mathbf{c}_2 d\epsilon_1 d\epsilon_2 - \\
& \quad \int \dots \int \varphi f_1 f_2 g \sigma d\mathbf{e}' h(\mathbf{s}) d\mathbf{s} d\mathbf{c}_1 d\mathbf{c}_2 d\epsilon_1 d\epsilon_2 \\
&= \int \dots \int (\varphi' - \varphi) f_1 f_2 g \sigma d\mathbf{e}' h(\mathbf{s}) d\mathbf{s} d\mathbf{c}_1 d\mathbf{c}_2 d\epsilon_1 d\epsilon_2,
\end{aligned} \tag{2.35}$$

where the analytical expression of $f_1 f_2$ is essential for taking moments of the collision term. The expression of $f_1 f_2$ in the collision term can be obtained by using the approximate distribution function Eq. (2.32):

$$\begin{aligned}
f_1 f_2 &= f_1^{(0)} f_2^{(0)} (1 + P_1) (1 + P_2) \\
&= f_1^{(0)} f_2^{(0)} (1 + P_1 + P_2 + P_1 P_2),
\end{aligned} \tag{2.36}$$

where P_1 and P_2 are the expansion polynomials of the approximate distribution function. The cross term $P_1 P_2$, due to its higher-order nonlinearity, introduces significant complexity to the integration process. However, as the contribution of cross term $P_1 P_2$ to key macroscopic quantities in typical flows is weak, the present study focuses on the linearized formulation. Therefore, neglecting the nonlinear terms in the pressure deviator $p_{\langle ij \rangle}$ and heat fluxes $q_{t,i}$, $q_{r,i}$, the distribution function product $f_1 f_2$ can be written as:

$$f_1 f_2 = f_1^{(0)} f_2^{(0)} \left(1 + \frac{P_{\langle ij \rangle}}{2n k T_t} \xi_{1,i} \xi_{1,j} + \frac{P_{\langle ij \rangle}}{2n k T_t} \xi_{2,i} \xi_{2,j} + \right. \\
\left. \frac{q_{t,i}}{5mn} \left(\frac{m}{k T_t} \right)^{\frac{3}{2}} \left(\xi_{1,i} \xi_1^2 - 5 \xi_{1,i} \right) + \frac{q_{t,i}}{5mn} \left(\frac{m}{k T_t} \right)^{\frac{3}{2}} \left(\xi_{2,i} \xi_2^2 - 5 \xi_{2,i} \right) + \right. \\
\left. \frac{2}{\nu} q_{r,i} \sqrt{\frac{m}{k T_t}} \frac{1}{n k T_r} \left(\varepsilon_1 - \frac{\nu}{2} \right) \xi_{1,i} + \frac{2}{\nu} q_{r,i} \sqrt{\frac{m}{k T_t}} \frac{1}{n k T_r} \left(\varepsilon_2 - \frac{\nu}{2} \right) \xi_{2,i} \right). \tag{2.37}$$

With the collision term simplified and the distribution function expressed approximately, the derivation of the relaxation rates can now be formally undertaken. When φ takes $mC_1^2/3nk$, $2\varepsilon_1/vnk$, $mC_{1,i}C_{1,j}$, $mC_1^2C_{1,i}/2$, $\varepsilon_1C_{1,i}$, the corresponding non-equilibrium quantities: the translational temperature relaxation rate \mathcal{T}_t , rotational temperature relaxation rate \mathcal{T}_r , pressure deviator relaxation rate \mathcal{P}_{ij} , translational heat flux relaxation rate Q_t , and rotational heat flux relaxation rate Q_r can be obtained from the simplified collision term Eq. (2.35). For a concise expression during the derivation, a set of non-dimensional quantities

is defined:

$$\begin{cases} \xi_i = \frac{C_i}{\sqrt{kT_t}}, \\ \varepsilon = \frac{\epsilon}{kT_r}, \\ G_i^* = \frac{G_i}{\sqrt{kT_t}}, \\ g_i^* = \frac{\sqrt{\frac{kT_t}{m}}}{\sqrt{\frac{kT_t}{m}}}, \end{cases} \quad \begin{cases} p_{\langle ij \rangle}^* = \frac{p_{\langle ij \rangle}}{nkT_t}, \\ q_{t,i}^* = \frac{q_{t,i}}{nm\left(\frac{kT_t}{m}\right)^{3/2}}, \\ q_{r,i}^* = \frac{q_{r,i}}{n\sqrt{\frac{kT_t}{m}} kT_r}. \end{cases} \quad (2.38)$$

It is noteworthy that during the non-dimensionalization process, the translational and rotational physical quantities are scaled using the translational and rotational temperatures, respectively.

In this work, to express the relaxation rate integrals compactly, an integral operator $\mathcal{I}_1 [A, B]$ is defined as follows:

$$\mathcal{I}_1 [A, B] = \left(\frac{kT_t}{m}\right)^{\frac{7}{2}} (kT_r)^2 \int (A' - A) f_1^{(0)} f_2^{(0)} (B) g^* \sigma d\mathbf{e}' h(\mathbf{s}) d\mathbf{s} d\xi_1 d\xi_2 d\varepsilon_2 d\varepsilon_1. \quad (2.39)$$

In the calculation of the relaxation rates, the integrals can be simplified according to the parity of the dimensionless thermal velocity ξ_1, ξ_2 to reduce the complexity of the derivation. Based on Eq. (2.39), the relaxation rates can be explicitly expressed as a combination of integral operators:

$$\mathcal{T}_t = \frac{\partial T_t}{\partial t} = \frac{kT_t}{3nk} \mathcal{I}_1 [\xi_1^2, 1], \quad (2.40)$$

$$\mathcal{T}_r = \frac{\partial T_r}{\partial t} = \frac{2kT_r}{vnk} \mathcal{I}_1 [\varepsilon_1, 1], \quad (2.41)$$

$$\mathcal{P}_{ij} = \frac{p_{\langle ij \rangle}}{\partial t} = \frac{kT_t}{2} \mathcal{I}_1 [\xi_{\langle 1,i} \xi_{1,j \rangle}, \xi_{\langle 1,k} \xi_{1,l \rangle} + \xi_{\langle 2,k} \xi_{2,l \rangle}] p_{\langle kl \rangle}^*, \quad (2.42)$$

$$Q_t = \frac{\partial q_{t,i}}{\partial t} = \left(\frac{kT_t}{m}\right)^{\frac{3}{2}} \frac{1}{2} m \left(\mathcal{I}_1 [\xi_1^2 \xi_{1,i}, \xi_1^2 \xi_{1,k} + \xi_1^2 \xi_{2,k}] \frac{q_{t,k}^*}{5} + \mathcal{I}_1 [\xi_1^2 \xi_{1,i}, \varepsilon_1 \xi_{1,k} + \varepsilon_2 \xi_{2,k}] \frac{2q_{r,k}^*}{\nu} \right. \\ \left. - \mathcal{I}_1 [\xi_1^2 \xi_{1,i}, \xi_{1,k} + \xi_{2,k}] (q_{t,k}^* + q_{r,k}^*) \right), \quad (2.43)$$

$$Q_r = \frac{\partial q_{r,i}}{\partial t} = \left(\frac{kT_t}{m}\right)^{\frac{1}{2}} kT_r \left(\mathcal{I}_1 [\xi_{1,i} \varepsilon_1, \xi_1^2 \xi_{1,k} + \xi_1^2 \xi_{2,k}] \frac{q_{t,k}^*}{5} + \mathcal{I}_1 [\xi_{1,i} \varepsilon_1, \varepsilon_1 \xi_{1,k} + \varepsilon_2 \xi_{2,k}] \frac{2q_{r,k}^*}{\nu} \right. \\ \left. - \mathcal{I}_1 [\xi_{1,i} \varepsilon_1, \xi_{1,k} + \xi_{2,k}] (q_{t,k}^* + q_{r,k}^*) \right). \quad (2.44)$$

In subsequent derivations, only a set of integrals in the $\mathcal{I}_1 [A, B]$ form need to be calculated. Since the integrals explicitly depend on $g = |\mathbf{g}|$, a variable transformation is required, replacing the thermal velocities $\mathbf{C}_1, \mathbf{C}_2$ of the colliding particle pair with their relative velocity \mathbf{g} and center-of-mass velocity \mathbf{G} . The pre-collision thermal velocities \mathbf{C}_1 and \mathbf{C}_2 and

post-collision thermal velocities \mathbf{C}'_1 and \mathbf{C}'_2 are expressed as:

$$\mathbf{C}_1 = \mathbf{G} - \frac{1}{2}\mathbf{g}, \quad \mathbf{C}_2 = \mathbf{G} + \frac{1}{2}\mathbf{g}, \quad \mathbf{C}'_1 = \mathbf{G}' - \frac{1}{2}\mathbf{g}', \quad \mathbf{C}'_2 = \mathbf{G}' + \frac{1}{2}\mathbf{g}'. \quad (2.45)$$

The corresponding transformation of integration variables gives $d\mathbf{C}_1 d\mathbf{C}_2 = d\mathbf{G} dg$. Noting momentum conservation implies $\mathbf{G} = \mathbf{G}'$, while energy exchange between translational and rotational modes leads to $|\mathbf{g}| \neq |\mathbf{g}'|$. Based on the assumption of decoupled velocity scattering and energy scattering in Pullin model, the integration over the relative velocity is separated into directional and magnitude components. The treatment of velocity scattering is first carried out. The differential cross-section can be expressed as $\sigma d\mathbf{e}' = bdbd\theta$, where b is the miss distance and θ is the azimuthal angle. The relative velocity \mathbf{g} is oriented along the x_3 -axis, without loss of generality, and the post-collision relative velocity is expressed in spherical coordinates (g, χ, θ) :

$$(\mathbf{g}) = g \begin{pmatrix} 0 \\ 0 \\ 1 \end{pmatrix}, \quad (\mathbf{g}') = g' \begin{pmatrix} \sin \chi \cos \theta \\ \sin \chi \sin \theta \\ \cos \chi \end{pmatrix}, \quad (2.46)$$

where χ and θ are the deflection angle and the azimuthal angle respectively. The transformations in Eqs. (2.45) and (2.46) are applied to the integral operator $\mathcal{I}_1 [A, B]$, followed by integrating the azimuthal angle θ over $(0, 2\pi)$. The deflection angle χ will be treated collectively at the final stage. After this treatment, integral operator $\mathcal{I}_1 [A, B]$ can be simplified to integral operator $\mathcal{I}_2 [A]$:

$$\begin{aligned} \mathcal{I}_2 [A] = \sqrt{\frac{kT_t}{m}} \int A \cdot n^2 \left(\frac{1}{2\pi} \right)^3 \frac{\varepsilon_1^{\frac{v}{2}-1}}{\Gamma(\frac{v}{2})} \frac{\varepsilon_2^{\frac{v}{2}-1}}{\Gamma(\frac{v}{2})} e^{-G^*} e^{-\frac{g^*}{4}} e^{-\varepsilon_1} e^{-\varepsilon_2} \\ \cdot g^* bdb h(\mathbf{s}) ds d\mathbf{G}^* d\mathbf{g}^* d\varepsilon_2 d\varepsilon_1. \end{aligned} \quad (2.47)$$

The correspondence between the specific integral operators $\mathcal{I}_1 [A, B]$ and $\mathcal{I}_2 [A]$ used in the relaxation rate integrals is provided in Appendix C. The center-of-mass velocity \mathbf{G} and the solid angle of relative velocity \mathbf{g} are subsequently integrated, while the magnitude of the relative velocity g is maintained. Specifically, dg can be expressed in spherical coordinates as $g^2 \sin(\theta_g) dg d\theta_g d\phi_g$, with θ_g and ϕ_g integrated over $(0, \pi)$ and $(0, 2\pi)$, respectively. With the treatment of velocity scattering largely complete here, Integral operator $\mathcal{I}_2 [A]$ can be further simplified to integral operator $\mathcal{I}_3 [A]$:

$$\mathcal{I}_3 [A] = \sqrt{\frac{kT_t}{m}} \int A \cdot \left(\frac{1}{2\pi} \right)^3 \frac{\varepsilon_1^{\frac{v}{2}-1}}{\Gamma(\frac{v}{2})} \frac{\varepsilon_2^{\frac{v}{2}-1}}{\Gamma(\frac{v}{2})} n^2 e^{-\frac{g^*}{4}} e^{-\varepsilon_1} e^{-\varepsilon_2} g^* bdb h(\mathbf{s}) ds d\mathbf{g}^* d\varepsilon_2 d\varepsilon_1. \quad (2.48)$$

The explicit computational steps from integral operator $\mathcal{I}_1 [A, B]$ to $\mathcal{I}_2 [A]$ and from $\mathcal{I}_2 [A, B]$ to $\mathcal{I}_3 [A]$ are provided in Appendix C. The subsequent treatment of energy scattering in the collision process is the core of this work and a key difference from previous studies on elastic collisions. In this integral step, calculating the post-collision translational and rotational energies is essential. According to the redistribution rule in Eq. (2.5), the post-collision rotational energies $\varepsilon_1', \varepsilon_2'$ and relative translational energy ε_t' of the colliding particle pair can be explicitly expressed in terms of the pre-collision variables $(\varepsilon_1, \varepsilon_2, \varepsilon_t)$ and the partition variables $\mathbf{s} = (s_1, s_2, s_3, s_4, s_5)$. Additionally, the post-collision relative velocity can be expressed as:

$$g' = \sqrt{\frac{4}{m} (1 - s_3) \varepsilon_t + (1 - s_5) (s_1 \varepsilon_1 + s_2 \varepsilon_2 + s_3 \varepsilon_t)}. \quad (2.49)$$

Based on the energy-scattering rules in Eqs. (2.5) and (2.49), the integration over the phase space $d\epsilon_1 d\epsilon_2 ds$, spanned by rotational energies ϵ_1, ϵ_2 , and partition variables s , can be carried out. Noting that the partition variable s represents the fraction of energy redistributed during the scattering process, its integration is carried out over the interval $(0, 1)$.

After completing the integration for energy scattering, integral operator $\mathcal{I}_3 [A]$ can be written as functions of a series of element integrals like the use of Ω in traditional gas kinetic theory. Once the molecular potential is specified, the values of the elementary integrals can be determined. Thus, the most compact form of the relaxation rates is presented first. At the end of this subsection, the specific expressions using the VHS model is provided. The integral over velocity scattering $bdbdg$, can be compactly expressed through the collision cross-section. The standard collision cross-section integral $\Omega_{l,r}$ and $\hat{\Omega}_r$ are defined as follows:

$$\Omega_{l,r} = \int e^{-\frac{g^{*2}}{4}} (g^*)^{2r+3} \left(1 - \cos^l [\chi] \right) b db dg^*, \quad (2.50)$$

$$\hat{\Omega}_r = \int e^{-\frac{g^{*2}}{4}} (g^*)^{2r+3} b db dg^*, \quad (2.51)$$

These standard collision cross-sections are analytically integrable. On the other hand, there are also the non-analytical integral terms in the heat flux relaxation rates, Eqs. (C 17) and (C 20). For the conciseness of relaxation rates, these non-analytical terms are temporarily denoted as:

$$\begin{aligned} \Omega_1^+ &= \int \frac{\pi^{\frac{1}{2}}}{48} \pi^{\frac{7}{2}} \cos [\chi] g'^* g^{*3} \left(10 + g^{*2} \right) (\epsilon_1 - \epsilon_2) \\ &\quad \cdot \frac{\epsilon_1^{\frac{v}{2}-1} \epsilon_2^{\frac{v}{2}-1}}{\Gamma(\frac{v}{2}) \Gamma(\frac{v}{2})} e^{-\frac{g^{*2}}{4}} e^{-\epsilon_1} e^{-\epsilon_2} g^* bdb h(s) ds dg^* d\epsilon_2 d\epsilon_1, \end{aligned} \quad (2.52)$$

$$\begin{aligned} \Omega_2^+ &= -\frac{1}{12} \pi^{\frac{1}{2}} \cos [\chi] g'^* g^{*3} \epsilon_1' (-\epsilon_1 + \epsilon_2) \\ &\quad \cdot \frac{\epsilon_1^{\frac{v}{2}-1} \epsilon_2^{\frac{v}{2}-1}}{\Gamma(\frac{v}{2}) \Gamma(\frac{v}{2})} e^{-\frac{g^{*2}}{4}} e^{-\epsilon_1} e^{-\epsilon_2} g^* bdb h(s) ds dg^* d\epsilon_2 d\epsilon_1. \end{aligned} \quad (2.53)$$

Once the adopted molecular potential is specified, the specific values of these non-analytical terms can be obtained via numerical integration. Using the Gaussian quadrature method, we evaluate Eqs. (2.52)–(2.53) under equilibrium temperature conditions ($T_t = T_r$). Table 1 lists the numerical values of Ω_1^+ and Ω_2^+ for the hard sphere (HS) model, the variable hard sphere (VHS) model, and the variable soft sphere (VSS) models, all normalized by d_{ref}^2 . Evidently, when the HS or VHS model is employed, both Ω_1^+ and Ω_2^+ are 0 (considered zero within numerical truncation error). This result can likewise be mathematically demonstrated by integrating Ω_1^+ and Ω_2^+ over the deflection angle χ . Notably, for the VSS model, Ω_1^+ is also zero while Ω_2^+ takes a non-negligible value. The role of the non-analytical term Ω_2^+ is reflected in the influence of the rotational heat flux on its own relaxation process.

Based on the defined collision cross-section integral, the integral operators $\mathcal{I}_1 [A, B]$ used in the relaxation rates can be expressed in the following form:

$$\mathcal{I}_1 [\xi_1^2, 1] = \frac{n^2 \sqrt{\pi} \sqrt{\frac{kT_r}{m}}}{4(v\phi + \eta\psi)} v\phi\psi \left(\frac{T_r}{T_t} 4\eta\hat{\Omega}_0 - \hat{\Omega}_1 \right), \quad (2.54)$$

	$\Omega_1^+/d_{\text{ref}}^2$	$\Omega_2^+/d_{\text{ref}}^2$
HS	8.11×10^{-31}	3.33×10^{-15}
VHS	1.41×10^{-30}	4.83×10^{-14}
VSS	1.82×10^{-15}	9.68

Table 1: Numerical values of non-analytic terms Ω_1^+ and Ω_2^+ .

$$\mathcal{I}_1 [\varepsilon_1, 1] = \frac{n^2 \sqrt{\pi} \sqrt{\frac{kT_t}{m}}}{8(v\phi + \eta\psi)} v\phi\psi \left(-4\eta\hat{\Omega}_0 + \frac{T_t}{T_r}\hat{\Omega}_1 \right), \quad (2.55)$$

$$\begin{aligned} & \mathcal{I}_1 [\xi_{\langle 1, i} \xi_{1, j \rangle}, \xi_{\langle 1, k} \xi_{1, l \rangle} + \xi_{\langle 2, k} \xi_{2, l \rangle}] \\ &= \frac{n^2 \sqrt{\pi} \sqrt{\frac{kT_t}{m}} (\delta_{ik}\delta_{jl} + \delta_{il}\delta_{jk})}{240(v\phi + \eta\psi)} \begin{pmatrix} 8\frac{T_r}{T_t} v\phi\psi\eta\hat{\Omega}_1 - 2v\phi\psi\hat{\Omega}_2 \\ -12\frac{T_r}{T_t} v\phi\psi\eta\Omega_{2,1} - 3(v\phi + \eta\psi - v\phi\psi)\Omega_{2,2} \end{pmatrix}, \end{aligned} \quad (2.56)$$

$$\begin{aligned} & \mathcal{I}_1 [\xi_1^2 \xi_{1,i}, \xi_1^2 \xi_{1,k} + \xi_2^2 \xi_{2,k}] \\ &= \frac{n^2 \sqrt{\pi} \sqrt{\frac{kT_t}{m}} \delta_{ik}}{48(v\phi + \eta\psi)} \begin{pmatrix} 200\frac{T_r}{T_t} v\phi\psi\eta\hat{\Omega}_0 + \left(-25 + 22\frac{T_r}{T_t}\eta \right) 2v\phi\psi\hat{\Omega}_1 - 11v\phi\psi\hat{\Omega}_2 \\ -16\frac{T_r}{T_t} v\phi\psi\eta\Omega_{2,1} - 4(v\phi + \eta\psi - v\phi\psi)\Omega_{2,2} \end{pmatrix}, \end{aligned} \quad (2.57)$$

$$\mathcal{I}_1 [\xi_1^2 \xi_{1,i}, \varepsilon_1 \xi_{1,k} + \varepsilon_2 \xi_{2,k}] = \frac{5n^2 \sqrt{\pi} \sqrt{\frac{kT_t}{m}} \delta_{ik}}{24(v\phi + \eta\psi)} v\phi\psi \left(\frac{T_r}{T_t} 4(1+\nu)\eta\hat{\Omega}_0 - v\hat{\Omega}_1 \right) + n^2 \sqrt{\frac{kT_t}{m}} \Omega_1^+, \quad (2.58)$$

$$\mathcal{I}_1 [\xi_1^2 \xi_{1,i}, \xi_{1,k} + \xi_{2,k}] = -\frac{5n^2 \sqrt{\pi} \sqrt{\frac{kT_t}{m}} \delta_{ik}}{12(v\phi + \eta\psi)} v\phi\psi \left(-\frac{T_r}{T_t} 4\eta\hat{\Omega}_0 + \hat{\Omega}_1 \right), \quad (2.59)$$

$$\mathcal{I}_1 [\xi_{1,i} \varepsilon_1, \xi_1^2 \xi_{1,k} + \xi_2^2 \xi_{2,k}] = \frac{5n^2 \sqrt{\pi} \sqrt{\frac{kT_t}{m}} \delta_{ik}}{96(v\phi + \eta\psi)} v\phi\psi \left(-24\eta\hat{\Omega}_0 + \left(6\frac{T_t}{T_r} - 4\eta \right) \hat{\Omega}_1 + \frac{T_t}{T_r} \hat{\Omega}_2 \right), \quad (2.60)$$

$$\begin{aligned} & \mathcal{I}_1 [\xi_{1,i} \varepsilon_1, \varepsilon_1 \xi_{1,k} + \varepsilon_2 \xi_{2,k}] \\ &= \frac{n^2 \sqrt{\pi} \sqrt{\frac{kT_t}{m}} \delta_{ik}}{48 (\nu\phi + \eta\psi)} \nu \left(-12 (1 + \nu) \eta\phi\psi \hat{\Omega}_0 + \left(3 \frac{T_t}{T_r} \nu\phi\psi - 2 (\nu\phi + \eta\psi) \right) \hat{\Omega}_1 \right) + n^2 \sqrt{\frac{kT_t}{m}} \Omega_2^+, \end{aligned} \quad (2.61)$$

$$\mathcal{I}_1 [\xi_{1,i} \varepsilon_1, \xi_{1,k} + \xi_{2,k}] = \frac{n^2 \sqrt{\pi} \sqrt{\frac{kT_t}{m}} \delta_{ik}}{8 (\nu\phi + \eta\psi)} \nu\phi\psi \left(-4\eta\hat{\Omega}_0 + \frac{T_t}{T_r} \hat{\Omega}_1 \right). \quad (2.62)$$

The integral operator $\mathcal{I}_1 [A, B]$ in its simplest form is obtained through the above mathematical derivation and integration. By substituting this simplest form into the definition of the relaxation rates Eqs. (2.40)-(2.44), the relaxation rate can be analytically expressed as:

$$\mathcal{T}_t = -\frac{2}{3nk} \sqrt{\frac{kT_t}{m}} \frac{\sqrt{\pi} n^2 k T_t \nu\phi\psi \left(\hat{\Omega}_1 - 4\eta \frac{T_r}{T_t} \hat{\Omega}_0 \right)}{8 (\nu\phi + \eta\psi)}, \quad (2.63)$$

$$\mathcal{T}_r = \frac{2}{vnk} \sqrt{\frac{kT_t}{m}} \frac{\sqrt{\pi} n^2 k T_r \nu\phi\psi \left(\frac{T_r}{T_t} \hat{\Omega}_1 - 4\eta \hat{\Omega}_0 \right)}{8 (\nu\phi + \eta\psi)}, \quad (2.64)$$

$$\mathcal{P}_{ij} = \frac{n \sqrt{\frac{\pi k T_t}{m}}}{240 (\nu\phi + \eta\psi)} \left(\begin{array}{l} -12\nu \frac{T_r}{T_t} \eta\phi\psi \Omega_{(2,1)} - 3 (\nu\phi + \eta\psi - \nu\phi\psi) \Omega_{(2,2)} \\ + 8\nu \frac{T_r}{T_t} \eta\phi\psi \hat{\Omega}_1 - 2\nu\phi\psi \hat{\Omega}_2 \end{array} \right) P_{\langle ij \rangle}, \quad (2.65)$$

$$\begin{aligned} Q_{t,i} &= \frac{n \sqrt{\frac{\pi k T_t}{m}}}{(\nu\phi + \eta\psi)} \left(\begin{array}{l} \frac{1}{120} \left(-4 \frac{T_r}{T_t} \eta\nu\phi\psi \Omega_{(2,1)} - (\nu\phi + \eta\psi - \nu\phi\psi) \Omega_{(2,2)} \right) q_{t,i} \\ + \frac{1}{480} \left(-200 \frac{T_r}{T_t} \eta\nu\phi\psi \hat{\Omega}_0 + \left(50 + 44 \frac{T_r}{T_t} \eta \right) \nu\phi\psi \hat{\Omega}_1 - 11\nu\phi\psi \hat{\Omega}_2 \right) q_{r,i} \\ + \frac{5}{6} \nu\eta\phi\psi \hat{\Omega}_0 q_{r,i} \end{array} \right) \\ &+ \frac{T_t}{T_r} \frac{n \sqrt{\frac{kT_t}{m}}}{\nu} \Omega_1^+ q_{r,i}, \end{aligned} \quad (2.66)$$

$$\begin{aligned} Q_{r,i} &= \frac{n \sqrt{\frac{\pi k T_t}{m}}}{(\nu\phi + \eta\psi)} \left(\begin{array}{l} \frac{\nu\phi\psi}{96} \left(24 \frac{T_r}{T_t} \eta\hat{\Omega}_0 - \left(6 + 4 \frac{T_r}{T_t} \eta \right) \hat{\Omega}_1 + \hat{\Omega}_2 \right) q_{t,i} \\ + \frac{1}{12} \left(6\eta\phi\psi \hat{\Omega}_0 + (\nu\phi + \eta\psi) \hat{\Omega}_1 \right) q_{r,i} \end{array} \right) \\ &+ \frac{2n \sqrt{\frac{kT_t}{m}}}{\nu} \Omega_2^+ q_{r,i}. \end{aligned} \quad (2.67)$$

An analytical relaxation rate applicable to arbitrary molecular collision models is obtained through mathematical derivation. Consistent with conventional gas kinetic theory, the relaxation rates derived in this work depend on standard collision cross-section integrals $\Omega_{l,r}$, $\hat{\Omega}_r$ and macroscopic quantities like n , m , T_t , T_r , with free parameters ϕ and ψ to be specified subsequently.

For the subsequent model validation, the relaxation rates implemented using the VHS model are provided. The collision cross-section integrals using the VHS model are given by:

$$\begin{cases} \hat{\Omega}_0 = 4 \left(\frac{2}{g_{\text{ref}}} \right)^{1-2\omega} d_{\text{ref}}^2 \Gamma \left[\frac{5}{2} - \omega \right], \\ \hat{\Omega}_1 = 4 \left(\frac{2}{g_{\text{ref}}} \right)^{1-2\omega} d_{\text{ref}}^2 \Gamma \left[\frac{7}{2} - \omega \right], \\ \hat{\Omega}_2 = 4 \left(\frac{2}{g_{\text{ref}}} \right)^{1-2\omega} d_{\text{ref}}^2 \Gamma \left[\frac{9}{2} - \omega \right], \\ \Omega_{2,1} = \frac{8}{3} \left(\frac{2}{g_{\text{ref}}} \right)^{1-2\omega} d_{\text{ref}}^2 \Gamma \left[\frac{7}{2} - \omega \right], \\ \Omega_{2,2} = \frac{8}{3} \left(\frac{2}{g_{\text{ref}}} \right)^{1-2\omega} d_{\text{ref}}^2 \Gamma \left[\frac{9}{2} - \omega \right], \\ \Omega_1^+ = 0, \\ \Omega_2^+ = 0. \end{cases} \quad (2.68)$$

The collision cross-section integrals of the VHS model are substituted into the relaxation rate integrals Eqs. (2.63)–(2.67). The relaxation time τ_t adopts the same definition as that in elastic collisions and can be evaluated from the ratio of the shear viscosity μ to the translational pressure p_t . The relaxation time for the VHS model is given by:

$$\tau_t = \frac{15}{4^{2-\omega} d_{\text{ref}}^2 g_{\text{ref}}^{2\omega-1} n \left(\frac{kT_t}{m} \right)^{1-\omega} \sqrt{\pi} \Gamma \left[\frac{9}{2} - \omega \right]}. \quad (2.69)$$

The relaxation rates for the VHS model are given as follows:

$$\mathcal{T}_t = \frac{(T - T_t)}{Z_{\text{rot}} \tau_t}, \quad (2.70)$$

$$\mathcal{T}_r = \frac{(T - T_r)}{Z_{\text{rot}} \tau_t}, \quad (2.71)$$

$$\mathcal{P}_{ij} = -\frac{p_{\langle ij \rangle}}{\tau_t}, \quad (2.72)$$

$$Q_{t,i} = - \left(\frac{2}{3} + \frac{5\nu \left(\frac{T_r}{T_t} (\omega - 1) - (\omega - 2) \right)}{6(3 + \nu) Z_{\text{rot}}} \right) \frac{q_{t,i}}{\tau_t} + \frac{5}{2(3 + \nu) Z_{\text{rot}}} \frac{q_{r,i}}{\tau_t}, \quad (2.73)$$

$$Q_{r,i} = \frac{\nu \left(\frac{T_t}{T_r} (\omega - 1) - (\omega - 2) \right) q_{t,i}}{2(3 + \nu) Z_{\text{rot}}} - \left(\frac{5}{(7 - 2\omega)} + \frac{3}{2(3 + \nu) Z_{\text{rot}}} \right) \frac{q_{r,i}}{\tau_t}, \quad (2.74)$$

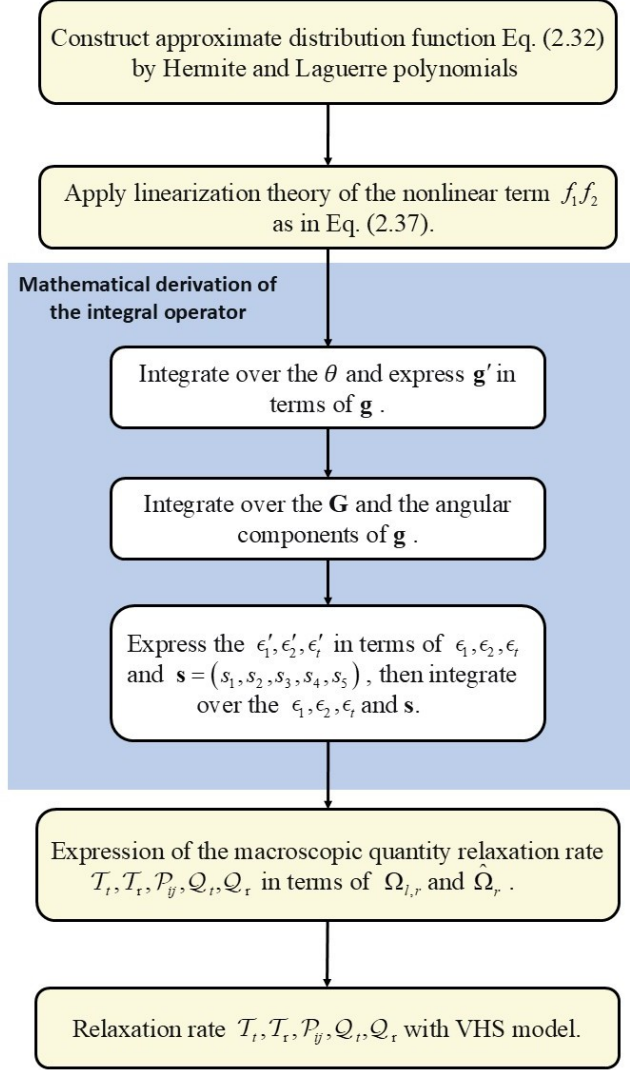


Figure 1: Mathematical derivation process of macroscopic quantity relaxation rate

where Z_{rot} represents the rotational collision number, defined as:

$$Z_{\text{rot}} = \frac{\tau_r}{\tau_t}. \quad (2.75)$$

The translational relaxation time τ_t and rotational relaxation time τ_r can be obtained from the previously derived temperature relaxation rate Eq. (2.64) $\mathcal{T}_r = (T - T_r) / \tau_r$ and pressure deviator relaxation rate Eq. (2.65) $\mathcal{P}_{ij} = -p_{\langle ij \rangle} / \tau_t$, respectively. Therefore, the rotational collision number can be explicitly expressed as:

$$Z_{\text{rot}} = \frac{(7 - 2\omega)(\nu\phi + \eta\psi)}{5(3 + \nu)\phi\psi}. \quad (2.76)$$

To clarify the derivation process of the relaxation rate, Figure 1 presents the complete procedure in a flowchart form.

2.2.3. Determination of free parameters

In the Pullin model, ϕ and ψ are key parameters that control the energy distribution ratio at the microscopic collision process. The selection of free parameters should ensure the accuracy of both microscopic processes and macroscopic parameters. Pullin derived the relationship between the rotational collision number and the parameters ϕ and ψ through the C-E expansion (Pullin 1978). However, if the goal is to ensure only the accuracy of the rotational collision number, one of the free parameters is redundant. Accordingly, Pullin introduced the assumption $\phi = \psi$ under the hard-sphere model. The explicit expressions of ϕ and ψ under this assumption are:

$$\phi = \psi = \frac{8(2+\nu)}{5\pi} \frac{1}{Z_{\text{rot}}}. \quad (2.77)$$

The approach of Pullin focuses on only recovering the rotational collision number while omitting the use of extra free parameters. In this work, the extra parameter is used to give more reasonable microscopic process. According to the energy equal-partition principle, the energy between two colliding particles is redistributed based on their respective degrees of freedom. In the energy partitioning function Eq. (2.10), $\beta \langle s_1 | \phi \zeta, (1-\phi)\zeta \rangle$ and $\beta \langle s_3 | \psi \eta, (1-\psi)\eta \rangle$ respectively control the energy distribution between rotational and translational energy during the collision process, where $\phi\zeta$ and $\psi\eta$ represent the allocation ratios of rotational energy and translational energy, respectively. According to the energy equal-partition principle, the relationship between the parameters $\phi\zeta$ and $\psi\eta$ in the energy partitioning function is given as follows:

$$\frac{\phi\zeta}{\psi\eta} = \frac{\nu}{3}. \quad (2.78)$$

Meanwhile, to ensure the accuracy of the rotational collision number, the correspondence between the rotational collision number and the free parameters given by Eq. (2.76) must also be satisfied. Likewise, the free parameters ϕ and ψ can be obtained from Eq. (2.76) and Eq. (2.78) as follows:

$$\phi = \frac{2(3+2\nu)\eta(1+\eta)}{15(3+\nu)Z_{\text{rot}}}, \quad (2.79)$$

$$\psi = \frac{(3+2\nu)(1+\eta)}{5(3+\nu)Z_{\text{rot}}}. \quad (2.80)$$

It is noteworthy that the determination of free parameters via either Eq. (2.77) or Eqs. (2.79)-(2.80), does not affect the relaxation rates of the non-equilibrium macroscopic quantities. In contrast, Eqs. (2.79)-(2.80), which are derived from the equipartition theorem, provide a more physically reasonable description of the microscopic partitioning process. Moreover, the new determination of free parameters extends the applicability of Pullin model from hard sphere model to the variable hard sphere model.

Thus far, the analytical relaxation rates for polyatomic gases considering rotational energy excitation have been derived by taking moments of the collision term in the Pullin model. The analytical expressions for the relaxation rates elucidate the fundamental relaxation behavior of key macroscopic physical quantities. Furthermore, it implies that the non-equilibrium degree T_t/T_r has a discernible influence on the relaxations of the heat flux. Meanwhile, these analytical relaxation rates can be directly linked to the macroscopic transport coefficients obtained from the C-E expansion. These points will be addressed in greater detail in the following subsections.

2.3. Theoretical analysis of the obtained relaxation rate

Compared with monoatomic gases, polyatomic gases contain additional rotational energy, which introduces energy exchange between translational and rotational modes during non-equilibrium relaxation. As a result, the relaxation process of polyatomic gases becomes inherently more complex. In spatially homogeneous systems, the temperature relaxation behavior can be described by the Jeans–Landau equation:

$$\mathcal{T}_t = \frac{p_t}{\mu} \frac{T - T_t}{Z_{\text{rot}}}, \quad (2.81)$$

$$\mathcal{T}_r = \frac{p_t}{\mu} \frac{T - T_r}{Z_{\text{rot}}}, \quad (2.82)$$

where p_t is kinetic pressure, μ is shear viscosity. The temperature relaxation rate can be controlled by adjusting the rotational collision number Z_{rot} . The relaxation processes of the translational and rotational heat fluxes can be described as follows (Mason & Monchick 1962; McCormack 1968):

$$\begin{aligned} Q_t &= -\frac{p_t}{\mu} (A_{tt} q_{t,i} + A_{tr} q_{r,i}), \\ Q_r &= -\frac{p_t}{\mu} (A_{rt} q_{t,i} + A_{rr} q_{r,i}). \end{aligned} \quad (2.83)$$

where $A_{tt}, A_{tr}, A_{rt}, A_{rr}$ are heat flux relaxation coefficients, which characterize the influence of translational and rotational heat fluxes on the heat flux relaxation rates. Eq. (2.83) provides the relaxation framework for heat flux, which also manifests in the DSMC simulation work (Li *et al.* 2021). Building upon this framework, the heat flux relaxation coefficient A_{ij} can be extracted from DSMC simulation data. However, due to its lack of theoretical foundation, this method does not lead to a clear understanding of the relaxation rate.

In this work, the heat flux relaxation rates Eqs. (2.73)-(2.74) obtained through theoretical derivation provide an explicit and analytical result, which establishes a theoretical foundation for analyzing the heat flux relaxation process. Specifically, the heat flux relaxation coefficients A_{ij} for the VHS model can be expressed analytically as:

$$\begin{aligned} A_{tt} &= \frac{2}{3} + \frac{5\nu}{6(3+\nu)Z_{\text{rot}}} \left(\frac{T_r}{T_t} (\omega - 1) - (\omega - 2) \right), \\ A_{tr} &= -\frac{5}{2(3+\nu)Z_{\text{rot}}}, \\ A_{rt} &= -\frac{\nu}{2(3+\nu)Z_{\text{rot}}} \left(\frac{T_r}{T_t} (\omega - 1) - (\omega - 2) \right), \\ A_{rr} &= \frac{5}{(7-2\omega)} + \frac{3}{2(3+\nu)Z_{\text{rot}}}. \end{aligned} \quad (2.84)$$

According to the derived heat flux relaxation coefficients in Eq. (2.84), the heat flux relaxation coefficients depend on the viscosity index ω , the rotational collision number Z_{rot} , and the translational-to-rotational temperature ratio T_t/T_r . The viscosity index ω and the rotational collision number Z_{rot} reflect the effects of shear viscosity and bulk viscosity on the thermal relaxation process respectively. This influence has a clear physical basis: exchanges of molecular momentum and energy between translational and rotational modes manifest macroscopically as shear viscosity Eq. (2.87) and bulk viscosity Eq. (2.88), and these momentum and energy exchanges also influence higher-order heat flux. In the limit

$Z_{\text{rot}} \rightarrow \infty$, A_{tt} approaches 2/3 (i.e., the Prandtl number), A_{rr} approaches the Schmidt number (Sc), while A_{tr} and A_{rt} tend to zero. This corresponds to the case of elastic collisions, where the relaxations of translational and rotational heat fluxes are decoupled. Notably, the dependence on $T_{\text{t}}/T_{\text{r}}$, which quantifies the degree of thermodynamic non-equilibrium in the flow, indicates that heat flux relaxation is affected by the evolving non-equilibrium conditions. Specifically, the relaxation coefficients characterizing the influence of translational heat flux, A_{tt} and A_{rt} , depend on $T_{\text{t}}/T_{\text{r}}$. Moreover, in terms of their specific numerical values, the self-influence coefficients A_{tt} and A_{rr} are positive. Because of the negative sign in Eq. (2.83), the translational and rotational heat fluxes effectively attenuate their own relaxation. Similarly, the cross-influence coefficients A_{tr} and A_{rt} are negative, which in practice leads to an reinforcing effect. For example, a large translational heat flux promotes an increase in the rotational heat flux via the coupled relaxation process.

The microscopic non-equilibrium relaxation behavior of gas molecules manifests macroscopically as constitutive relations in the Navier-Stokes (N-S) framework. This connection can be rigorously established through the C-E expansion (see Appendix A). Within the N-S framework, the pressure tensor and the heat flux are described by the laws of Navier-Stokes and Fourier, respectively:

$$p_{ij} = \left(p - \mu_b \frac{\partial U_r}{\partial x_r} \right) \delta_{ij} - 2\mu \frac{\partial U_{\langle i}}{\partial x_{j\rangle}} \quad (2.85)$$

$$q_i = -\kappa \frac{\partial T}{\partial x_i} \quad (2.86)$$

where μ is the shear viscosity, μ_b is the bulk viscosity and κ is the thermal conductivity. The particle momentum exchange during non-equilibrium relaxation is characterized by the pressure tensor relaxation rate. This exchange produces a shear stress during shear expansion or compression of the gas, which is quantified by the shear viscosity within the N-S framework. In the Pullin model, the shear viscosity can be written via the C-E expansion as:

$$\mu = \tau_t p_t. \quad (2.87)$$

Compared to monatomic gases, polyatomic molecular gases exhibit an additional exchange between translational and internal (rotational) energy during non-equilibrium processes, which can be described by the temperature relaxation rate. During shear-free expansion or compression of a gas, the translational energy adjusts preferentially due to pressure work, whereas the adjustment of internal energy relies on inelastic collisions with a finite relaxation time and therefore typically lags behind the translational energy. This dissipative effect arising from the delayed relaxation of internal energy is phenomenologically represented by the bulk viscosity within the N-S framework. In the Pullin equation, the bulk viscosity can be written via the C-E expansion as:

$$\mu_b = \frac{2\nu}{3(3+\nu)} Z_{\text{rot}} \tau_t p_t. \quad (2.88)$$

Via the C-E expansion, constitutive relation Eqs. (A 21) and (A 22) can be extracted from the relaxation rates in the near-equilibrium relaxation. The correspondence between the thermal conductivity and the heat flux relaxation coefficient therein can be written as:

$$\begin{bmatrix} \kappa_t \\ \kappa_r \end{bmatrix} = \frac{k\mu}{2m} \begin{bmatrix} A_{\text{tt}} & A_{\text{tr}} \\ A_{\text{rt}} & A_{\text{rr}} \end{bmatrix}^{-1} \begin{bmatrix} 5 \\ \nu \end{bmatrix}. \quad (2.89)$$

Conventionally, to concisely express the relationship between thermal conductivity and shear

viscosity, Eucken (Eucken 1913) defined dimensionless factors f_{eu} , f_t and f_r :

$$f_{\text{eu}} = \frac{3}{3+\nu} f_t + \frac{\nu}{3+\nu} f_r = \frac{2}{3+\nu} \frac{\kappa m}{\mu k}, \quad (2.90)$$

$$f_t = \frac{2 \kappa_t m}{3 \mu k}, \quad f_r = \frac{2 \kappa_r m}{\nu \mu k}. \quad (2.91)$$

Under Eucken's framework, the total Eucken factor f_{eu} is a result of combining the translational Eucken factor f_t and rotational Eucken factor f_r at equilibrium temperature. Based on the thermal conductivities κ_t and κ_r derived from the C-E expansion, the translational and rotational Eucken factors can be directly expressed in terms of the heat flux relaxation coefficient A_{ij} as:

$$\begin{bmatrix} f_t \\ f_r \end{bmatrix} = \begin{bmatrix} 3A_{tt} & \nu A_{tr} \\ 3A_{rt} & \nu A_{rr} \end{bmatrix}^{-1} \begin{bmatrix} 5 \\ \nu \end{bmatrix}. \quad (2.92)$$

The explicit expression of the Eucken factors can be derived from the heat flux relaxation coefficient A_{ij} in Eq. (2.84):

$$f_t = \frac{(3+\nu)((7-2\omega)+2Z_{\text{rot}})}{20(3+\nu)Z_{\text{rot}}+6(7-2\omega)+25\nu\left(\frac{T_r}{T_t}(\omega-1)-(\omega-2)\right)}, \quad (2.93)$$

$$f_r = \frac{(3+\nu)(7-2\omega)\left(4Z_{\text{rot}}+5\left(\frac{T_r}{T_t}(\omega-1)-(\omega-2)\right)\right)}{20(3+\nu)Z_{\text{rot}}+6(7-2\omega)+25\nu\left(\frac{T_r}{T_t}(\omega-1)-(\omega-2)\right)}, \quad (2.94)$$

$$f_{\text{eu}} = \frac{(150+4\nu(7-2\omega))Z_{\text{rot}}+(7-2\omega)\left(15+5\nu\left(\frac{T_r}{T_t}(\omega-1)-(\omega-2)\right)\right)}{20(3+\nu)Z_{\text{rot}}+6(7-2\omega)+25\nu\left(\frac{T_r}{T_t}(\omega-1)-(\omega-2)\right)}. \quad (2.95)$$

Evidently, the dependence of the heat flux relaxation process on the non-equilibrium temperature T_t/T_r leads to the dependence of the macroscopic Eucken factor on the non-equilibrium temperature T_t/T_r , stemming from reliance on identical elementary integrals. The similar dependence of gas property on non-equilibrium degrees T_t/T_r is also found in the classic research on rotation number Z_{rot} by Parker (Parker 1959) and Zhang (Zhang *et al.* 2014). Prior to the establishment of Eqs. (2.93)-(2.95), as research on transport coefficients was predominantly carried out under thermal equilibrium conditions (Mason & Monchick 1962), the dependence on the non-equilibrium degree remained largely unrecognized.

Moreover, to provide a more intuitive analysis of the influence of non-equilibrium temperature on the heat flux, Figure 2 illustrates the relationship between the Eucken factor and the ratio of translational-to-rotational temperature T_t/T_r . The curves are constructed for nitrogen molecules, with the rotational degrees of freedom set as $\nu = 2$, the rotational collision number as $Z_{\text{rot}} = 3$, and the viscosity index as $\omega = 0.74$. The solid red and blue lines show the variation trends of the translational and rotational Eucken factors, respectively. The black dashed line indicates the equilibrium condition $T_t/T_r = 1$, with the corresponding Eucken factor values $f_t = 2.317$ and $f_r = 1.224$ annotated. As $\log(T_t/T_r)$ increases, the translational Eucken factor f_t decreases while the rotational Eucken factor f_r increases.

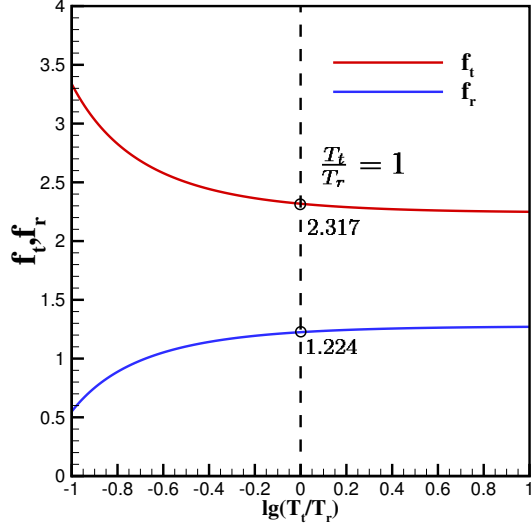


Figure 2: Variation of the Eucken factor with the degree of non-equilibrium

Furthermore, f_t and f_r approach asymptotic values of 2.242 and 1.275, respectively, in the limit $\log(T_t/T_r) \rightarrow 0$ (i.e., the limiting state approaching absolute zero with rotational modes unexcited). When $T_t > T_r$, the non-equilibrium temperature T_t/T_r exerts limited influence on the Eucken factor. This corresponds to compressive flows, such as those encountered in aerospace re-entry problems, where macroscopic kinetic energy is first converted into translational thermal energy. Conversely, when $T_r > T_t$, the ratio T_t/T_r exerts a significant influence on the Eucken factor. This corresponds to expansion or jet flows in applications such as aerospace propulsion or micro/nanofabrication, where T_t decreases along the jet.

In this work, under thermal equilibrium condition ($T_t = T_r$), the results of Eqs. (2.93)-(2.94) can first be reduced and then compared with results from prior study. In earlier work, Mason and Monchick (Mason & Monchick 1962) derived analytical expressions for thermal conductivity and the Eucken factor based on the WCU equation using a modified C-E expansion, with a special thermal equilibrium assumption $T_t = T_r$. Furthermore, an elastic collision assumption and the rough-sphere model were used for calculating the complex integrals. For comparison with results of Mason and Monchick, Eqs. (2.93)-(2.94) are first simplified under the conditions of thermal equilibrium $T_t/T_r = 1$ and the relation $\rho D/\mu = (7 - 2\omega)/5$, yielding:

$$f_t = \frac{5}{2} \left[1 - \frac{5\nu}{4(3+\nu)} \cdot \frac{4(3+\nu) \left(1 - \frac{2\rho D}{5\mu} \right)}{4(3+\nu)Z_{\text{rot}} + \left\{ 6\frac{\rho D}{\mu} + 5\nu \right\}} \right], \quad (2.96)$$

$$f_r = \frac{\rho D}{\mu} \left[1 + \frac{15}{4(3+\nu)} \cdot \frac{4(3+\nu) \left(1 - \frac{2\rho D}{5\mu} \right)}{4(3+\nu)Z_{\text{rot}} + \left\{ 6\frac{\rho D}{\mu} + 5\nu \right\}} \right], \quad (2.97)$$

where D denotes the diffusion coefficient. A further simplification of the Eucken factor is achieved by adopting Mason's approach, keeping only first-order terms of $1/Z_{\text{rot}}$. This is equivalent to neglecting the terms enclosed in curly braces, leading to:

$$\begin{aligned} f_t &= \frac{5}{2} \left[1 - \frac{5\nu}{4(3+\nu)Z_{\text{rot}}} \left(1 - \frac{2\rho D}{5\mu} \right) \right], \\ f_r &= \frac{\rho D}{\mu} \left[1 + \frac{15}{4(3+\nu)Z_{\text{rot}}} \left(1 - \frac{2\rho D}{5\mu} \right) \right]. \end{aligned} \quad (2.98)$$

Clearly, within the equilibrium-temperature framework, the results derived in this work reduce to the classical results of Mason and Monchick (Mason & Monchick 1962).

To further check the derived result in this work, the shear viscosity μ and thermal conductivity κ of nitrogen gas are compared with the experimentally fitted data from the National Institute of Standards and Technology (NIST) (NIST 2025) over the temperature range of 100–1000 K. The NIST data include both physical experiments and their fitted values. It is noteworthy that most measurements of viscosity and thermal conductivity are conducted under thermal equilibrium conditions. The comparative results of viscosity using the VHS model ($\omega = 0.74$) are presented in Figure 3a, where the blue solid line represents results obtained under the equilibrium temperature assumption and black circles represent NIST data. The red dashed and dotted-dashed lines represent the viscosity under different non-equilibrium temperatures, which remains identical to that at equilibrium temperature. This stems from the decoupling of velocity and energy collisions in the Pullin model, and thus the viscosity is unaffected by thermal non-equilibrium temperature. Comparison with the NIST data shows that shear viscosity achieve good agreement. In the thermal conductivity calculation, the rotational collision number adopts the fitting results of Larina and Rykov (Larina & Rykov 1976; Rykov *et al.* 2007):

$$Z_{\text{rot}} = \frac{3}{4}\pi \frac{\Phi(t)}{t^{1/6}} \frac{9t}{t+8} \left(\frac{T_r}{T_t} \right) \left[0.461 + 0.5581 \left(\frac{T_r}{T_t} \right) + 0.0358 \left(\frac{T_r}{T_t} \right)^2 \right], \quad (2.99)$$

$$\Phi(t) = 0.767 + 0.233t^{-\frac{1}{6}} \exp[-1.17(t-1)], \quad (2.100)$$

$$t = \frac{T_{\text{tran}}}{\tilde{T}}, \quad (2.101)$$

where \tilde{T} is the reduced temperature; for nitrogen $\tilde{T} = 91.5K$. The thermal conductivity using the VHS model ($\omega = 0.74$) under the equilibrium temperature ($T_t/T_r = 1$) is presented as blue solid line in Figure 3b. Furthermore, by substituting the self-diffusion coefficient D of the VSS model ($\alpha = 1.36$) into Eqs. (2.96)–(2.97), the corresponding thermal conductivity under the equilibrium temperature ($T_t/T_r = 1$) and different non-equilibrium temperature conditions ($T_t/T_r = 0.1, 10$) is represented by the red lines. The comparison shows that, under equilibrium temperature conditions, the results obtained using the VSS model demonstrate better accuracy than using the VHS model. Moreover, as T_t/T_r decreases, the total thermal conductivity exhibits an increasing trend, which becomes more pronounced when $T_t/T_r < 1$.

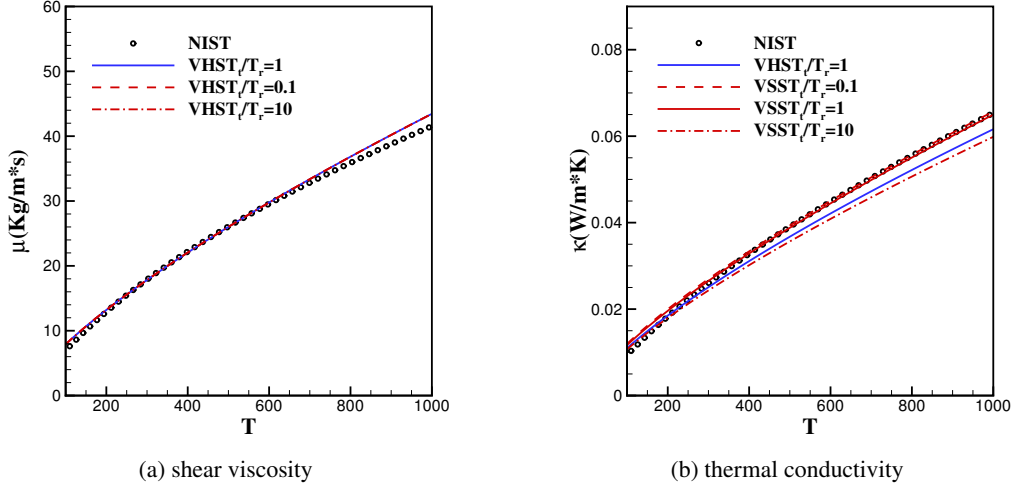


Figure 3: Comparison of calculated macroscopic transport coefficients with the NIST database

3. Kinetic Model

Due to the high computational cost of directly solving the extended Boltzmann equation, there is a need to develop simplified models that are both efficient and accurate. The establishment of a simplified model requires explicit and accurate relaxation rates to recover the correct relaxation process. In the past, when relaxation rates were unavailable, some studies resorted to the C-E expansion to calibrate transport coefficients for model construction such as relaxation-type(BGK-type) model equations and Fokker-Planck-type model equations. However, due to insufficient understanding of the relaxation process, modeling conducted this way is often incomplete.

To yield accurate relaxation rates and transport coefficients simultaneously, a new relaxation-type model equation is constructed based on the accurate analytical relaxation rates provided in Eqs. (2.70)–(2.74). In reviewing previous work, the basic framework of the Rykov model was sound. However, due to the absence of relaxation rates as a basis for modeling, its description of near-equilibrium relaxation remains incomplete. Therefore, constructing an appropriate equilibrium state to recover the relaxation rates is key to modeling. The subsequent sections are organized as follows. In subsection 3.1, a brief review of the Rykov model is provided to highlight its key assumptions and limitations. In subsection 3.2, the model construction procedure based on macroscopic relaxation rates is presented. The relaxation behavior and the recovery of transport coefficients in the proposed kinetic model are then examined.

3.1. The Rykov kinetic model

The original Rykov model was developed for diatomic gases and later extended to polyatomic gases. Its construction adopts the approach of treating elastic and full-inelastic collisions separately. Without external forces, the evolution of the molecular distribution function is described by:

$$\frac{\partial f}{\partial t} + \mathbf{c} \cdot \frac{\partial f}{\partial \mathbf{x}} = \frac{g_{t,\text{Rykov}} - f}{\tau_t} + \frac{g_{r,\text{Rykov}} - g_{t,\text{Rykov}}}{Z_{\text{rot}} \tau_t}. \quad (3.1)$$

where the left hand side of this equation represents the free-transport term, the right-hand side represents elastic and inelastic collisions terms respectively. All molecules first relax

to the equilibrium state g_t via elastic collisions, which mediate the exchange of momentum between molecules, with a concurrent redistribution of translational energy occurring across different spatial directions. Then, a fraction $1/Z_{\text{rot}}$ of the molecules undergo further inelastic collisions, relaxing to the equilibrium state g_r , during which translational and rotational energy are exchanged. Analogous to the approach of constructing approximate distribution functions in theoretical analysis, $g_{t,\text{Rykov}}$ and $g_{r,\text{Rykov}}$ are similarly expressed as the product of perturbation polynomial and equilibrium state functions:

$$g_{t,\text{Rykov}} = E_t(T_t) E_r(T_r) \left[1 + \frac{2m q_{t,i} C_i}{15k T_t p_t} \left(\frac{m C^2}{2k T_t} - \frac{5}{2} \right) + \frac{2(1-\delta)}{\nu} \frac{m q_{r,i} C_i}{k T_t p_r} \left(\frac{\epsilon}{k T_r} - \frac{\nu}{2} \right) \right], \quad (3.2)$$

$$g_{r,\text{Rykov}} = E_t(T) E_r(T) \left[1 + \omega_0 \frac{2m q_{t,i} C_i}{15k T p} \left(\frac{m C^2}{2k T} - \frac{5}{2} \right) + \frac{2\omega_1(1-\delta)}{\nu} \frac{m q_{r,i} C_i}{k T p} \left(\frac{\epsilon}{k T} - \frac{\nu}{2} \right) \right], \quad (3.3)$$

where $E_t(T)$ and $E_r(T)$ are the equilibrium state functions as:

$$E_t(T) = n \left(\frac{m}{2\pi k T} \right)^{\frac{3}{2}} \exp \left(-\frac{m C^2}{2k T_t} \right), \quad (3.4)$$

$$E_r(T) = \frac{\epsilon^{\frac{\nu}{2}-1}}{\Gamma(\frac{\nu}{2})(k T)^{\frac{\nu}{2}}} \exp \left(-\frac{\epsilon}{k T} \right). \quad (3.5)$$

The Rykov model obtains its transport coefficients through the C-E expansion and recovers the correct bulk viscosity, shear viscosity, and thermal conductivity by adjusting its free parameters. Specifically, the Rykov model adjusts the collision number Z_{rot} to control the proportion of inelastic collisions, thereby recovering the correct bulk viscosity. For the shear viscosity, the model sets the relaxation time for elastic collisions as $\tau_t = \mu/p_t$ to achieve its recovery. Regarding thermal conductivity, the model matches the correct thermal conductivity values by tuning the free parameters ω_0 and ω_1 in the heat flux correction term (where $\delta = \mu/\rho D$ characterizes diffusion properties).

More significantly, the relaxation behavior of the Rykov model is analyzed. By taking the third-order moment of the collision term, the heat flux relaxation rates for the Rykov model can be obtained. Following the heat flux relaxation relationship Eq. (2.83), the corresponding heat flux relaxation coefficients can be extracted for analysis:

$$\begin{aligned} A_{tt} &= \frac{2}{3} + \frac{1-\omega_0}{3Z_{\text{rot}}}, & A_{tr} &= 0, \\ A_{rt} &= 0, & A_{rr} &= \frac{\mu}{\rho D} + \frac{\left(1 - \frac{\mu}{\rho D}\right)(1-\omega_1)}{Z_{\text{rot}}}. \end{aligned} \quad (3.6)$$

Notably, the heat flux relaxation coefficients A_{tr} and A_{rt} are set to zero. This implies the model assumes independent relaxation between translational and rotational heat fluxes without mutual influence. The Rykov model does not accurately capture the relaxation process due to the assumption of independently relaxing translational and rotational heat fluxes, which consequently results in incorrect thermal relaxation coefficients. This demonstrates that recovering the transport coefficients does not guarantee the correct relaxation rates.

3.2. A kinetic model based on relaxation rates

In Section 2, we derived analytical expressions for relaxation rates of key macroscopic quantities (i.e., temperature, pressure tensor and heat flux) within Pullin model framework. These theoretical results provide complete and explicit information on the constraints for constructing relaxation-type model equations that can recover accurate relaxation rates. The new kinetic model adopts the same form as Rykov's model:

$$\frac{\partial f}{\partial t} + \mathbf{c} \cdot \frac{\partial f}{\partial \mathbf{x}} = \frac{g_{t,\text{new}} - f}{\tau_t} + \frac{g_{r,\text{new}} - g_{t,\text{new}}}{Z_{\text{rot}} \tau_t}. \quad (3.7)$$

The collision term on the right-hand side of the equation adopts a framework similar to that of the Rykov model. However, as the relaxation rates are now more clearly expressed, the perturbative polynomials within the equilibrium states $g_{t,\text{new}}$ and $g_{r,\text{new}}$ can be constructed in a simpler and more compact form:

$$g_{t,\text{new}} = E_t(T_t) E_r(T_r) \left[1 + \frac{2}{5nm} \left(\frac{m}{kT_t} \right)^2 q_{0,i} C_i \left(\frac{m}{2kT_t} C^2 - \frac{5}{2} \right) \right], \quad (3.8)$$

$$g_{r,\text{new}} = E_t(T) E_r(T) \left[1 + \frac{2}{\nu nm} \left(\frac{m}{kT} \right)^2 q_{1,i} \sqrt{\frac{m}{kT}} C_i \left(\frac{1}{kT} \epsilon - \frac{\nu}{2} \right) \right], \quad (3.9)$$

where $q_{0,i}$ and $q_{1,i}$ are linear combinations of the translational heat flux $q_{t,i}$ and rotational heat flux $q_{r,i}$ designed specifically to recover heat flux relaxation rates:

$$q_{0,i} = \frac{Z_{\text{rot}}}{Z_{\text{rot}} - 1} \left(\left(\frac{1}{3} - \frac{\frac{T_r}{T_t}(\omega - 1) - (\omega - 2)}{3Z_{\text{rot}}} \right) q_{t,i} + \frac{\left(\frac{T_r}{T_t}(\nu - 1) - (\nu - 2) \right)}{2Z_{\text{rot}}} q_{r,i} \right),$$

$$q_{1,i} = Z_{\text{rot}} \left(\frac{\frac{T_t}{T_r}(\omega - 1) - (\omega - 2)}{5Z_{\text{rot}}} q_{t,i} + \left(1 - \frac{5\nu}{2(7 - 2\omega)} - \frac{3 \left((\nu - 1) - (\nu - 2) \frac{T_t}{T_r} \right)}{10Z_{\text{rot}}} \right) q_{r,i} \right). \quad (3.10)$$

The new reference distribution function is constructed around the equilibrium distribution and orthogonal polynomials in thermal velocity C_i , rotational energy ϵ , and their corresponding moments $q_{0,i}$, $q_{1,i}$. To achieve practical application, we now detail the determination of parameters τ_t , Z_{rot} , $q_{0,i}$, $q_{1,i}$, and examine both the microscopic relaxation processes and the macroscopic transport coefficients of the new kinetic model equation.

3.2.1. Relaxation of pressure deviator

Regarding pressure and the pressure tensor relaxations, multiplying the collision term in the kinetic equation Eq. (3.7) by $mC^2/3$ and $mC_i C_j$, and integrating over the thermal velocity \mathbf{C} and the rotational energy ϵ yields:

$$\frac{\partial p_t}{\partial t} = \frac{p - p_t}{Z_{\text{rot}} \tau_t}, \quad (3.11)$$

$$\frac{\partial p_{ij}}{\partial t} = \frac{p_t \delta_{ij} - p_{ij}}{\tau_t} + \frac{p \delta_{ij} - p_t \delta_{ij}}{Z_{\text{rot}} \tau_t}. \quad (3.12)$$

The relaxation rates for the pressure deviator $\partial p_{\langle ij \rangle} = p_{ij} - p\delta_{ij}$ can be derived from Eqs. (3.11) and (3.12) as follows:

$$\frac{\partial p_{\langle ij \rangle}}{\partial t} = -\frac{p_{\langle ij \rangle}}{\tau_t}. \quad (3.13)$$

To recover accurate relaxation rates for the pressure deviator, the relaxation time τ_t employed in the kinetic model equations should be determined according to the pressure deviator relaxation Eq. (2.65) derived previously. Specifically, taking the results of the VHS model as an example, the relaxation time τ_t is given by:

$$\tau_t = \frac{15}{4^{2-\omega} d_{\text{ref}}^2 g_{\text{ref}}^{2\omega-1} n \left(\frac{kT_t}{m} \right)^{1-\omega} \sqrt{\pi} \Gamma \left[\frac{9}{2} - \omega \right]}. \quad (3.14)$$

Moreover, it is essential to verify the accuracy of the shear viscosity while ensuring the correct recovery of the pressure deviator relaxation rate. The shear viscosity for the kinetic model equation can be derived via the C-E expansion as (see Appendix B):

$$\mu = p_t \tau_t. \quad (3.15)$$

Comparison with the result derived from the Pullin model, Eq. (2.87), demonstrates that correctly recovering the pressure tensor relaxation rate ensures the accuracy of the model's shear viscosity.

3.2.2. Relaxation of energy

The relaxation process of energy can be described by the temperature relaxation rate. The translational and rotational temperature relaxation rates can be obtained by multiplying the collision term in the kinetic equation Eq. (3.7) by $mC^2/3nk$ and $2\epsilon/vnk$, and integrating over the thermal velocity C and the rotational energy ϵ :

$$\frac{\partial T_t}{\partial t} = \frac{T - T_t}{Z_{\text{rot}} \tau_t}, \quad (3.16)$$

$$\frac{\partial T_r}{\partial t} = \frac{T - T_r}{Z_{\text{rot}} \tau_t}. \quad (3.17)$$

Based on the previously derived temperature relaxation rates Eq. (2.63) and Eq. (2.64), adjusting the rotational collision number Z_{rot} enables the kinetic model to accurately describe the relaxation processes of translational and rotational energies. Specifically, the rotational collision number under the VHS model is adopted as follows:

$$Z_{\text{rot}} = \frac{(7 - 2\omega)(\nu\phi + \eta\psi)}{5(3 + \nu)\phi\psi}. \quad (3.18)$$

Furthermore, since the bulk viscosity coefficient μ_b fundamentally originates from dissipative effects during translational-rotational energy exchange, the correctly recovered energy relaxation rates naturally should ensure the accuracy of the bulk viscosity coefficient. This correspondence is rigorously established through C-E expansion (see Appendix B). The bulk viscosity of the kinetic model equation can be expressed as:

$$\mu_b = \frac{2\nu}{3(3 + \nu)} Z_{\text{rot}} \mu. \quad (3.19)$$

By comparison with the bulk viscosity derived from the Pullin model Eq. (2.88), this demonstrates that the kinetic model equation can recover the correct bulk viscosity provided accurate temperature relaxation is maintained.

3.2.3. Relaxation of heat flux

For the relaxation of heat flux in the kinetic model equation, multiplying the collision term in the kinetic equation Eq. (3.7) by $mC^2C_i/2$ and ϵC_i , then integrating over thermal velocity C_i and rotational energy ϵ to obtain translational and rotational heat flux relaxation rates:

$$\frac{\partial q_{t,i}}{\partial t} = \frac{1}{\tau_t} \left(\frac{Z_{\text{rot}} - 1}{Z_{\text{rot}}} q_{0,i} - q_{t,i} \right), \quad (3.20)$$

$$\frac{\partial q_{r,i}}{\partial t} = \frac{1}{\tau_t} \left(\frac{1}{Z_{\text{rot}}} q_{1,i} - q_{r,i} \right). \quad (3.21)$$

where $q_{0,i}$ and $q_{1,i}$ are the free parameters that serve to restore the correct thermal conductivity. The analytical expressions Eqs. (2.66)-(2.67) for the relaxation rates of translational and rotational heat fluxes have been previously derived from the Pullin equation. Using the heat flux relaxation framework in Eq. (2.83), for brevity, the free parameters $q_{0,i}$ and $q_{1,i}$ can be solved as follows:

$$\begin{bmatrix} q_{0,i} \\ q_{1,i} \end{bmatrix} = \begin{bmatrix} Z_{\text{rot}} & -Z_{\text{rot}} \\ \frac{Z_{\text{rot}} - 1}{Z_{\text{rot}}} (1 - A_{tt}) & \frac{Z_{\text{rot}}}{Z_{\text{rot}} - 1} A_{tr} \\ -Z_{\text{rot}} A_{rt} & Z_{\text{rot}} (1 - A_{rr}) \end{bmatrix} \begin{bmatrix} q_{t,i} \\ q_{r,i} \end{bmatrix}. \quad (3.22)$$

Specifically, under the VHS model, the heat flux relaxation coefficients A_{ij} in Eq. (3.22) adopt the result from Eq. (2.84). The corresponding free parameters can be written as:

$$\begin{aligned} q_{0,i} &= \frac{Z_{\text{rot}}}{Z_{\text{rot}} - 1} \left(\left(\frac{1}{3} - \frac{\frac{T_r}{T_t}(\omega - 1) - (\omega - 2)}{3Z_{\text{rot}}} \right) q_{t,i} + \frac{\left(\frac{T_r}{T_t}(\nu - 1) - (\nu - 2) \right)}{2Z_{\text{rot}}} q_{r,i} \right), \\ q_{1,i} &= Z_{\text{rot}} \left(\frac{\frac{T_t}{T_r}(\omega - 1) - (\omega - 2)}{5Z_{\text{rot}}} q_{t,i} + \left(1 - \frac{5\nu}{2(7 - 2\omega)} - \frac{3\left((\nu - 1) - (\nu - 2) \frac{T_t}{T_r} \right)}{10Z_{\text{rot}}} \right) q_{r,i} \right). \end{aligned} \quad (3.23)$$

Furthermore, to simultaneously verify the accuracy of thermal conductivity, we derived the translational thermal conductivity κ_t and rotational thermal conductivity κ_r from the kinetic model equation via the C-E expansion in the continuous limit:

$$\begin{bmatrix} \kappa_t \\ \kappa_r \end{bmatrix} = \frac{k\mu}{2m} \begin{bmatrix} A_{tt} & A_{tr} \\ A_{rt} & A_{rr} \end{bmatrix}^{-1} \begin{bmatrix} 5 \\ \nu \end{bmatrix}. \quad (3.24)$$

Result confirms that the κ_t and κ_r obtained from C-E expansion are identical to the thermal conductivity results theoretically derived from Pullin model. This conclusively demonstrates that when the model accurately describes the heat flux relaxation process (i.e., with correct relaxation coefficients A_{ij}), the accuracy of thermal conductivities is ensured.

At this stage, all free parameters in the new kinetic model are determined. The examination of the relaxation rates and transport coefficients shows that, while ensuring the accuracy of the relaxation rates, the transport coefficients naturally match those in Pullin model.

This demonstrates that kinetic modeling based on relaxation rates is more complete. The new kinetic model is founded on theoretically derived relaxation rates, thereby achieving more accurate relaxation processes compared to Rykov's model. Moreover, by employing relaxation-rate-based kinetic modeling, the theoretically derived relaxation rates not only serve for theoretical analysis but are also applied to the simulation and prediction of actual flows.

4. Validation of the kinetic model

We solve the newly developed kinetic model (hereafter referred to as “the kinetic model”) using the unified gas kinetic scheme (UGKS) method, which employs a discrete velocity space to capture the non-equilibrium distribution function, and we perform numerical simulations for classical test cases. To validate the kinetic model, the numerical results are compared with the results from the Rykov model and with DSMC data. Notably, in DSMC simulations employing the VHS model, the temperature relaxation process is described by:

$$\frac{\partial T_r}{\partial t} = \frac{30(T - T_r)}{(7 - 2\omega)(5 - 2\omega)Z_{r,DSMC}}. \quad (4.1)$$

While the kinetic model strictly follows the Jeans-Landau relaxation equation, for the convenience of model validation, it is necessary to clarify the relationship between the rotational collision numbers in DSMC and the kinetic model:

$$Z_{rot,DSMC} = \frac{30}{(7 - 2\omega)(5 - 2\omega)}Z_{rot}. \quad (4.2)$$

4.1. Unified gas-kinetic scheme

4.1.1. General framework of unified gas-kinetic scheme

The gas-kinetic relaxation model equation adopted in the UGKS can be expressed in the following form:

$$\frac{\partial f}{\partial t} + \mathbf{c} \cdot \frac{\partial f}{\partial \mathbf{x}} = \frac{g - f}{\tau_t}, \quad (4.3)$$

where g is the equilibrium distribution function. The collision term in the new kinetic model can be recast into the general form on the right-hand side of Eq. (4.3), where $g = g_{t,new} + g_{r,new}$. The construction of UGKS for diatomic gas is based on reduced model equations in the classical finite volume framework. By discretizing the model equation Eq. (4.3) at time t_{n+1} by a backward Euler method, we can obtain the discrete governing equation:

$$f_i^{n+1} - f_i^n + \frac{\Delta t}{|V_i|} F_i^{n+1/2} = \frac{\Delta t}{2} \left(\frac{g_i^{n+1} - f_i^{n+1}}{\tau_{t,i}^{n+1}} + \frac{g_i^n - f_i^n}{\tau_{t,i}^n} \right). \quad (4.4)$$

The V_i is the volume of cell i , and \mathbf{c}_k is the discrete particle velocity space. $\Delta t = t_{n+1} - t_n$ is the time step. The microscopic flux $F_i^{n+1/2}$ can be calculated as follows:

$$F_i^{n+1/2} = \sum_j \mathbf{c}_k \cdot \mathbf{A}_i^j f \left(\mathbf{x}_i^j, \mathbf{c}_k, t_{n+1/2} \right), \quad (4.5)$$

where \mathbf{A}_i^j is the outward normal vector of the j th face of cell i with an area of $|\mathbf{A}_i^j|$, and \mathbf{x}_i^j is the center of this face. In this work, a simplified multi-scale flux is adopted. By integrating relaxation model equation Eq. (4.3) along the characteristic line (in the direction

of particle velocity) from t_n to $t_{n+1/2}$, the interface distribution function $f(\mathbf{x}_i^j, \mathbf{c}_k, t_{n+1/2})$ can be expressed as:

$$f(\mathbf{x}_i^j, \mathbf{c}_k, t_{n+1/2}) = \frac{2\tau^{n+1/2}}{2\tau^{n+1/2} + \Delta t} f\left(\mathbf{x}_i^j - \mathbf{c}_k \frac{\Delta t}{2}, \mathbf{c}_k, t_n\right) + \frac{\Delta t}{2\tau^{n+1/2} + \Delta t} g(\mathbf{x}_i^j, \mathbf{c}_k, t_{n+1/2}) \quad (4.6)$$

where the free transport distribution (representing the microscopic mechanism) and equilibrium distribution (representing the macroscopic mechanism) are coupled rationally, resulting in the multi-scale property of the present UGKS. Take the moment of Eq (4.6) and we can directly obtain the macroscopic flow variable $\mathbf{W}(\mathbf{x}_i^j, \mathbf{c}_k, t_{n+1/2})$, which is used to evaluate the equilibrium state $g(\mathbf{x}_i^j, \mathbf{c}_k, t_{n+1/2})$.

To perform the microscopic evolution for obtaining f_i^{n+1} , the equilibrium state g_i^{n+1} is required. The equilibrium distribution g depends on the macroscopic variables $\mathbf{W} = (\rho, \rho\mathbf{U}, \rho E, \rho E_t, \rho E_r)^T$, where ρ , $\rho\mathbf{U}$, ρE , ρE_t , and ρE_r are the density, momentum, total energy, translational energy, and rotational energy, respectively. Therefore, by taking the moments of Eq. (4.4), the macroscopic evolution equation can be obtained:

$$\mathbf{W}_i^{n+1} = \mathbf{W}_i^n - \frac{\Delta t}{|V_i|} \int \psi F_i^{n+1/2} d\mathbf{c}_k + \frac{1}{2} (S_i^{n+1} + S_i^n), \quad (4.7)$$

where $\int \psi F_i^{n+1/2} d\mathbf{c}_k$ is the macroscopic flux, ψ is the collision invariant, and S is the source term. Once the macroscopic variables are updated, the implicit equation Eq. (4.4) can be explicitly expressed as:

$$f_i^{n+1} = \left(1 + \frac{\Delta t}{2\tau_i^{n+1}}\right)^{-1} \left[f_i^n - \frac{\Delta t}{|V_i|} F_i^{n+1/2} + \frac{\Delta t}{2} \left(\frac{g_i^{n+1}}{\tau_i^{n+1}} + \frac{g_i^n - f_i^n}{\tau_i^n} \right) \right]. \quad (4.8)$$

In summary, the calculation procedure of the UGKS with simplified multi-scale numerical flux from time level t_n to t_{n+1} is summarized in the following steps:

Step 1. Given the initial macroscopic flow variables \mathbf{W}_i^0 and calculate the equilibrium distribution functions g_i^{n+1} .

Step 2. Compute the micro-flux $F_i^{n+1/2}$ across the cell interface of control volumes.

(a) Calculate the macroscopic flow variables $\mathbf{W}(\mathbf{x}_i^j, \mathbf{c}_k, t_{n+1/2})$ by taking the moment of Eq. (4.6).

(b) Calculate the equilibrium distribution functions $g(\mathbf{x}_i^j, \mathbf{c}_k, t_{n+1/2})$ from the macroscopic flow variables $\mathbf{W}(\mathbf{x}_i^j, \mathbf{c}_k, t_{n+1/2})$.

(c) Calculate the distribution functions $f(\mathbf{x}_i^j, \mathbf{c}_k, t_{n+1/2})$ at the cell interface using Eq. (4.6).

(d) Calculate the micro-flux $F_i^{n+1/2}$ using Eq. (4.5).

Step 3. Update the macroscopic flow variables \mathbf{W}_i^{n+1} in each cell i according to Eq. (4.7).

Step 4. Update the distribution function f_i^{n+1} in each cell i according to Eq. (4.8).

Therefore, in the UGKS, the gas-kinetic relaxation model equations can be solved by sequentially updating the macroscopic variables and distribution functions respectively.

4.1.2. Reduced distribution function

Because of the quasi-linear nature common to BGK-type relaxation model equations, their dimensionality can often be reduced when energy is treated continuously, achieving lower

computational cost. For the reader's convenience, the following reduced distribution functions are employed: $R_1 = \int f(t, \mathbf{x}, \mathbf{c}, \epsilon) d\epsilon$, $R_2 = \int \epsilon f(t, \mathbf{x}, \mathbf{c}, \epsilon) d\epsilon$. This effectively reduces solution complexity. Eliminating the rotational energy variable decreases computational memory requirements and costs. Multiplying Eq. (3.7) by 1 and ϵ , then integrating over ϵ from $(0, \infty)$, yields equations for the reduced distribution functions R_1 and R_2 :

$$\frac{\partial R_1}{\partial t} + \mathbf{c} \cdot \frac{\partial R_1}{\partial \mathbf{x}} = \frac{R_{1,t} - R_1}{\tau_t} + \frac{R_{1,r} - R_{1,t}}{Z_{\text{rot}} \tau_t}, \quad (4.9)$$

$$\frac{\partial R_2}{\partial t} + \mathbf{c} \cdot \frac{\partial R_2}{\partial \mathbf{x}} = \frac{R_{2,t} - R_2}{\tau_t} + \frac{R_{2,r} - R_{2,t}}{Z_{\text{rot}} \tau_t}, \quad (4.10)$$

where the reference reduced distribution functions $R_{1,t}$, $R_{1,r}$, $R_{2,t}$ and $R_{2,r}$ are given by:

$$R_{1,t}(t, \mathbf{x}, \mathbf{c}) = E_t(T_t) \left[1 + \frac{2}{5nm} \left(\frac{m}{kT_t} \right)^2 q_{0,i} C_i \left(\frac{m}{2kT_t} C^2 - \frac{5}{2} \right) \right], \quad (4.11)$$

$$R_{1,r}(t, \mathbf{x}, \mathbf{c}) = E_t(T_t), \quad (4.12)$$

$$R_{2,t}(t, \mathbf{x}, \mathbf{c}) = E_t(T_t) \frac{\nu k T_r}{2} \left[1 + \frac{2}{5nm} \left(\frac{m}{kT_t} \right)^2 q_{0,i} C_i \left(\frac{m}{2kT_t} C^2 - \frac{5}{2} \right) \right], \quad (4.13)$$

$$R_{2,r}(t, \mathbf{x}, \mathbf{c}) = E_t(T_t) \frac{\nu k T}{2} \left[1 + \frac{2}{\nu nm} \left(\frac{m}{kT} \right)^2 q_{1,i} C_i \right]. \quad (4.14)$$

Finally, the macroscopic quantities are calculated as:

$$\begin{aligned} n &= \int R_1 d\mathbf{c}, \quad \mathbf{U} = \int R_1 \frac{\mathbf{c}}{n} d\mathbf{c}, \quad p_{ij} = \int R_1 m C_i C_j d\mathbf{c}, \quad T_t = \int R_1 \frac{m C^2}{3nk} d\mathbf{c}, \\ T_r &= \int R_2 \frac{2}{\nu nk} d\mathbf{c}, \quad \mathbf{q}_t = \int R_1 \frac{1}{2} m C^2 \mathbf{C} d\mathbf{c}, \quad \mathbf{q}_r = \int R_2 \mathbf{C} d\mathbf{c}. \end{aligned} \quad (4.15)$$

4.2. Dimensionless analysis

In the calculations, the dimensionless quantities normalized by the reference length, density, temperature, and velocity are introduced as follows:

$$L_{\text{ref}} = L_c, \quad \rho_{\text{ref}} = \rho_\infty, \quad T_{\text{ref}} = T_\infty, \quad U_{\text{ref}} = \sqrt{2RT_{\text{ref}}}, \quad (4.16)$$

where L_c is the characteristic length scale of the flow, ρ_∞ , T_∞ are the density and temperature of the free-stream, respectively. Then the following dimensionless quantities can be obtained:

$$\begin{aligned} \hat{L} &= \frac{L}{L_{\text{ref}}}, \quad \hat{\rho} = \frac{\rho}{\rho_{\text{ref}}}, \quad \hat{T} = \frac{T}{T_{\text{ref}}}, \quad \hat{U} = \frac{U}{U_{\text{ref}}}, \\ \hat{t} &= \frac{t}{L_{\text{ref}} U_{\text{ref}}^{-1}}, \quad \hat{n} = \frac{n}{L_{\text{ref}}^{-3}}, \quad \hat{m} = \frac{m}{\rho_{\text{ref}} L_{\text{ref}}^3}, \quad \hat{\mu} = \frac{\mu}{\rho_{\text{ref}} U_{\text{ref}} L_{\text{ref}}}, \\ \hat{p} &= \frac{p}{\rho_{\text{ref}} U_{\text{ref}}^2}, \quad \hat{\mathbf{q}} = \frac{\mathbf{q}}{\rho_{\text{ref}} U_{\text{ref}}^3}, \quad \hat{\tau} = \frac{\tau}{L_{\text{ref}} U_{\text{ref}}^{-1}}. \end{aligned} \quad (4.17)$$

Finally, a complete dimensionless system is obtained. In the following, all variables without the "hat" are nondimensionalized by default, unless stated otherwise.

4.3. 0-Dimensional homogenous relaxation

In the zero-dimensional homogeneous relaxation case, the flow field is spatially uniform, allowing us to neglect the transport terms on the left-hand side of the model equation and focus exclusively on the effects of intermolecular collisions. This configuration is particularly suitable for investigating non-equilibrium relaxation processes in flow fields. Given the spatial homogeneity, the governing equation simplifies to:

$$\frac{\partial f}{\partial t} = \frac{g_t - f}{\tau_t} + \frac{g_r - g_t}{Z_{\text{rot}} \tau_t}. \quad (4.18)$$

In this zero-dimensional case, all particles are considered to reside within a single computational cell. To facilitate observation of the relaxation process, the flow field is initialized in a non-equilibrium state, evolving toward equilibrium through collisional relaxation. We initialize the particle distribution using two distinct groups following Maxwellian distributions, mimicking the strongly non-equilibrium velocity distribution functions found in shock waves. The macroscopic variables for these two initial Maxwellian distributions, corresponding to Mach numbers $\text{Ma} = 8$, are specified as follows:

$$\text{Ma} = 8 \quad \begin{cases} \rho_A = 4.65 \times 10^{-6} \text{ kg/m}^3, U_A = 2695.2 \text{ m/s}, T_A = 273 \text{ K} \\ \rho_B = 4.65 \times 10^{-6} \text{ kg/m}^3, U_B = 336.9 \text{ m/s}, T_B = 2730 \text{ K} \end{cases} \quad (4.19)$$

In this case study, we solve both the kinetic model and Rykov model with rotational collision number fixed at $Z_{\text{rot,DSMC}} = 3$. To examine the impact of collision models on relaxation processes, we implement three distinct molecular interaction models: hard sphere molecules ($\omega = 0.5$), nitrogen molecules ($\omega = 0.74$), Maxwell molecules ($\omega = 1$). Parallel DSMC simulations are performed with 10^5 simulator particles to minimize statistical fluctuations. Crucially, the collision number of the kinetic model is determined through Eq. (4.2). Figure 4 presents zero-dimensional homogeneous relaxation simulations within normal shock wave at $\text{Ma} = 8$, comparing results from the new kinetic model, Rykov model and DSMC simulations. For temperature relaxation, the kinetic model exhibits excellent agreement with DSMC data, confirming its accuracy in energy exchange processes; regarding heat flux relaxation, the kinetic model maintains consistent alignment with DSMC across all three collision models (hard sphere, nitrogen, Maxwell), while Rykov model shows varying degrees of deviation attributable to its neglect of translational-rotational heat flux coupling. The new model overcomes this limitation by explicitly incorporating cross-coupling effects, non-equilibrium intensity dependence, and molecular collision model sensitivity into heat flux relaxation dynamics.

4.4. normal shock wave

Normal shock wave represents prevalent phenomena in high-speed flows and constitute a focal point in non-equilibrium flow research. The normal shock wave manifests as a strong discontinuity, with its thickness typically spanning approximately 20 molecular mean free paths. Gas compression within confined space induces severe non-equilibrium effects, particularly intense energy exchange processes for molecular gases within the normal shock wave. Consequently, this scenario serves as both a benchmark and challenging test case for numerical methods predicting rarefied and multiscale flows. The Rankine-Hugoniot relations

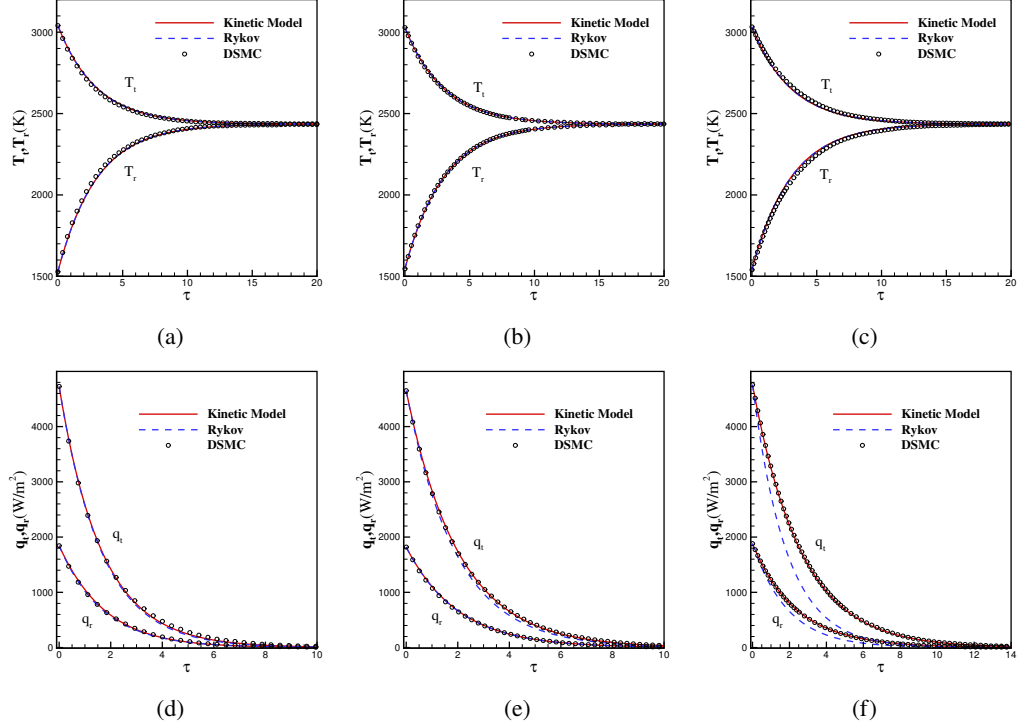


Figure 4: Time evolution of temperature and heat flux during zero-dimensional homogeneous relaxation from a strongly non-equilibrium initial state corresponding to a $\text{Ma}=8$ normal shock. (a)-(c) are the temperature profiles with HS, VHS and Maxwell molecules. (d)-(f) are the heat flux profiles with HS, VHS and Maxwell molecules.

prescribe the inlet and outlet boundary conditions as follows:

$$\begin{aligned} \frac{\rho_2}{\rho_1} &= \frac{(\gamma + 1) \text{Ma}^2}{(\gamma - 1) \text{Ma}^2 + 2}, \\ \frac{T_2}{T_1} &= \frac{\left(1 + \frac{\gamma - 1}{2} \text{Ma}^2\right) \left(\frac{2\gamma}{\gamma - 1} \text{Ma}^2 - 1\right)}{\text{Ma}^2 \left(\frac{2\gamma}{\gamma - 1} + \frac{\gamma - 1}{2}\right)}, \end{aligned} \quad (4.20)$$

The subscripts “1” and “2” denote variables upstream and downstream of the normal shock wave, respectively, with specific heat ratio $\gamma = 5/3$ and inlet Mach number Ma . Three sets of numerical simulations were conducted on nitrogen normal shock wave at Mach numbers 1.53, 4.0, and 7.0. Viscosity is calculated using the VHS model. For all cases, the pre-shock density $\rho_1 = 1.7413 \times 10^{-2} \text{kg/m}^3$ and temperature $T_1 = 226.149 \text{K}$ remain identical. Dimensionless quantities are adopted in computations. Reference values are defined as: $L_{\text{ref}} = \lambda_1$, $\rho_{\text{ref}} = \rho_1$, $T_{\text{ref}} = T_1$, $U_{\text{ref}} = \sqrt{2kT_{\text{ref}}/m}$ where the mean free path λ_1 is computed by:

$$\lambda = \frac{2\mu (7 - 2\omega) (5 - 2\omega)}{15n(2\pi mkT)^{1/2}}. \quad (4.21)$$

The computational domain spans $[-100\lambda_1, 100\lambda_1]$ discretized with a uniform grid of 500

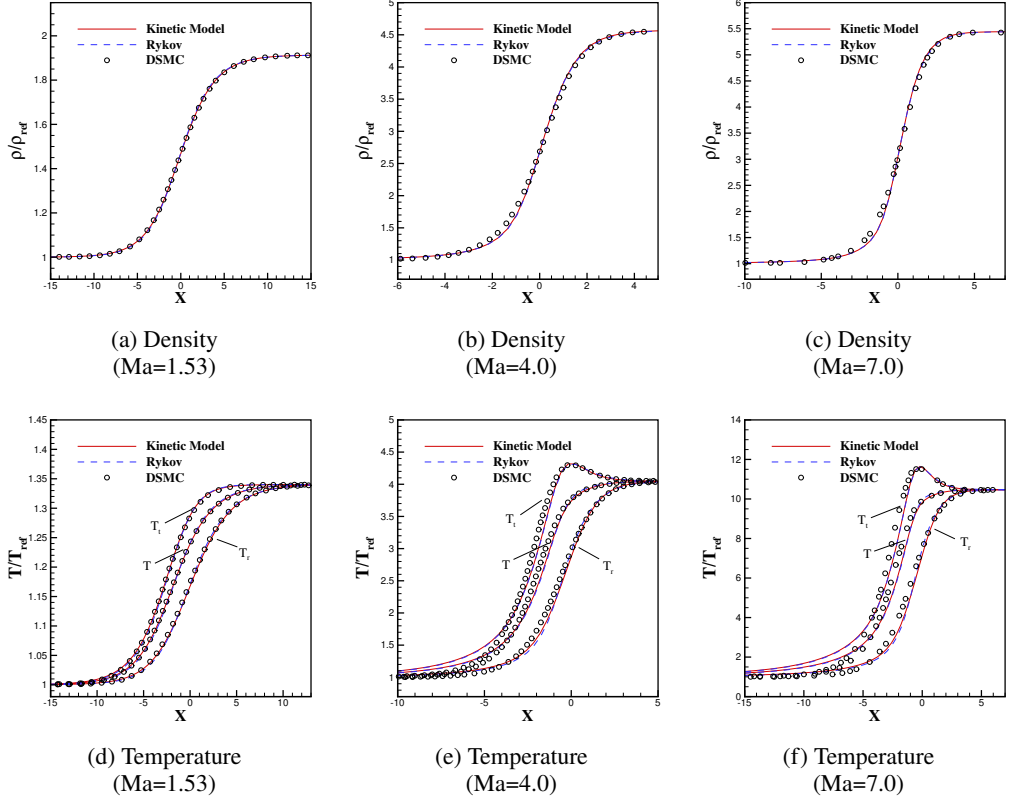


Figure 5: Profiles for nitrogen gas shock structure at $\text{Ma} = 1.53, 4.0, 7.0$. (a)-(c) are the density distribution at $\text{Ma} = 1.53, 4.0, 7.0$. (d)-(f) are the temperature distribution at $\text{Ma} = 1.53, 4.0, 7.0$.

cells ($\Delta x = 0.5\lambda_1$). Velocity space is discretized into 401 uniformly distributed points within $[-18, 18]$, with numerical integration carried out via the Newton-Cotes quadrature method.

In this case study, we solve both the kinetic model and the Rykov model, setting the viscosity index $\omega = 0.72$ and rotational collision number $Z_{\text{rot}} = 2.4$ to benchmark against DSMC results from (Liu *et al.* 2014). Figure 5 compares density and temperature distributions, revealing excellent agreement between the kinetic model and DSMC for density profiles across Mach numbers. While temperature distributions align well with DSMC at low Mach numbers, the kinetic model exhibits premature upstream temperature rise at high Mach numbers, primarily due to insufficient relaxation of backstreaming high-velocity particles from downstream—a discrepancy addressable through relaxation time modifications for high-energy particles (Xu *et al.* 2021). Subsequently, we adjust parameters to $\omega = 0.74$ and $Z_{\text{rot}} = 2.6671$ to compare heat flux distributions with (Zeng *et al.* 2022) (Figure 6). Translational heat fluxes show essential agreement with Rykov model simulations, whereas rotational heat flux peaks exhibit smaller absolute magnitudes and upstream positional shifts relative to Rykov. Compared to DSMC, the kinetic model accurately captures translational heat flux peaks but underpredicts rotational heat flux magnitudes.

4.5. Planar Couette flow

This case examines planar Couette flow between two parallel plates separated by distance L , both maintained at temperature T_0 . The lower plate moves with velocity $U = -V_m$, while

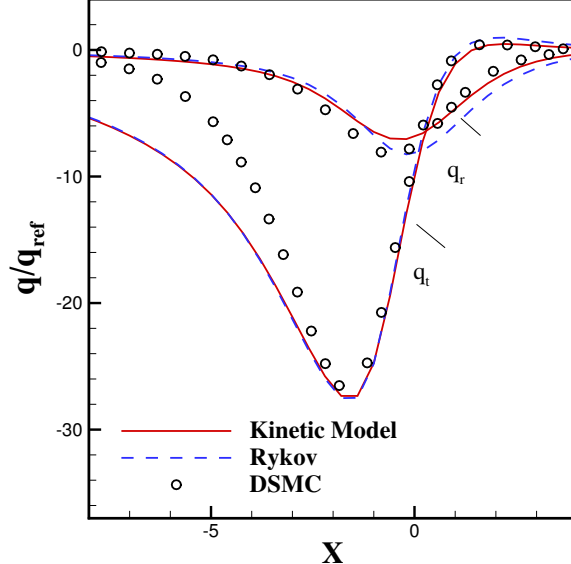


Figure 6: Heat flux distribution for nitrogen gas shock structure at $\text{Ma} = 7.0$.

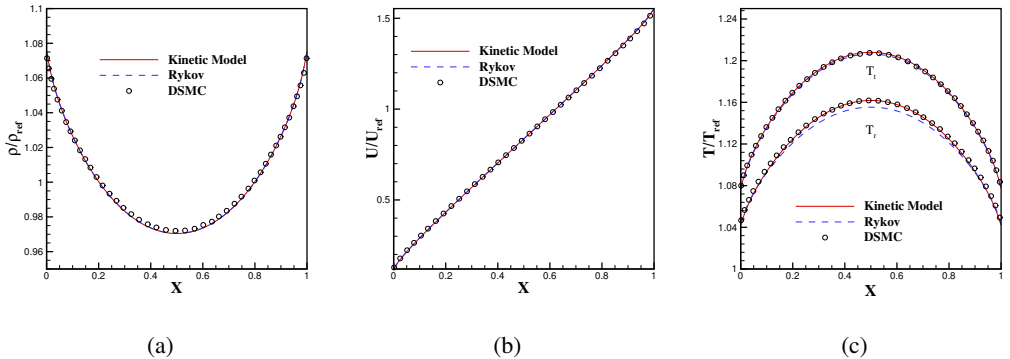


Figure 7: Profiles for planar Couette flows of nitrogen at $\text{Kn}=0.1$. (a) density, (b) velocity and (c) temperature.

the upper plate moves in the opposite direction, with diffuse reflection boundary conditions applied. Nitrogen gas is simulated using the VHS model with viscosity index $\omega = 0.74$. For the $\text{Kn} = 0.1$ condition, the rotational collision number is set to $Z_{\text{rot}} = 3.2384$ in the kinetic and Rykov model solutions, and to $Z_{\text{rot}} = 5$ in DSMC simulations according to Eq. (4.2). Figure 7 compares density, velocity, and temperature distributions between the plates. Results demonstrate excellent agreement between the kinetic model predictions and DSMC for all macroscopic quantities. The Rykov model shows nearly identical density and velocity profiles to the kinetic model but underpredicts rotational temperature distributions near the centerline. This discrepancy may arise because the translational heat flux slightly exceeds the rotational heat flux in this case, whereas the Rykov model's neglect of the coupling between these heat fluxes leads to an underprediction of the rotational heat flux, consequently resulting in a lower peak rotational temperature.

4.6. Lid-driven cavity flow

The lid-driven cavity flow benchmark serves as an excellent test case for validating the capability of proposed model to accurately simulate viscous effects. This study simulates cavity flows across a wide range of Knudsen numbers (0.075, 1, 10) to verify the model's effectiveness. For nitrogen under standard conditions, the reference lengths $L = 8.27 \times 10^{-7} \text{ m}$, $6.2 \times 10^{-8} \text{ m}$, $6.2 \times 10^{-9} \text{ m}$ corresponding to Knudsen numbers of $\text{Kn} = 0.075, 1, 10$ respectively. The cavity features walls of length L , with the top wall moving rightward at constant velocity U_w while other walls remain stationary, all employing diffuse reflection boundary conditions. Nitrogen gas is simulated using a VHS molecular model with viscosity index $\omega = 0.74$ and rotational collision number $Z_{\text{rot}} = 5$. All walls and the initial flow field maintain 273 K temperature, with the lid velocity set at 54.7 m/s and speed of sound at 336.9 m/s.

We solve both the current kinetic model and Rykov model using the UGKS method for Knudsen numbers 0.075, 1, and 10. Figure 8 compares centerline velocity profiles, demonstrating the kinetic model's accuracy in predicting flow velocities across rarefaction regimes, confirming proper recovery of viscous effects. Figure 9 presents the translational and rotational temperature distributions, with the kinetic model's results shown as colored fields and the Rykov model's as white dashed lines. Comparative results show that while the translational temperature distributions essentially match Rykov's, the rotational temperatures exhibit discrepancies, with the kinetic model demonstrating more concentrated rotational energy. This concentration is analyzed by comparing the translational and rotational heat fluxes distributions in Figures 10-12. While both models agree well on the translational heat flux, a key difference emerges in the rotational component: the Rykov model's rotational heat flux always opposes the temperature gradient (defined as pointing from low to high temperature), whereas the kinetic model's displays a direction reversal that intensifies with the Knudsen number. This reversal occurs because the kinetic model incorporates coupling between the heat flux. The rotational heat flux is approximately two orders of magnitude smaller than the translational heat flux. Therefore, the influence of the rotational heat flux on the translational component is negligible. However, as the Knudsen number rises, the translational heat flux increases while the rotational heat flux decreases. According to the coupling mechanism outlined by the heat flux relaxation Equations (2.73)-(2.74), the translational heat flux exerts a stronger influence on the rotational component in more rarefied flows. Consequently, the rotational heat flux is pulled toward the direction of the counter-gradient translational heat flux. This mechanism enables more rotational heat flux in the kinetic model to flow from low- to high-temperature regions, leading to the more concentrated rotational temperature distribution shown in Figure 9. This difference underscores the importance of the heat flux coupling relaxation mechanism for accurate thermal flow prediction.

4.7. hypersonic flow past cylinder

In high-speed molecular gas flows past objects within rarefied environments, thermodynamic non-equilibrium arises not only from translational non-equilibrium (manifested as bimodal distributions and significant velocity slip) but also from disparities in translational and rotational temperatures within shock layers, boundary layers, and wake regions. While earlier studies emphasized shock and boundary layers, the wake region is in fact equally important and requires models to possess the ability to capture detailed flow information. To validate the kinetic model's reliability for high-speed flows, we solve both the current kinetic model and Rykov model using the UGKS method, comparing results against each other and against DSMC simulations. This study simulates hypersonic nitrogen flow ($\text{Ma} = 5$) past a cylinder

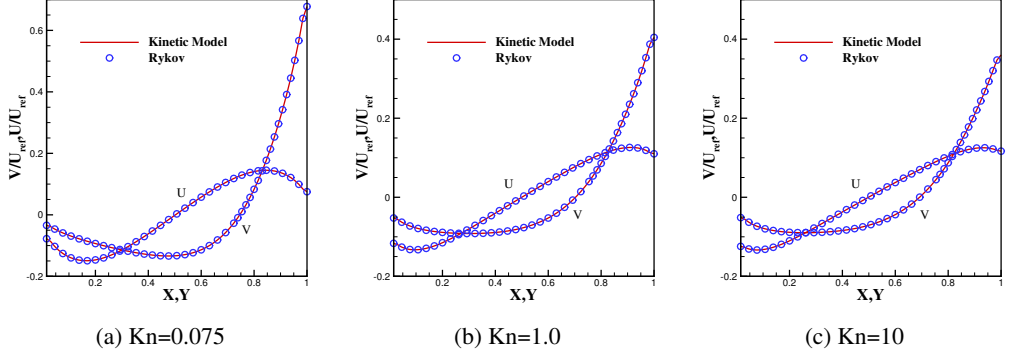


Figure 8: Velocity profiles of centerline in lid-driven cavity flows at $\text{Kn} = 0.075, 1.0$, and 10 .

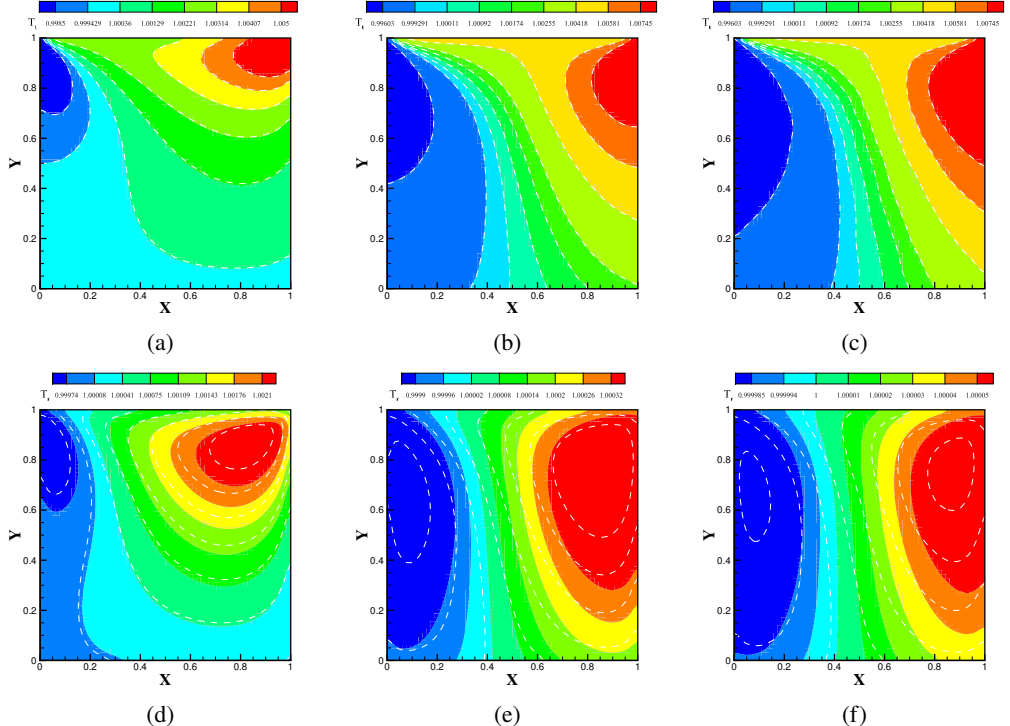


Figure 9: The contours of temperature in lid-driven cavity flows at $\text{Kn} = 0.075, 1.0$, and 10 . The white dash line: UGKS with Rykov model, color band: kinetic model. (a)-(c) are translational temperature at $\text{Kn} = 0.075, 1.0, 10$. (d)-(f) are rotational temperature at $\text{Kn} = 0.075, 1.0, 10$.

at Knudsen numbers ($\text{Kn} = 0.01, 0.1, 1$). The cylinder radius is $R_c = 0.5\text{m}$ with freestream temperature $T_\infty = 273\text{K}$. VHS molecular model ($\omega = 0.74$) is employed under isothermal wall conditions ($T_w = 273\text{K}$). Rotational collision numbers are set to $Z_{\text{rot}} = 3.5$ for the kinetic model and $Z_{\text{rot}} = 5.404$ for DSMC according to Eq. (4.2). Boundaries employ fully accommodated diffuse reflection (Cercignani *et al.* 1969) at walls, inlet and outlet.

Figures 14, 16, 18 present density, velocity, and temperature distributions along the

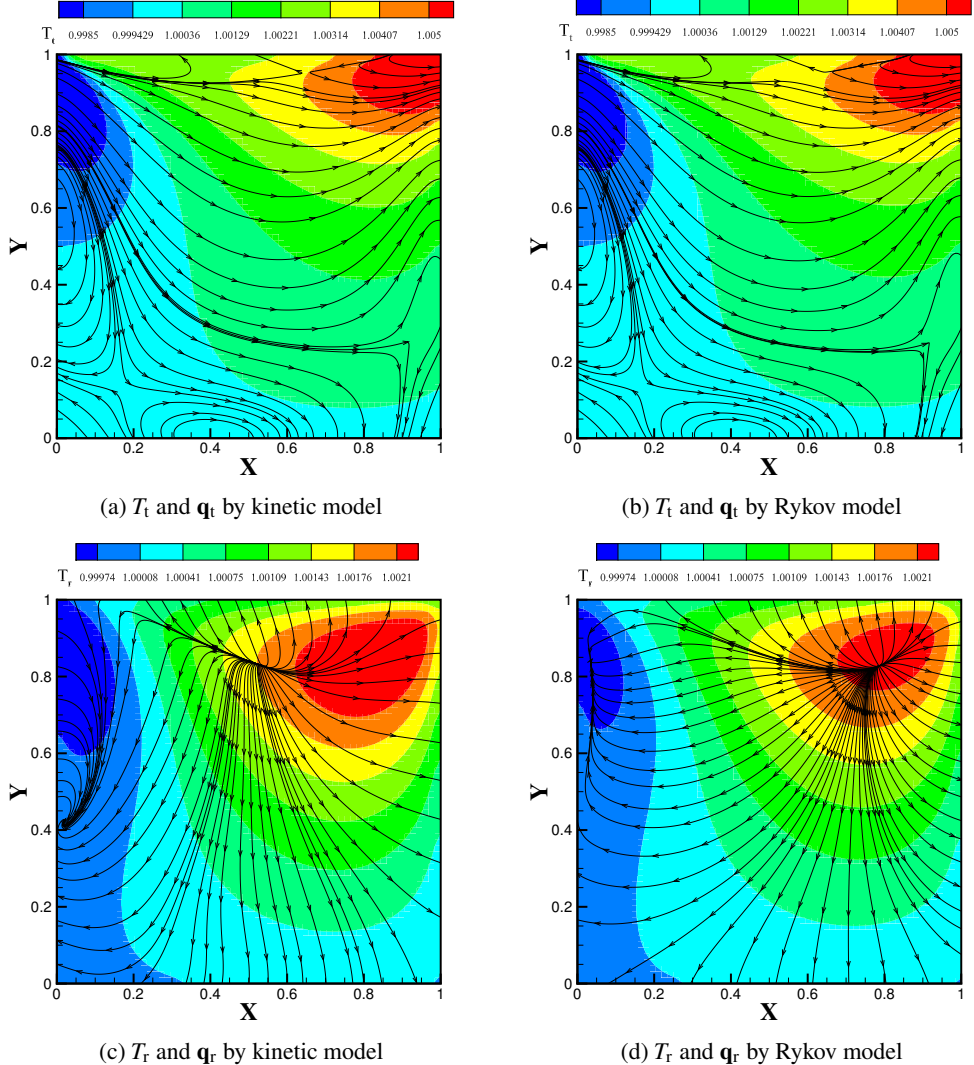


Figure 10: Comparison of the temperature fields (colored fields) and heat flux (black solid lines) in lid-driven cavity flows at $\text{Kn} = 0.075$. (a)-(b) are translational temperature and heat flux. (c)-(d) are rotational temperature and heat flux.

stagnation streamline for $\text{Kn} = 0.01, 0.1, 1$. The kinetic model shows essential agreement with Rykov simulations. Compared to DSMC results, density distributions match closely, while velocity profiles exhibit minor deviations. Temperature distributions display an early rise upstream of the shock, which is primarily attributed to insufficient relaxation of backstreaming high-energy particles from downstream. This limitation can be addressed by modifying the relaxation times for energetic particles (Xu *et al.* 2021). Figures 13, 15, 17 show distributions of normal stress, shear stress, and heat transfer coefficients on the cylinder surface. The kinetic model demonstrates good agreement with both Rykov and DSMC simulations, confirming its capability to accurately predict surface forces and heat transfer in high-speed flows.

In compressive flows, sufficient collisions make the coupling effect in heat flux relaxation

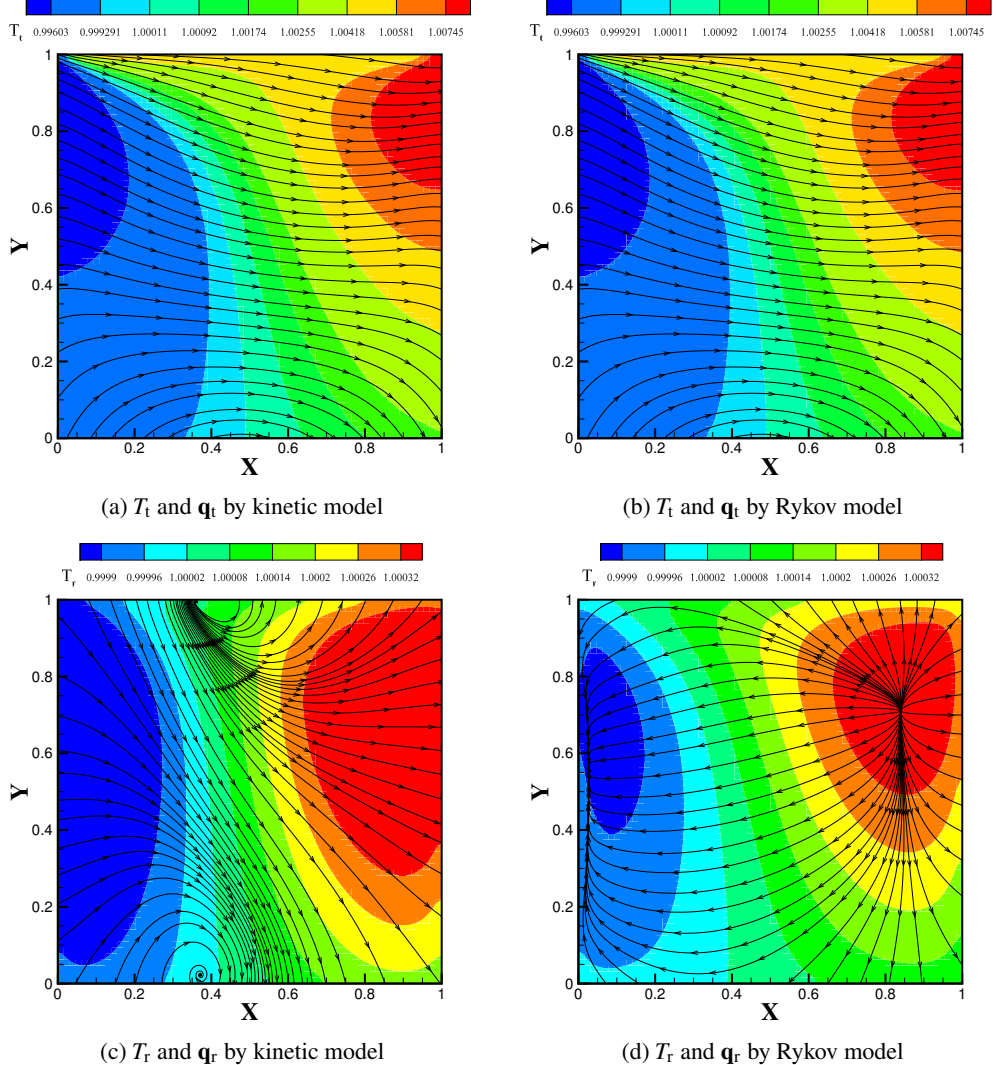


Figure 11: Comparison of the temperature fields (colored fields) and heat flux (black solid lines) in lid-driven cavity flows at $\text{Kn} = 1.0$. (a)-(b) are translational temperature and heat flux. (c)-(d) are rotational temperature and heat flux.

less evident in the flow field. However, in wake flows with insufficient collisions, the situation is markedly different. Figures 19, 20, 21 present the distributions of heat flux behind a cylinder at Knudsen numbers of 0.01, 0.1, and 1.0, respectively. The predictions of translational temperature and translational heat flux show good agreement between the kinetic and Rykov models, whereas discrepancies of varying degrees are observed for the rotational temperature and rotational heat flux. These differences in the rotational distributions become more pronounced as the degree of rarefaction increases. It is noteworthy that for the case of $\text{Kn} = 1.0$, the kinetic model exhibits a significant phenomenon wherein the rotational heat flux becomes aligned with the temperature gradient in parts of the flow field. For heat flux distributions in high Knudsen number flows, accurate description cannot be achieved through constitutive relations alone, as it requires simultaneous consideration of heat flux

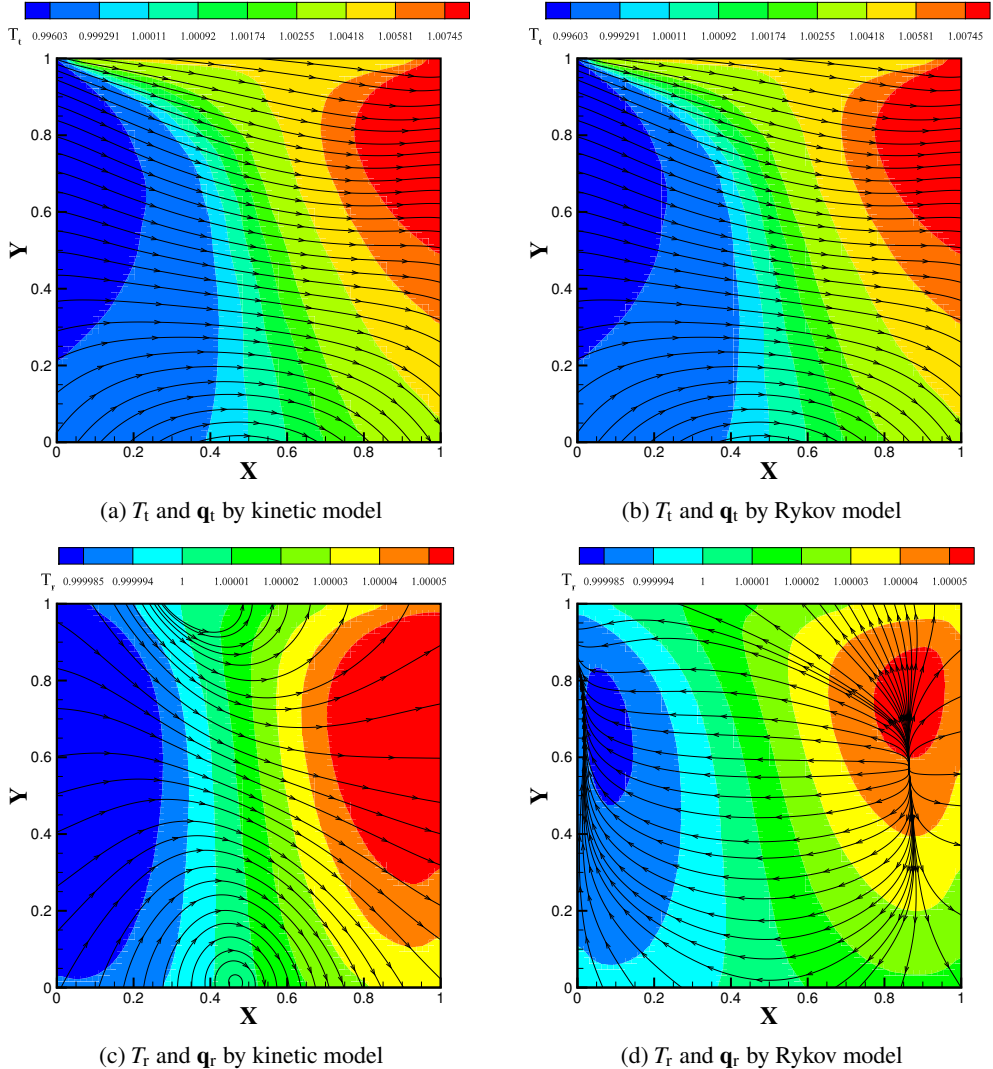


Figure 12: Comparison of the temperature fields (colored fields) and heat flux (black solid lines) in lid-driven cavity flows at $Kn = 10$. (a)-(b) are translational temperature and heat flux. (c)-(d) are rotational temperature and heat flux.

generation and transport. However, results in Figure 21 shows that the heat flux is nearly parallel to the isotherms of the temperature field, indicating that the heat flux in the wake region is primarily governed by thermal relaxation (generation) rather than thermal transport. Consequently, our analysis focuses on heat flux generation, i.e., the relaxation driven by molecular collisions. Similar to the Lid-driven cavity flow case, the differences in rotational heat flux may be attributed to the kinetic model's more comprehensive consideration of the coupling mechanism between the relaxation processes of translational and rotational heat fluxes, compared to the Rykov model. In the central wake region where differences arise, the dimensionless translational heat flux is on the order of 10^{-1} to 10^{-2} , while the rotational heat flux is on the order of 10^{-3} to 10^{-4} . As indicated by the relaxation formula Eqs. (2.73) and (2.74), the translational heat flux exerts a strong influence on the rotational

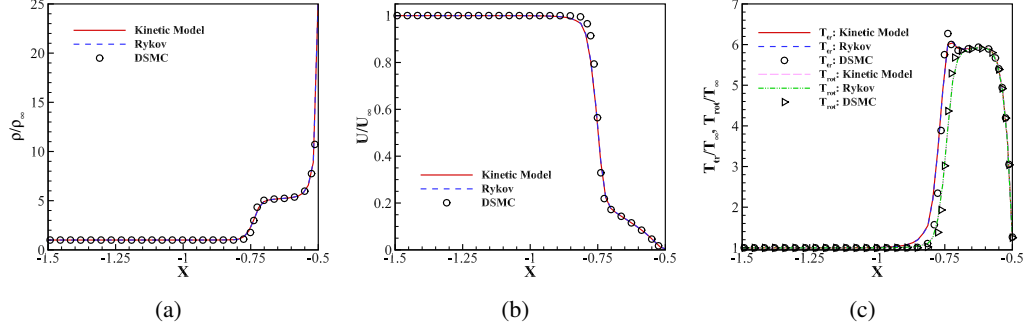


Figure 13: Comparison of the (a) density, (b) the velocity and (c) the translational and rotational temperatures along the forward stagnation line for the cylinder at $\text{Kn} = 0.01$.

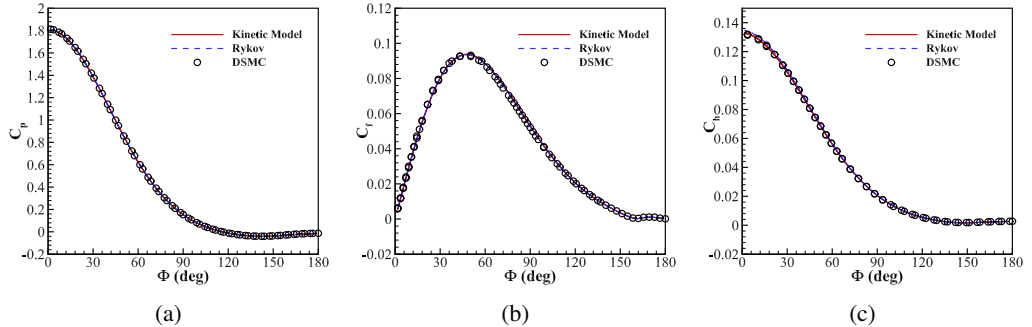


Figure 14: Comparisons of the (a) pressure, (b) shear stress, and (c) heat transfer coefficients at the wall surface of cylinder at $\text{Kn} = 0.01$.

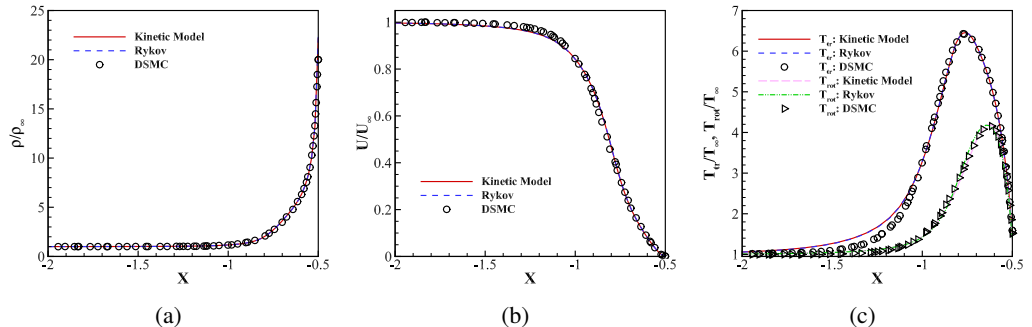


Figure 15: Comparison of the (a) density, (b) the velocity and (c) the translational and rotational temperatures along the forward stagnation line for the cylinder at $\text{Kn} = 0.1$.

component here, while the effect of the rotational on the translational component can be ignored. This coupling in the relaxation process ultimately leads to heat flux reversal within the wake. In summary, in rarefied flows where thermal relaxation mechanisms dominate, the influence of the translational-rotational heat flux relaxation coupling becomes more pronounced. Therefore, the kinetic model, established upon more accurate relaxation rates, is expected to yield superior results in thermal predictions for such flow conditions.

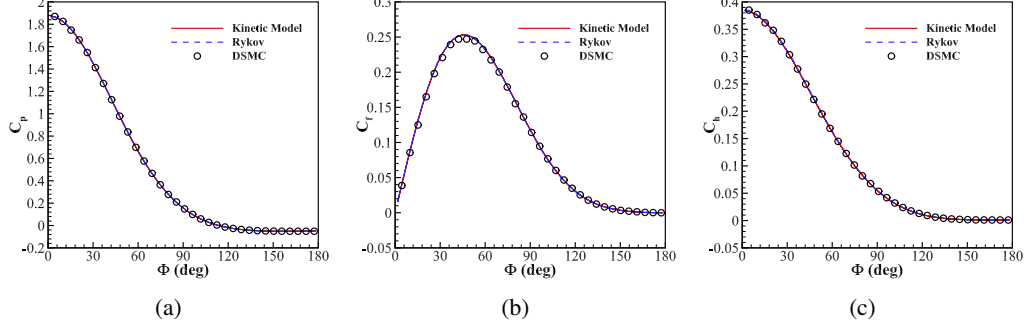


Figure 16: Comparisons of the (a) pressure, (b) shear stress, and (c) heat transfer coefficients at the wall surface of cylinder at $\text{Kn} = 0.1$.

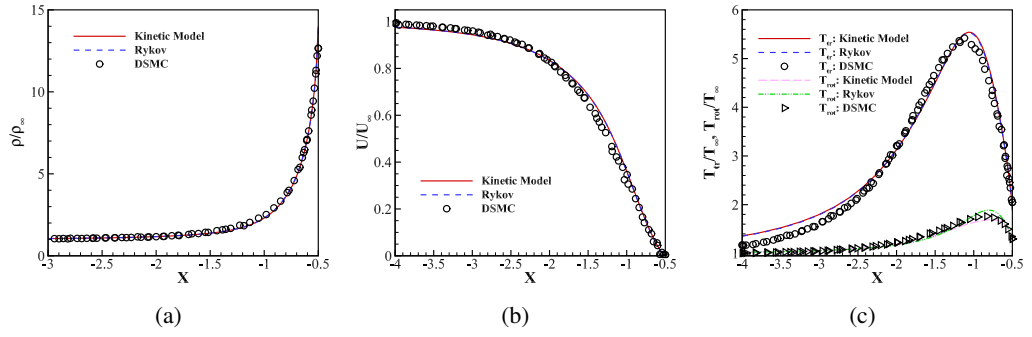


Figure 17: Comparison of the (a) density, (b) the velocity and (c) the translational and rotational temperatures along the forward stagnation line for the cylinder at $\text{Kn} = 1.0$.

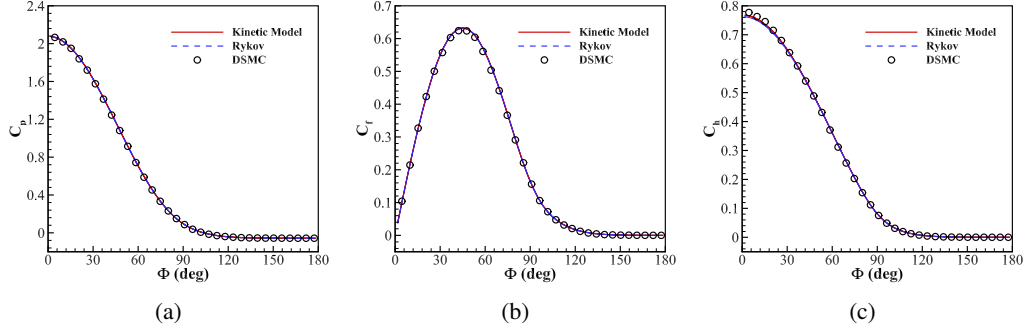


Figure 18: Comparisons of the (a) pressure, (b) shear stress, and (c) heat transfer coefficients at the wall surface of cylinder at $\text{Kn} = 1.0$.

5. Conclusions

In summary, we adopt the Pullin model with an integrable collision kernel that abides by the detailed balance principle as the extended Boltzmann equation, and derive the analytical expressions of the temporal relaxation rates for key macroscopic quantities via theoretical derivation for the first time. These quantities include the stress tensor, translational and rotational temperatures, as well as translational and rotational heat fluxes. Meanwhile, based on the C-E expansion framework with the same fundamental integrals for the collision term, the corresponding transport coefficients are derived, thereby establishing the fundamental

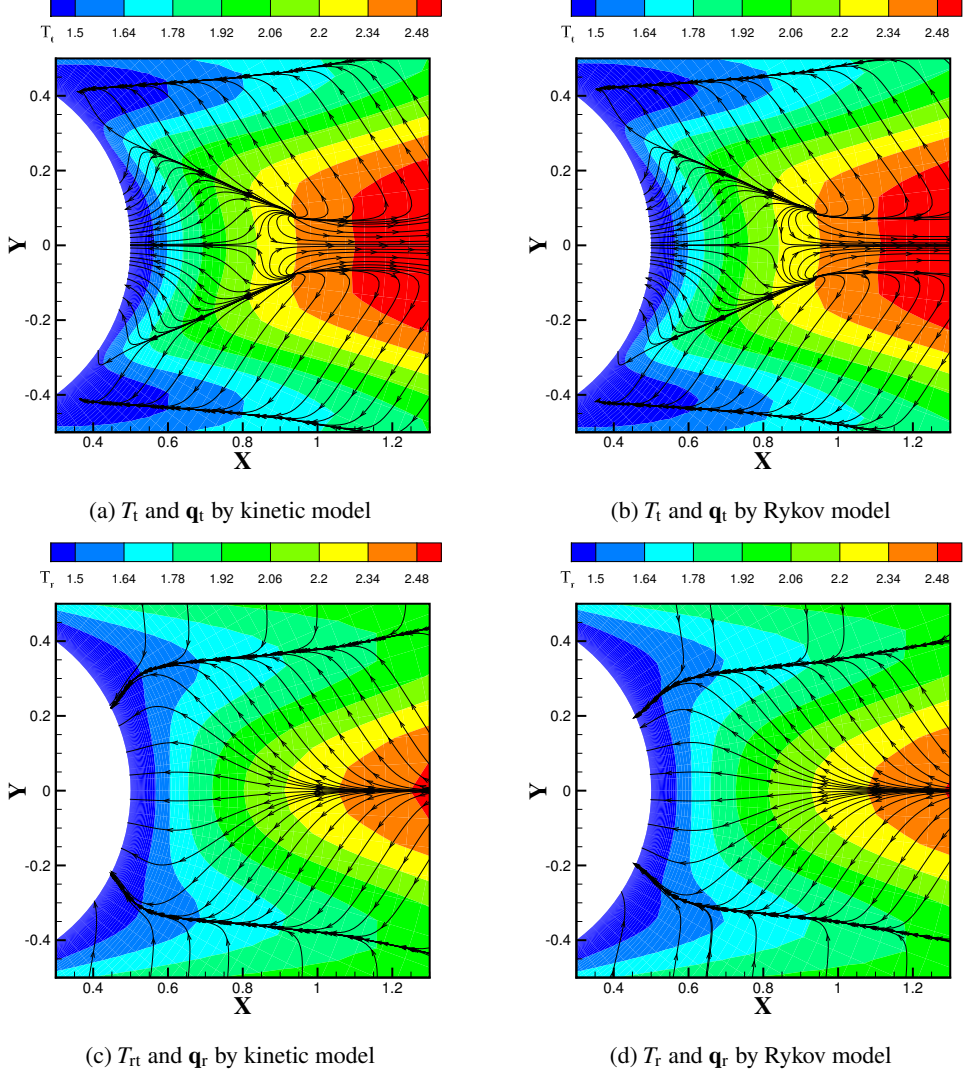


Figure 19: Comparison of the temperature fields (colored fields) and heat flux (black solid lines) in the wake region of flow past cylinder at $\text{Kn} = 0.01$. (a)-(b) are translational temperature and heat flux. (c)-(d) are rotational temperature and heat flux.

physical connection between non-equilibrium relaxation rates and transport coefficients. The primary results revealed from the theoretical analysis are that translational and rotational heat fluxes relax in a coupled manner, and that both the heat-flux relaxation process and the thermal conductivity are influenced by the non-equilibrium temperature ratio T_t/T_r . We quantify and evaluate the influence of non-equilibrium temperatures on thermal conductivity, and the results demonstrate that extreme non-equilibrium temperatures can induce drastic variations in thermal conductivity. Additionally, the derived results are compared separately with the theoretical and experimental results under the more common equilibrium temperature condition ($T_t = T_r$). The Eucken factor derived in this work reduces to the classical result obtained by Mason and Monchick from the WCU equation under equilibrium temperature condition. On the other hand, comparisons with the viscosity and thermal conductivity data

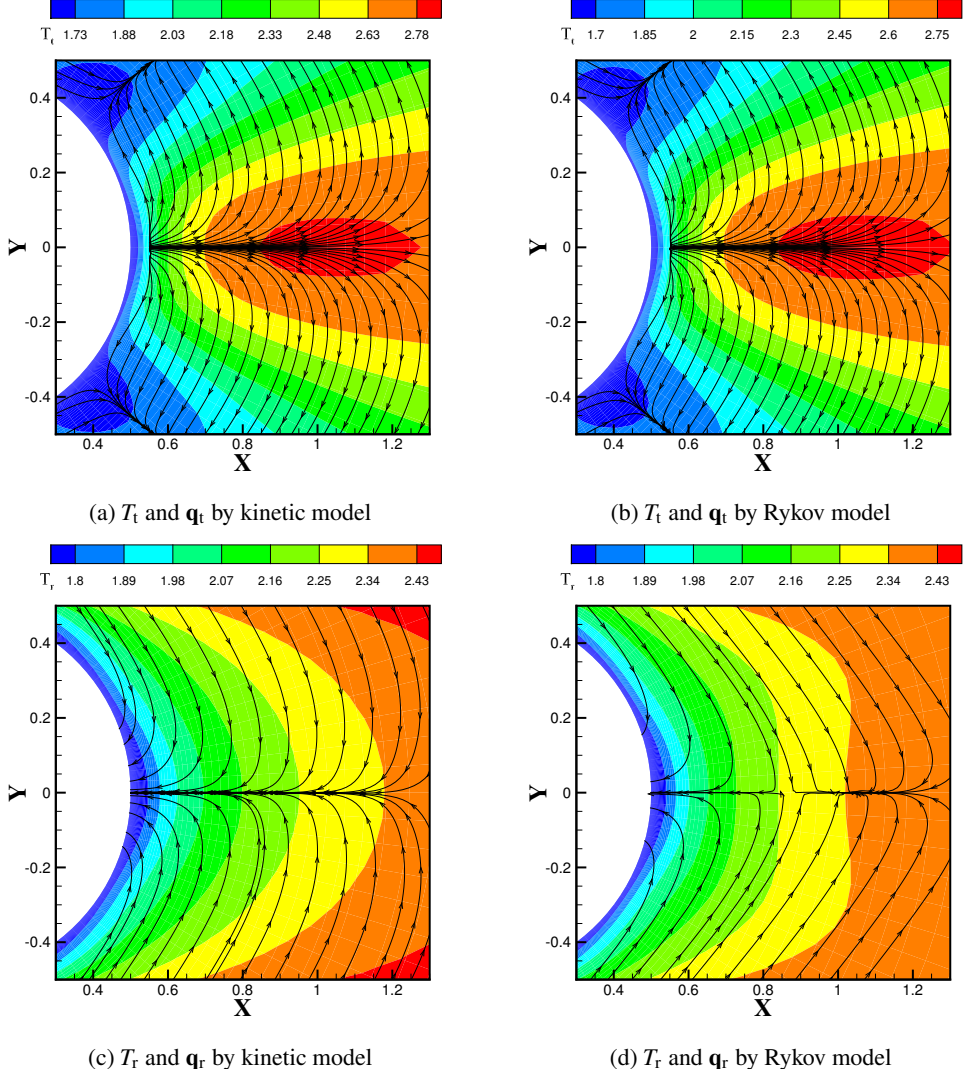


Figure 20: Comparison of the temperature fields (colored fields) and heat flux (black solid lines) in the wake region of flow past cylinder at $Kn = 0.1$. (a)-(b) are translational temperature and heat flux. (c)-(d) are rotational temperature and heat flux.

of nitrogen from the NIST experimental database show that the results derived in this work exhibit excellent agreement with the experimental values.

Based on the analytically derived relaxation rates, we have proposed a tractable relaxation-type kinetic model. The kinetic model can not only recover transport coefficients including shear viscosity, bulk viscosity and thermal conductivity, but also accurately capture the relaxation processes of non-equilibrium macroscopic quantities. The accuracy of the proposed model is evaluated by comparisons with DSMC simulation results. The kinetic model demonstrates excellent accuracy in zero-dimensional homogeneous relaxation, planar Couette flow, and hypersonic flow past a cylinder, while it exhibits certain deviations in the normal shock waves. This issue can be resolved by modifying the relaxation time of high-energy particles during the solution process.

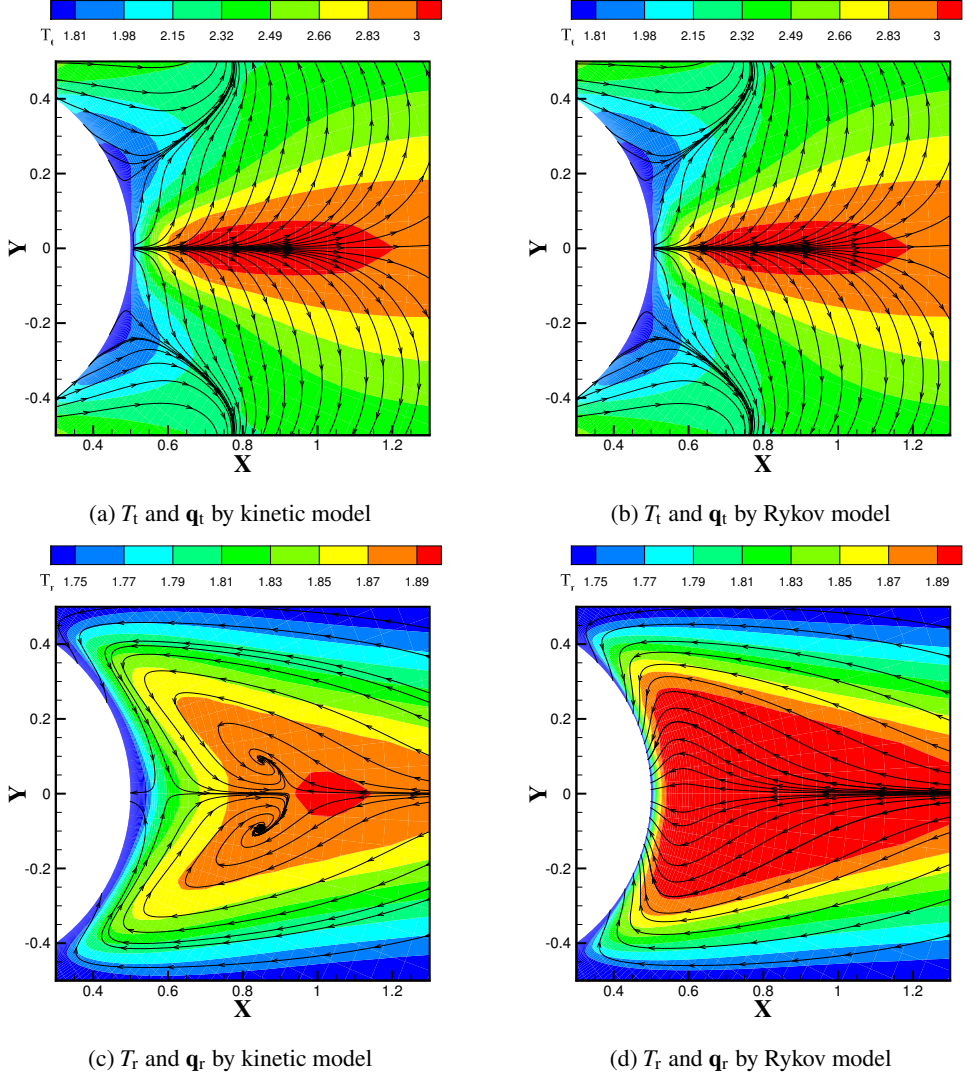


Figure 21: Comparison of the temperature fields (colored fields) and heat flux (black solid lines) in the wake region of flow past cylinder at $\text{Kn} = 1.0$. (a)-(b) are translational temperature and heat flux. (c)-(d) are rotational temperature and heat flux.

Then, the influence of the coupled relaxation mechanism between translational and rotational heat fluxes and the role of the non-equilibrium temperature ratio T_t/T_r on the flow are assessed by comparing solutions of the proposed kinetic model with those of the widely used Rykov model, which neglects these mechanisms. In simulations of 0-dimensional homogeneous relaxation and Planar Couette flow, the proposed kinetic model yields more accurate predictions of heat fluxes and temperatures than the Rykov model. Furthermore, under rarefied conditions, significant differences in rotational temperature and heat flux distributions are observed in lid-driven cavity flows and in the wake region of hypersonic flow past a cylinder. This demonstrates that it is essential to account for the coupled relaxation of heat fluxes and the effect of the non-equilibrium temperature ratio T_t/T_r in the thermal prediction of rarefied flows.

Although the derivation of relaxation rates and kinetic modeling in this study considers only rotational excitation, the extension to include vibrational relaxation rates and modeling can be achieved within our general framework. Furthermore, the increasingly complete state-to-state database can provide a foundation for achieving higher-precision modeling within this theoretically derived framework. In future work, these elements will be incorporated into the establishment of relaxation-rate models that account for vibrational excitation, to study high-temperature rarefied gas flows with strong thermal non-equilibrium.

Appendix A. Chapman-Enskog expansion of Pullin equation

The macroscopic transport coefficients of the Pullin model can be derived through C-E expansion (Chapman & Cowling 1990) and related to macroscopic relaxation rates. Expanding the distribution function and the time derivative operator $\mathcal{D} \equiv \frac{\partial}{\partial t} + U_i \frac{\partial}{\partial x_i}$ as power series in ε_{ce} , we retain terms up to second-order approximation.

$$\mathcal{D} = \mathcal{D}^{(0)} + \varepsilon_{ce} \mathcal{D}^{(1)} \quad (\text{A } 1)$$

$$f = f^{(0)} + \varepsilon_{ce} f^{(1)} = f^{(0)} + \varepsilon_{ce} f^{(0)} \phi_{ce} \quad (\text{A } 2)$$

where

$$f_1^{(0)} = n \left(\frac{m}{2\pi k T_t} \right)^{\frac{3}{2}} \exp \left(-\frac{m C^2}{2k T_t} \right) \frac{\epsilon^{\frac{\nu}{2}-1}}{\Gamma \left(\frac{\nu}{2} \right) (k T_r)^{\frac{\nu}{2}}} \exp \left(-\frac{\epsilon}{k T_r} \right) \quad (\text{A } 3)$$

The parameter ε_{ce} is introduced into the collision term of the Pullin equation, resulting in:

$$\mathcal{D} f_1^{(0)} + \mathbf{C}_1 \frac{\partial f_1^{(0)}}{\partial \mathbf{x}} = \frac{1}{\varepsilon_{ce}} Q(f, f) \quad (\text{A } 4)$$

Substituting the expanded distribution function Eq. (A 2) and time derivative Eq. (A 1) into the above Eq. (A 4), then classifying the resulting equations by order of ε_{ce} , yields:

$$\mathcal{D} f_1^{(0)} + \mathbf{C}_1 \frac{\partial f_1^{(0)}}{\partial \mathbf{x}} = 0 \quad (\text{A } 5)$$

$$\mathcal{D} f_1^{(0)} + \mathbf{C}_1 \frac{\partial f_1^{(0)}}{\partial \mathbf{x}} = \int f_1^{(0)} f_2^{(0)} (\phi'_1 + \phi'_2 - \phi_1 - \phi_2) g \sigma h(\mathbf{s}) ds d\Omega d\mathbf{c}_2 d\epsilon_2 = \mathcal{I} [\phi_{ce}] \quad (\text{A } 6)$$

Taking moments of the first-order approximate Eq. (A 5) with respect to collisional invariants yields the Euler-type equations:

$$\mathcal{D} \rho + \rho \frac{\partial U_i}{\partial x_i} = 0 \quad (\text{A } 7)$$

$$\rho \mathcal{D} U_i + \frac{\partial p_t}{\partial x_i} = 0 \quad (\text{A } 8)$$

$$\left(\frac{3}{2} n k \mathcal{D} T_t + n k T_t \frac{\partial U_i}{\partial x_i} \right) + \frac{\nu}{2} n k \mathcal{D} T_r = 0 \quad (\text{A } 9)$$

decomposing the energy equation gives:

$$\left(\frac{3}{2} n k \mathcal{D} T_t + n k T_t \frac{\partial U_i}{\partial x_i} \right) = \mathcal{E}_t = \frac{3 \nu n k}{2 (3 + \nu)} \frac{T_r - T_t}{Z_{\text{rot}} \tau_t} \quad (\text{A } 10)$$

$$\frac{\nu}{2} nk \mathcal{D} T_r = \mathcal{E}_r = \frac{3\nu nk}{2(3+\nu)} \frac{T_t - T_r}{Z_{\text{rot}} \tau_t} \quad (\text{A 11})$$

where \mathcal{E}_t and \mathcal{E}_r denote the translational and rotational energy relaxation rates, respectively. From the decomposed energy equations, we derive:

$$\mathcal{D} (T_t - T_r) = -\frac{2}{3} T_t \frac{\partial U_i}{\partial x_i} - \frac{2(3+\nu)}{3\nu} \mathcal{E}_r = -\frac{2}{3} T_t \frac{\partial U_i}{\partial x_i} - \frac{T_t - T_r}{Z_{\text{rot}} \tau_t} \quad (\text{A 12})$$

Expanding $T_t - T_r$ in powers of τ_t as $T_t - T_r = T_t \tau_t + O(\tau_t^2)$ reveals that the left-hand time derivative is negligible compared to the right-hand terms, yielding:

$$T_t - T_r \approx -\frac{2}{3} Z_{\text{rot}} \tau_t T_t \frac{\partial U_i}{\partial x_i} \approx -\frac{2}{3} Z_{\text{rot}} \tau_t T \frac{\partial U_i}{\partial x_i} \quad (\text{A 13})$$

Internal energy relaxation transforms the original pressure $p = nkT$ into translational pressure $p_t = nkT_t$. Thus, the translational pressure is expressed as:

$$p_t = nkT_t = nkT \left(1 + \frac{\nu}{3+\nu} (T_t - T_r) \right) = nkT \left(1 - \frac{2\nu}{3(3+\nu)} Z_{\text{rot}} \tau_t \frac{\partial U_i}{\partial x_i} \right) \quad (\text{A 14})$$

On the other hand, by reformulating the left-hand side of the second-order approximate Eq. (A 6) as:

$$\left(\left(\frac{\partial f^{(0)}}{\partial \rho} \mathcal{D} \rho + \frac{\partial f^{(0)}}{\partial v_i} \mathcal{D} v_i + \frac{\partial f^{(0)}}{\partial T_t} \mathcal{D} T_t + \frac{\partial f^{(0)}}{\partial T_r} \mathcal{D} T_r \right) + \right. \\ \left. C_i \left(\frac{\partial f^{(0)}}{\partial \rho} \frac{\partial \rho}{\partial x_i} + \frac{\partial f^{(0)}}{\partial v_j} \frac{\partial v_j}{\partial x_i} + \frac{\partial f^{(0)}}{\partial T_t} \frac{\partial T_t}{\partial x_i} + \frac{\partial f^{(0)}}{\partial T_r} \frac{\partial T_r}{\partial x_i} \right) \right) \quad (\text{A 15})$$

the function ϕ_{ce} can be expressed as:

$$\phi = \mathbf{A}_1 \left(-\frac{3}{2} + \frac{m}{2kT_t} C^2 \right) \frac{2}{3nkT_t} \mathcal{E}_t + \mathbf{A}_2 \left(-\frac{\nu}{2} + \frac{1}{kT_r} \epsilon_r \right) \frac{2}{\nu nkT_r} \mathcal{E}_r + \mathbf{B} \frac{m}{kT_t} C_i C_j \frac{\partial U_{\langle j \rangle}}{\partial x_i} + \\ \mathbf{D}_1 C_i \frac{1}{T_t} \left(-\frac{5}{2} + \frac{m}{2kT_t} C^2 \right) \frac{\partial T_t}{\partial x_i} + \mathbf{D}_2 C_i \frac{1}{T_r} \left(-\frac{\nu}{2} + \frac{1}{kT_r} \epsilon_r \right) \frac{\partial T_r}{\partial x_i} \quad (\text{A 16})$$

Taking moments of Eq. (A 16) yields:

$$\mathbf{A}_1 = 0, \mathbf{A}_2 = 0 \quad (\text{A 17})$$

$$\mathbf{B} = \tau_t \quad (\text{A 18})$$

$$\begin{bmatrix} \frac{5}{2} \mathbf{D}_1 \\ \frac{\nu}{2} \mathbf{D}_2 \end{bmatrix} = \frac{nk^2 T_t}{m} \begin{bmatrix} A_{tt} & A_{tr} \\ A_{rt} & A_{rr} \end{bmatrix}^{-1} \begin{bmatrix} \frac{5}{2} \\ \frac{\nu}{2} \end{bmatrix} \quad (\text{A 19})$$

Taking moments of the distribution function $f = f^{(0)} (1 + \phi_{ce})$ yields:

$$p_{t,\langle ij \rangle} = 2 \mathbf{B} n k T_t \frac{\partial U_{\langle i \rangle}}{\partial x_{j \rangle}} \quad (\text{A 20})$$

$$q_{t,i} = \mathbf{D}_1 \frac{5nk^2 T_t}{2m} \frac{\partial T_t}{\partial x_i} \quad (\text{A 21})$$

$$q_{r,i} = \mathbf{D}_2 \frac{nk^2 T_t}{m} \frac{\partial T_r}{\partial x_i} \quad (\text{A 22})$$

From Eq. (A 20), the shear viscosity is obtained as:

$$\mu = -nkT_t \mathbf{B} \quad (\text{A 23})$$

From Eq. (A 14), the bulk viscosity is derived as:

$$\mu_b = \frac{2\nu}{3(3+\nu)} Z_{\text{rot}} \tau_t n k T = \frac{2\nu}{3(3+\nu)} Z_{\text{rot}} \mu \quad (\text{A 24})$$

From Eq. (A 21) and Eq. (A 22), the translational and rotational thermal conductivities are given by:

$$\kappa_t = \frac{5nk^2 T_t}{2m} \mathbf{D}_1 \quad (\text{A 25})$$

$$\kappa_r = \frac{nk^2 T_t}{m} \mathbf{D}_2 \quad (\text{A 26})$$

Appendix B. Chapman-Enskog expansion of kinetic equation

The macroscopic transport coefficients of the kinetic model can also be derived through C-E expansion((Chapman & Cowling 1990)). Introducing the parameter ε_{ce} into the kinetic model equation yields:

$$\mathcal{D}f_1 + \mathbf{C}_1 \frac{\partial f_1}{\partial \mathbf{x}} = \frac{1}{\varepsilon_{\text{ce}}} \left(\frac{f_t - f_1}{\tau_t} + \frac{f_r - f_t}{Z_{\text{rot}} \tau_t} \right) \quad (\text{B 1})$$

The expanded distribution function and the time derivative are substituted into the Pullin equation. By truncating to the first-order approximation and setting $\varepsilon_{\text{ce}} = 1$, we obtain:

$$\mathcal{D}f_1^{(0)} + \mathbf{C}_1 \frac{\partial f_1^{(0)}}{\partial \mathbf{x}} = \frac{f_t - f_1^{(0)}}{\tau_t} + \frac{f_r - f_t}{Z_{\text{rot}} \tau_t} \quad (\text{B 2})$$

where

$$f_1^{(0)} = n \left(\frac{m}{2\pi k T_t} \right)^{\frac{3}{2}} \exp \left(-\frac{m C^2}{2k T_t} \right) \frac{\epsilon^{\frac{\nu}{2}-1}}{\Gamma \left(\frac{\nu}{2} \right) (k T_r)^{\frac{\nu}{2}}} \exp \left(-\frac{\epsilon}{k T_r} \right) \quad (\text{B 3})$$

Taking moments of Eq. (B 2) yields the Euler-type equations:

$$\mathcal{D}\rho + \rho \frac{\partial U_i}{\partial x_i} = 0 \quad (\text{B 4})$$

$$\rho \mathcal{D}U_i + \frac{\partial p_t}{\partial x_i} = 0 \quad (\text{B 5})$$

$$\left(\frac{3}{2} nk \mathcal{D}T_t + nk T_t \frac{\partial U_i}{\partial x_i} \right) + \frac{\nu}{2} nk \mathcal{D}T_r = 0 \quad (\text{B 6})$$

decomposing the energy equation gives:

$$\left(\frac{3}{2} nk \mathcal{D}T_t + nk T_t \frac{\partial U_i}{\partial x_i} \right) = \frac{3\nu nk}{2(3+\nu)} \frac{T_r - T_t}{Z_{\text{rot}} \tau_t} \quad (\text{B 7})$$

$$\frac{\nu}{2} nk \mathcal{D}T_r = \frac{3\nu nk}{2(3+\nu)} \frac{T_t - T_r}{Z_{\text{rot}} \tau_t} \quad (\text{B 8})$$

From the decomposed energy equations, we derive:

$$\mathcal{D}(T_t - T_r) = -\frac{2}{3}T_t \frac{\partial U_i}{\partial x_i} - \frac{2(3+\nu)}{3\nu} \mathcal{E}_r = -\frac{2}{3}T_t \frac{\partial U_i}{\partial x_i} - \frac{T_t - T_r}{Z_{\text{rot}}\tau_t} \quad (\text{B 9})$$

Expanding $T_t - T_r$ in powers of τ_t as $T_t - T_r = T_t\tau_t + O(\tau_t^2)$ reveals that the left-hand time derivative is negligible compared to the right-hand terms, yielding:

$$T_t - T_r \approx -\frac{2}{3}Z_{\text{rot}}\tau_t T_t \frac{\partial U_i}{\partial x_i} \approx -\frac{2}{3}Z_{\text{rot}}\tau_t T \frac{\partial U_i}{\partial x_i} \quad (\text{B 10})$$

Internal energy relaxation transforms the original pressure $p_0 = nkT$ into translational pressure $p_t = nkT_t$. Thus, the translational pressure is expressed as:

$$p_t = nkT_t = nkT \left(1 + \frac{\nu}{3+\nu} (T_t - T_r)\right) = nkT \left(1 - \frac{2\nu}{3(3+\nu)} Z_{\text{rot}}\tau_t \frac{\partial U_i}{\partial x_i}\right) \quad (\text{B 11})$$

, the bulk viscosity is derived as:

$$\mu_b = \frac{2\nu}{3(3+\nu)} Z_{\text{rot}}\tau_t nkT = \frac{2\nu}{3(3+\nu)} Z_{\text{rot}}\mu \quad (\text{B 12})$$

By truncating to the second-order approximation and setting $\varepsilon_{\text{ce}} = 1$, we obtain:

$$\mathcal{D}^{(0)} f_1^{(0)} + \mathbf{C}_1 \frac{\partial f_1^{(0)}}{\partial \mathbf{x}} = \frac{f_t - (f_1^{(0)} + f_1^{(1)})}{\tau_t} + \frac{f_r - f_t}{Z_{\text{rot}}\tau_t} \quad (\text{B 13})$$

By transforming the left-hand side of the equation into the form of Eq. (A 15), the second-order approximate part of the distribution function can be solved from Eq. (B 13):

$$f_1^{(1)} = \frac{f_t - f_1^{(0)}}{\tau_t} + \frac{f_r - f_t}{Z_{\text{rot}}\tau_t} - F_{\text{ce}} \quad (\text{B 14})$$

where

$$F_{\text{ce}} = f_1^{(0)} \left(\left(-\frac{3}{2} + \frac{m}{2kT_t} C^2 \right) \frac{1}{T_t} \frac{T - T_t}{Z_{\text{rot}}\tau_t} + \left(-\frac{\nu}{2} + \frac{1}{kT_r} \epsilon_r \right) \frac{1}{T_r} \frac{T - T_r}{Z_{\text{rot}}\tau_t} \right) + C_1 \left(\frac{m}{kT_t} C_j \frac{\partial U_{\langle j \rangle}}{\partial x_i} + \frac{1}{T_t} \left(-\frac{5}{2} + \frac{m}{2kT_t} C^2 \right) \frac{\partial T_t}{\partial x_i} + \frac{1}{T_r} \left(-\frac{\nu}{2} + \frac{1}{kT_r} \epsilon_r \right) \frac{\partial T_r}{\partial x_i} \right) \quad (\text{B 15})$$

Taking moments of the distribution function $f = f^{(0)} + f^{(1)}$ yields:

$$p_{t,\langle ij \rangle} = 2\mu \frac{\partial U_{\langle i \rangle}}{\partial x_{j\rangle}} = 2\tau_t nkT_t \frac{\partial U_{\langle i \rangle}}{\partial x_{j\rangle}} \quad (\text{B 16})$$

$$q_i = q_{t,i} + q_{r,i} \quad (\text{B 17})$$

$$q_{t,i} = \kappa_t \frac{\partial T_t}{\partial x_i} \quad (\text{B 18})$$

$$q_{r,i} = \kappa_r \frac{\partial T_r}{\partial x_i} \quad (\text{B 19})$$

where

$$\begin{bmatrix} \kappa_t \\ \kappa_r \end{bmatrix} = \frac{nk^2 T_t}{m} \begin{bmatrix} A_{tt} & A_{tr} \\ A_{rt} & A_{rr} \end{bmatrix}^{-1} \begin{bmatrix} \frac{5}{2} \\ \frac{\nu}{2} \end{bmatrix} \quad (\text{B 20})$$

Appendix C. integral operator

In the calculation of relaxation rates, the integral operator $\mathcal{I}_1 [A, B]$ is used to split and separately compute the integrals of the rates. The definition of $\mathcal{I}_1 [A, B]$ is as follows:

$$\mathcal{I}_1 [A, B] = \left(\frac{kT_t}{m} \right)^{\frac{7}{2}} (kT_r)^2 \int (A' - A) f_1^{(0)} f_2^{(0)} (B) g^* \sigma d\mathbf{e}' h(\mathbf{s}) d\mathbf{s} d\boldsymbol{\xi}_1 d\boldsymbol{\xi}_2 d\boldsymbol{\varepsilon}_2 d\boldsymbol{\varepsilon}_1. \quad (C1)$$

Key intermediate results in the derivation of the relaxation rates are respectively presented by the integral operators $\mathcal{I}_2 [A]$ and $\mathcal{I}_3 [A]$, which are defined as follows:

$$\begin{aligned} \mathcal{I}_2 [A] = \sqrt{\frac{kT_t}{m}} \int A \cdot n^2 \left(\frac{1}{2\pi} \right)^3 \frac{\varepsilon_1^{\frac{v}{2}-1}}{\Gamma(\frac{v}{2})} \frac{\varepsilon_2^{\frac{v}{2}-1}}{\Gamma(\frac{v}{2})} e^{-G^{*2}} e^{-\frac{g^{*2}}{4}} e^{-\varepsilon_1} e^{-\varepsilon_2} \\ \cdot g^* bdb h(\mathbf{s}) d\mathbf{s} d\mathbf{G}^* d\mathbf{g}^* d\boldsymbol{\varepsilon}_2 d\boldsymbol{\varepsilon}_1. \end{aligned} \quad (C2)$$

$$\mathcal{I}_3 [A] = \sqrt{\frac{kT_t}{m}} \int A \cdot \left(\frac{1}{2\pi} \right)^3 \frac{\varepsilon_1^{\frac{v}{2}-1}}{\Gamma(\frac{v}{2})} \frac{\varepsilon_2^{\frac{v}{2}-1}}{\Gamma(\frac{v}{2})} n^2 e^{-\frac{g^{*2}}{4}} e^{-\varepsilon_1} e^{-\varepsilon_2} g^* bdb h(\mathbf{s}) d\mathbf{s} d\mathbf{g}^* d\boldsymbol{\varepsilon}_2 d\boldsymbol{\varepsilon}_1. \quad (C3)$$

The correspondence between the $\mathcal{I}_1 [A, B]$ and $\mathcal{I}_2 [A]$ used in the relaxation rate integrals is written as follows:

$$\mathcal{I}_1 [\xi_1^2, 1] = \mathcal{I}_2 \left[\frac{\pi}{2} (g'^* - g^*) \right] \quad (C4)$$

$$\mathcal{I}_1 [\varepsilon_1, 1] = \mathcal{I}_2 [2\pi (\varepsilon_1' - \varepsilon_1)] \quad (C5)$$

$$\begin{aligned} \mathcal{I}_1 [\xi_{\langle 1, i} \xi_{1, j \rangle}, \xi_{\langle 1, k} \xi_{1, l \rangle} + \xi_{\langle 2, k} \xi_{2, l \rangle}] \\ = \mathcal{I}_2 \left[\pi \left(\frac{1}{2} (3\cos^2 [\chi] - 1) \frac{|g'^*|^2}{|g^*|^2} g_{\langle i}^* g_{j \rangle}^* - g_{\langle i}^* g_{j \rangle}^* \right) \left(G_k^* G_l^* + \frac{1}{4} g_k^* g_l^* \right) \right] \end{aligned} \quad (C6)$$

$$\begin{aligned} \mathcal{I}_1 [\xi_1^2 \xi_{1, i}, \xi_1^2 \xi_{1, k} + \xi_2^2 \xi_{2, k}] \\ = \mathcal{I}_2 \left[\left(\frac{\pi}{2} (3\cos^2 [\chi] - 1) \frac{|g'^*|^2}{|g^*|^2} g_i^* g_j^* G_j^* + \frac{\pi}{2} (\sin^2 [\chi] + 1) g'^* G_i^* - \pi g_i^* g_j^* G_j^* + \frac{\pi}{2} g^* G_i^* \right) \right. \\ \left. \cdot 2 \left(G^2 G_k + \frac{1}{2} g_k G_j g_j + \frac{1}{4} g^2 G_k \right) \right] \end{aligned} \quad (C7)$$

$$\begin{aligned} \mathcal{I}_1 [\xi_1^2 \xi_{1, i}, \varepsilon_1 \xi_{1, k} + \varepsilon_2 \xi_{2, k}] \\ = \mathcal{I}_2 \left[\left(\frac{\pi}{2} (3\cos^2 [\chi] - 1) \frac{|g'^*|^2}{|g^*|^2} g_i^* g_j^* G_j^* + \frac{\pi}{2} (\sin^2 [\chi] + 1) g'^* G_i^* \right) G_k (\varepsilon_1 + \varepsilon_2) \right. \\ \left. - \pi g_i^* g_j^* G_j^* + \frac{\pi}{2} g^* G_i^* \right] \\ + \mathcal{I}_2 \left[\pi \left(1 - \cos [\chi] \frac{|g'^*|}{|g^*|} \right) \left(G^2 \frac{1}{2} g_i + G_i G_j g_j + \frac{1}{8} g^2 g_i \right) g_k (-\varepsilon_1 + \varepsilon_2) \right] \end{aligned} \quad (C8)$$

$$\begin{aligned}
& \mathcal{I}_1 [\xi_1^2 \xi_{1,i}, \xi_{1,k} + \xi_{2,k}] \\
= & \mathcal{I}_2 \left[\frac{\pi}{2} \left(3\cos^2 [\chi] - 1 \right) \frac{|g'^*|^2}{|g^*|^2} g_i^* g_j^* G_j^* + \frac{\pi}{2} \left(\sin^2 [\chi] + 1 \right) g'^* G_i^* - \pi g_i^* g_j^* G_j^* + \frac{\pi}{2} g'^* G_i^* \right] 2G_k \quad (C9)
\end{aligned}$$

$$\begin{aligned}
& \mathcal{I}_1 [\xi_{1,i} \varepsilon_1, \xi_1^2 \xi_{1,k} + \xi_2^2 \xi_{2,k}] \\
= & \mathcal{I}_2 \left[4\pi G_i (\varepsilon_1' - \varepsilon_1) \left(G^2 G_k + \frac{1}{2} g_k G_j g_j + \frac{1}{4} g^2 G_k \right) \right] \quad (C10)
\end{aligned}$$

$$\begin{aligned}
& \mathcal{I}_1 [\xi_{1,i} \varepsilon_1, \varepsilon_1 \xi_{1,k} + \varepsilon_2 \xi_{2,k}] \\
= & \mathcal{I}_2 [2\pi G_i (\varepsilon_1' - \varepsilon_1) G_k (\varepsilon_1 + \varepsilon_2)] + \\
& \mathcal{I}_2 \left[\frac{\pi}{2} \left(-\cos [\chi] \frac{|g'^*|}{|g^*|} g_i \varepsilon_1' + g_i \varepsilon_1 \right) g_k (-\varepsilon_1 + \varepsilon_2) \right] \quad (C11)
\end{aligned}$$

$$\mathcal{I}_1 [\xi_{1,i} \varepsilon_1, \xi_{1,k} + \xi_{2,k}] = \mathcal{I}_2 [4\pi G_i (\varepsilon_1' - \varepsilon_1) G_k] \quad (C12)$$

Furthermore, the correspondence between the $\mathcal{I}_1 [A, B]$ and $\mathcal{I}_3 [A]$ used in the relaxation rate integrals is given by:

$$\mathcal{I}_1 [\xi_1^2, 1] = \mathcal{I}_3 \left[2\pi^{\frac{7}{2}} \left(g'^* - g^* \right) g^* \right] \quad (C13)$$

$$\mathcal{I}_1 [\varepsilon_1, 1] = \mathcal{I}_3 \left[8\pi^{\frac{7}{2}} (\varepsilon_1' - \varepsilon_1) g^* \right] \quad (C14)$$

$$\mathcal{I}_1 [\xi_{\langle 1,i} \xi_{1,j \rangle}, \xi_{\langle 1,k} \xi_{1,l \rangle} + \xi_{\langle 2,k} \xi_{2,l \rangle}] = \mathcal{I}_3 \left[\frac{1}{15} \pi^{\frac{7}{2}} g^{*4} \left(g'^* (3\cos^2 [\chi] - 1) - 2g^* \right) \right] \quad (C15)$$

$$\begin{aligned}
\mathcal{I}_1 [\xi_1^2 \xi_{1,i}, \xi_1^2 \xi_{1,k} + \xi_2^2 \xi_{2,k}] = & \mathcal{I}_3 \left[\frac{1}{3} \pi^{\frac{7}{2}} g^{*2} \left(10 + 3g^* \right) \left(\frac{1}{2} \left(3\cos^2 [\chi] - 1 \right) g'^* - g^* \right) \right] \\
& + \mathcal{I}_3 \left[\frac{5}{6} \pi^{\frac{7}{2}} g^{*2} \left(6 + g^* \right) \left(\left(\sin^2 [\chi] + 1 \right) g'^* - g^* \right) \right] \quad (C16)
\end{aligned}$$

$$\begin{aligned}
\mathcal{I}_1 [\xi_1^2 \xi_{1,i}, \varepsilon_1 \xi_{1,k} + \varepsilon_2 \xi_{2,k}] = & \mathcal{I}_3 \left[\frac{2}{3} \pi^{\frac{7}{2}} g^{*2} (\varepsilon_1 + \varepsilon_2) \left(\frac{1}{2} \left(3\cos^2 [\chi] - 1 \right) g'^* - g^* \right) \right] \\
& + \mathcal{I}_3 \left[\pi^{\frac{7}{2}} g^{*2} (\varepsilon_1 + \varepsilon_2) \left(\left(\sin^2 [\chi] + 1 \right) g'^* - g^* \right) \right] \\
& + \mathcal{I}_3 \left[\frac{1}{6} \pi^{\frac{7}{2}} g^{*2} \left(10 + g^* \right) (-\varepsilon_1 + \varepsilon_2) \left(g^* - \cos [\chi] g'^* g^* \right) \right] \quad (C17)
\end{aligned}$$

$$\begin{aligned}
\mathcal{I}_1 [\xi_1^2 \xi_{1,i}, \xi_{1,k} + \xi_{2,k}] = & \mathcal{I}_3 \left[\frac{4}{3} \pi^{\frac{7}{2}} g^{*2} \left(\frac{1}{2} \left(3\cos^2 [\chi] - 1 \right) g'^* - g^* \right) \right] \\
& + \mathcal{I}_3 \left[2\pi^{\frac{7}{2}} g^{*2} \left(\left(\sin^2 [\chi] + 1 \right) g'^* - g^* \right) \right] \quad (C18)
\end{aligned}$$

$$\mathcal{I}_1 [\xi_{1,i}\varepsilon_1, \xi_1^2\xi_{1,k} + \xi_2^2\xi_{2,k}] = \mathcal{I}_3 \left[\frac{10}{3}\pi^{\frac{7}{2}}g^{*^2} (6 + g^{*^2}) (\varepsilon_1' - \varepsilon_1) \right] \quad (C19)$$

$$\begin{aligned} \mathcal{I}_1 [\xi_{1,i}\varepsilon_1, \varepsilon_1\xi_{1,k} + \varepsilon_2\xi_{2,k}] = & \mathcal{I}_3 \left[\frac{2}{3}\pi^{\frac{7}{2}}g^{*^3} (-\cos[\chi] g'^*\varepsilon_1' + g^*\varepsilon_1) (-\varepsilon_1 + \varepsilon_2) \right] \\ & + \mathcal{I}_3 \left[4\pi^{\frac{7}{2}}g^{*^2} (\varepsilon_1' - \varepsilon_1) (\varepsilon_1 + \varepsilon_2) \right] \end{aligned} \quad (C20)$$

$$\mathcal{I}_1 [\xi_{1,i}\varepsilon_1, \xi_{1,k} + \xi_{2,k}] = \mathcal{I}_3 \left[8\pi^{\frac{7}{2}}g^{*^2} (\varepsilon_1' - \varepsilon_1) \right] \quad (C21)$$

REFERENCES

AKHLAGHI, H., ROOHI, E. & STEFANOV, S. 2023 A comprehensive review on micro-and nano-scale gas flow effects: Slip-jump phenomena, knudsen paradox, thermally-driven flows, and knudsen pumps. *Phys. Reports* **997**, 1–60.

ARISTOV, V.V. 2001 *Direct methods for solving the Boltzmann equation and study of nonequilibrium flows*, , vol. 60.

BHATNAGAR, P.L., GROSS, E.P. & KROOK, M. 1954 A model for collision processes in gases. i. small amplitude processes in charged and neutral one-component systems. *Phys. Rev.* **94** (3), 511.

BILLING, G.D. 2003 *The quantum classical theory*.

BIRD, G.A. 1970 Direct simulation and the boltzmann equation. *Phys. Fluids* **13** (11), 2676–2681.

BIRD, G.A. 1976 Molecular gas dynamics. *NASA STI/Recon Tech. Rep. A* **76**, 40225.

BIRD, G.A. 1978 Monte carlo simulation of gas flows. *Annu. Rev. Fluid Mech.* **10**, 11–31.

BORGNAKKE, C. & LARSEN, P.S. 1975 Statistical collision model for monte carlo simulation of polyatomic gas mixture. *J. Comput. Phys.* **18** (4), 405–420.

BOYD, I.D. 1993 Temperature dependence of rotational relaxation in shock waves of nitrogen. *J. Fluid Mech.* **246**, 343–360.

CAI, Z. & LI, R. 2010 Numerical regularized moment method of arbitrary order for boltzmann-bbgk equation. *SIAM J. Sci. Comput.* **32** (5), 2875–2907.

CERCIGNANI, C. 2000 *Rarefied gas dynamics: from basic concepts to actual calculations*, , vol. 21.

CERCIGNANI, C. & LAMPIS, M. 1971 Kinetic models for gas-surface interactions. *Transport Theory Stat. Phys.* **1** (2), 101–114.

CERCIGNANI, C. & OTHERS 1969 *Mathematical methods in kinetic theory*, , vol. 1.

CHAPMAN, S. & COWLING, T.G. 1990 *The mathematical theory of non-uniform gases: an account of the kinetic theory of viscosity, thermal conduction and diffusion in gases*.

CHEN, J., LIU, S., WANG, Y. & ZHONG, C. 2019 Conserved discrete unified gas-kinetic scheme with unstructured discrete velocity space. *Phys. Rev. E* **100** (4), 043305.

CLARKE, P., VARGHESE, P., GOLDSTEIN, D., MORRIS, A., BAUMAN, P. & HEGERMILLER, D. 2012 A novel discrete velocity method for solving the boltzmann equation including internal energy and non-uniform grids in velocity space. In *AIP Conference Proceedings*, , vol. 1501, pp. 373–380. American Institute of Physics.

CRUDEN, B.A. 2014 Absolute radiation measurements in earth and mars entry conditions. *Tech. Rep.*.

DESVILLETTES, L. & VILLANI, C. 2005 On the trend to global equilibrium for spatially inhomogeneous kinetic systems: the boltzmann equation. *Inventiones mathematicae* **159** (2), 245–316.

DREICER, H 1964 Kinetic theory of an electron-photon gas. *Phys. Fluids* **7** (5), 735–753.

EBNER, C., SAAM, W.F. & STROUD, D. 1976 Density-functional theory of simple classical fluids. i. surfaces. *Phys. Rev. A* **14** (6), 2264.

EUCKEN, A. 1913 Über das wärmeleitvermögen, die spezifische wärme und die innere reibung der gase. *Phys. Z.* **14** (8), 324–332.

FEI, F. 2023 A time-relaxed monte carlo method preserving the navier-stokes asymptotics. *J. Comput. Phys.* **486**, 112128.

FEI, F., ZHANG, J., LI, J. & LIU, Z. 2020 A unified stochastic particle bhatnagar-gross-krook method for multiscale gas flows. *J. Comput. Phys.* **400**, 108972.

GALLIS, M.A. & TORCZYNSKI, J.R. 2011 Investigation of the ellipsoidal-statistical bhatnagar–gross–krook kinetic model applied to gas-phase transport of heat and tangential momentum between parallel walls. *Phys. Fluids* **23** (3).

GAMBA, I.M. & PAVIĆ-ČOLIĆ, M. 2023 On the cauchy problem for boltzmann equation modeling a polyatomic gas. *J. Math. Phys.* **64** (1).

GORJI, M.H., TORRILHON, M. & JENNY, P. 2011 Fokker–planck model for computational studies of monatomic rarefied gas flows. *J. fluid Mech.* **680**, 574–601.

GRAD, H. 1958 Principles of the kinetic theory of gases. In *Thermodynamik der Gase/Thermodynamics of Gases*, pp. 205–294.

GUO, Z. & XU, K. 2016 Discrete unified gas kinetic scheme for multiscale heat transfer based on the phonon boltzmann transport equation. *Intl J. Heat and Mass Transfer* **102**, 944–958.

GUO, Z., XU, K. & WANG, R. 2013 Discrete unified gas kinetic scheme for all knudsen number flows: Low-speed isothermal case. *Phys. Rev. E* **88** (3), 033305.

GUO, Z. & ZHENG, C. 2008 Analysis of lattice boltzmann equation for microscale gas flows: relaxation times, boundary conditions and the knudsen layer. *Intl J. Comput. Fluid Dyn.* **22** (7), 465–473.

GUSAROV, A.V. & SMUROV, I. 2002 Gas-dynamic boundary conditions of evaporation and condensation: numerical analysis of the knudsen layer. *Phys. Fluids* **14** (12), 4242–4255.

HOLWAY, L.H. 1966 New statistical models for kinetic theory: methods of construction. *Phys. fluids* **9** (9), 1658–1673.

HONG, Q., STORCHI, L., SUN, Q., BARTOLOMEI, M., PIRANI, F. & COLETTI, C. 2023 Improved quantum-classical treatment of n2–n2 inelastic collisions: Effect of the potentials and complete rate coefficient data sets. *J. Chem. Theory and Comput.* **19** (23), 8557–8571.

HONG, Q., SUN, Q., BARTOLOMEI, M., PIRANI, F. & COLETTI, C. 2020 Inelastic rate coefficients based on an improved potential energy surface for n2+ n2 collisions in a wide temperature range. *Phys. Chem. Chem. Phys.* **22** (17), 9375–9387.

HU, Y., GUO, C., SONG, H. & MA, J. 2025 Thermal nonequilibrium relaxation of methane–nitrogen system investigated by state-resolved deep-potential-energy molecular dynamics. *Phys. Rev. A* **111** (6), 062821.

JIANG, J., YANG, J., HONG, Q., SUN, Q. & LI, J. 2024 Global potential energy surfaces by compressed-state multistate pair-density functional theory for hyperthermal collisions in the o2+ o2 system. *Chem. Phys. Chem.* **25** (12), e202400078.

JIANG, Z., ZHAO, W., YUAN, Z., CHEN, W. & MYONG, R.S. 2019 Computation of hypersonic flows over flying configurations using a nonlinear constitutive model. *AIAA J.* **57** (12), 5252–5268.

KARPLUS, M., PORTER, R.N. & SHARMA, R.D. 1965 Exchange reactions with activation energy. i. simple barrier potential for (h, h2). *J. Chem. Phys.* **43** (9), 3259–3287.

KREMER, G.M. 2010 *An introduction to the Boltzmann equation and transport processes in gases*.

LARINA, I.N. & RYKOV, V.A. 1976 Numerical study of the transverse supersonic flow of a diatomic rarefied gas past a plate. *Dokl. Akad. Nauk SSSR* **227** (1), 60–62.

LEBOWITZ, J.L., FRISCH, H.L. & HELFAND, E. 1960 Nonequilibrium distribution functions in a fluid. *Phys. Fluids* **3** (3), 325–338.

LI, J., VARGA, Z., TRUHLAR, D.G. & GUO, H. 2020a Many-body permutationally invariant polynomial neural network potential energy surface for n4. *J. Chem. Theory and Comput.* **16** (8), 4822–4832.

LI, Q., ZENG, J., SU, W. & WU, L. 2021 Uncertainty quantification in rarefied dynamics of molecular gas: rate effect of thermal relaxation. *J. Fluid Mech.* **917**, A58.

LI, W., LIU, C., ZHU, Y., ZHANG, J. & XU, K. 2020b Unified gas-kinetic wave-particle methods iii: Multiscale photon transport. *J. Comput. Phys.* **408**, 109280.

LIU, C. & XU, K. 2017 A unified gas kinetic scheme for continuum and rarefied flows v: Multiscale and multi-component plasma transport. *Commun. Comput. Phys.* **22** (5), 1175–1223.

LIU, S., YU, P., XU, K. & ZHONG, C. 2014 Unified gas-kinetic scheme for diatomic molecular simulations in all flow regimes. *J. Comput. Phys.* **259**, 96–113.

LIU, W., FENG, Y., LI, R., BAI, C. & NIU, B. 2024 Peridynamic modeling for multiscale heat transport of phonon boltzmann transport equation. *Comput. Phys. Commun.* **299**, 109157.

MASON, E.A. & MONCHICK, L. 1962 Heat conductivity of polyatomic and polar gases. *J. Chem. Phys.* **36** (6), 1622–1639.

MCCORMACK, F.J. 1968 Kinetic equations for polyatomic gases: The 17-moment approximation. *Phys. Fluids* **11** (12), 2533–2543.

MORRIS, A.B., VARGHESE, P.L. & GOLDSTEIN, D.B. 2011 Monte carlo solution of the boltzmann equation via a discrete velocity model. *J. Comput. Phys.* **230** (4), 1265–1280.

MORSE, T.F. 1964 Kinetic model for gases with internal degrees of freedom. *Phys. fluids* **7** (2), 159–169.

MÜLLER-PLATHE, F. 1997 A simple nonequilibrium molecular dynamics method for calculating the thermal conductivity. *J. Chem. Phys.* **106** (14), 6082–6085.

NAGNIBEDA, E. & KUSTOVA, E. 2009 *Non-equilibrium reacting gas flows: kinetic theory of transport and relaxation processes*.

NIST 2025 NIST database. <https://www.nist.gov>, accessed: 2025-07-14.

PARK, C. 1989 Nonequilibrium hypersonic aerothermodynamics .

PARKER, J.G. 1959 Rotational and vibrational relaxation in diatomic gases. *Phys. Fluids* **2** (4), 449–462.

PAVIĆ-ČOLIĆ, M. & SIMIĆ, S. 2022 Kinetic description of polyatomic gases with temperature-dependent specific heats. *Phys. Rev. Fluids* **7** (8), 083401.

PAWULA, R.F. 1967 Approximation of the linear boltzmann equation by the fokker-planck equation. *Phys. Rev.* **162** (1), 186.

PU, Z. & XU, K. 2025 Unified gas-kinetic wave-particle method for multiscale flow simulation of partially ionized plasma. *J. Comput. Phys.* **530**, 113918.

PULLIN, D.I. 1978 Kinetic models for polyatomic molecules with phenomenological energy exchange. *Phys. Fluids* **21** (2), 209–216.

REN, W., LIU, H. & JIN, S. 2014 An asymptotic-preserving monte carlo method for the boltzmann equation. *J. Comput. Phys.* **276**, 380–404.

RYKOV, V.A. 1975 A model kinetic equation for a gas with rotational degrees of freedom. *Fluid Dyn.* **10** (6), 959–966.

RYKOV, V.A. & SKOBELKIN, V.N. 1978 Macroscopic description of the motions of a gas with rotational degrees of freedom. *Fluid Dyn.* **13** (1), 144–147.

RYKOV, V.A., TITAREV, V.A. & SHAKHOV, E.M. 2007 Numerical study of the transverse supersonic flow of a diatomic rarefied gas past a plate. *Comput. Mathematics and Math. Phys.* **47** (1), 136–150.

SCHATZ, G.C. 1989 The analytical representation of electronic potential-energy surfaces. *Rev.s Mod. Phys.* **61** (3), 669.

SHAKHOV, E.M. 1968 Approximate kinetic equations in rarefied gas theory. *Fluid Dyn.* **3** (1), 112–115.

STRUCHTRUP, H. & TORRILHON, M. 2003 Regularization of grad's 13 moment equations: Derivation and linear analysis. *Phys. Fluids* **15** (9), 2668–2680.

SUN, W., JIANG, S. & XU, K. 2017 A multidimensional unified gas-kinetic scheme for radiative transfer equations on unstructured mesh. *J. Comput. Phys.* **351**, 455–472.

SUN, W., JIANG, S., XU, K. & LI, S. 2015 An asymptotic preserving unified gas kinetic scheme for frequency-dependent radiative transfer equations. *J. Comput. Phys.* **302**, 222–238.

SZABO, A. & OSLUND, N.S. 2012 *Modern quantum chemistry: introduction to advanced electronic structure theory*.

TAN, S., SUN, W., WEI, J. & NI, G. 2019 A parallel unified gas kinetic scheme for three-dimensional multi-group neutron transport. *J. Comput. Phys.* **391**, 37–58.

TAN, S., SUN, W., XU, K., WEI, J. & NI, G. 2020 Time implicit unified gas kinetic scheme for 3d multi-group neutron transport simulation. *Commun. Comput. Phys.* **28** (3), 1189–1218.

TORRILHON, M. 2016 Modeling nonequilibrium gas flow based on moment equations. *Annu. Rev. Fluid Mech.* **48** (1), 429–458.

VALENTINI, P., GROVER, M.S., VERHOFF, A.M. & BISEK, N.J. 2023 Near-continuum, hypersonic oxygen flow over a double cone simulated by direct simulation monte carlo informed from quantum chemistry. *J. Fluid Mech.* **966**, A32.

TE VRUGT, M., LÖWEN, H. & WITTKOWSKI, R. 2020 Classical dynamical density functional theory: from fundamentals to applications. *Adv. Phys.* **69** (2), 121–247.

WANG-CHANG, C.S. & UHLENBECK, G.E. 1951 Transport phenomena in polyatomic gases. *Tech. Rep.*..

WU, L., REESE, J.M. & ZHANG, Y. 2014 Solving the boltzmann equation deterministically by the fast spectral method: application to gas microflows. *J. Fluid Mech.* **746**, 53–84.

WU, L., WHITE, C., SCANLON, T.J., REESE, J.M. & ZHANG, Y. 2015 A kinetic model of the boltzmann equation for non-vibrating polyatomic gases. *J. Fluid Mech.* **763**, 24–50.

XU, K. & HUANG, J. 2010 A unified gas-kinetic scheme for continuum and rarefied flows. *J. Comput. Phys.* **229** (20), 7747–7764.

XU, X., CHEN, Y. & XU, K. 2021 Modeling and computation for non-equilibrium gas dynamics: Beyond single relaxation time kinetic models. *Phys. Fluids* **33** (1).

YANG, L.M., SHU, C., YANG, W.M. & WU, J. 2019 An improved three-dimensional implicit discrete velocity method on unstructured meshes for all knudsen number flows. *J. Comput. Phys.* **396**, 738–760.

YANO, R., SUZUKI, K. & KURODA, H. 2009 Analytical and numerical study on the nonequilibrium relaxation by the simplified fokker–planck equation. *Phys. Fluids* **21** (4).

ZENG, J., QI, L. & LEI, W. 2022 Kinetic modeling of rarefied molecular gas dynamics. *Acta Aerodyn. Sin.* **40** (2), 1–30.

ZHANG, C. & GUO, Z. 2021 A transient heat conduction phenomenon to distinguish the hydrodynamic and (quasi) ballistic phonon transport. *Intl J. Heat and Mass Transfer* **181**, 121847.

ZHANG, C., GUO, Z. & CHEN, S. 2017 Unified implicit kinetic scheme for steady multiscale heat transfer based on the phonon boltzmann transport equation. *Phys. Rev. E* **96** (6), 063311.

ZHANG, C., VALENTINI, P. & SCHWARTZENTRUBER, T.E. 2014 Nonequilibrium-direction-dependent rotational energy model for use in continuum and stochastic molecular simulation. *AIAA J.* **52** (3), 604–617.

ZHANG, J., JOHN, B., PFEIFFER, M., FEI, F. & WEN, D. 2019 Particle-based hybrid and multiscale methods for nonequilibrium gas flows. *Adv. Aerodyn.* **1** (1), 12.

ZHANG, Y., GU, X., BARBER, R.W. & EMERSON, D.R. 2006 Capturing knudsen layer phenomena using a lattice boltzmann model. *Phys. Rev. E* **74** (4), 046704.

ZHOU, X. & GUO, Z. 2020 Discrete unified gas kinetic scheme for steady multiscale neutron transport. *J. Comput. Phys.* **423**, 109767.